



Final Report, February 2015

PM-THIN PROJECT (2011-2014)

Optimization of Thin Film Module Testing and PV Module Energy Rating at SUPSI

QUALITY AND ENERGY YIELD OF PHOTOVOLTAIC MODULES

Auftraggeber:

Bundesamt für Energie BFE
Forschungsprogramm Photovoltaik
CH-3003 Bern
www.bfe.admin.ch

Kofinanzierung:

Azienda Elettrica Ticinese (AET), CH-6500 Bellinzona

Auftragnehmer:

Scuola Universitaria Professionale della Svizzera Italiana (SUPSI)
Via Trevano
CH-6952 Canobbio
www.isaac.supsi.ch

Autoren:

Gabi Friesen, SUPSI, gabi.friesen@supsi.ch
Mauro Pravettoni, SUPS , mauro.pravettoni@supsi.ch
Sebastian Dittmann, SUPSI, sebastian.dittmann@supsi.ch
Alessandro Virtuani, SUPSI, alessandro.virtuani@supsi.ch

BFE-Bereichsleiter: Stefan Oberholzer

BFE-Programmleiter: Stefan Nowak

BFE-Vertrags- und Projektnummer: 500691-01

Für den Inhalt und die Schlussfolgerungen ist ausschliesslich der Autor dieses Berichts verantwortlich.

Acknowledgments

The authors of this report would like to thank all colleagues of ISAAC without whom all this work would not have been possible, particularly:

- **Loris Manni, Michele Denicolà, Mauro Bernasocchi, Moreno Ronchi and Flavio Serrano** for their help in the execution of all measurements and the setup and upgrade of the various test facilities.
- **Enrico Burà, Boris Margna and Sylvain Pittet** for the installation and maintenance of the outdoor test facility and again **Enrico Burà** for the preparation of the new calibration procedure for our MPPT3000.
- **Davide Strepparava, Ronny Meoli and Marco Nicola** for the continuous improvement of all software and data acquisition tools, their support in the definition of error flags, the maintenance and upgrade of our database and their support in all data analysis activities.
- **Antonella Realini** for her great support in the accreditation of new test procedures.
- **Thomas Friesen and Matteo Marzoli** for their scientific support.

Index

Acknowledgments	3
1. FOREWORD	5
2. ABSTRACT	6
3. CHARACTERIZATION OF THIN FILM MODULES	7
3.1 Spectral responsivity (SR) measurement.....	8
3.2 Spectral mismatch (MM) error calculation.....	10
3.3 Current-voltage (IV) measurements	13
3.4 Measurement uncertainties	18
4. PRE-CONDITIONING OF THIN FILM MODULES	25
4.1 Meta-stability of polycrystalline thin film modules	26
4.2 Preconditioning of thin film PV modules with light.....	27
4.3 Dark current soaking (CS).....	31
4.4 CIGS and CdTe pre-conditioning procedure	33
5. OUTDOOR PERFORMANCE OF THIN FILM MODULES.....	35
5.1 Outdoor test facility.....	36
5.2 Module characterization	39
5.3 Energy yield (EY) inter-comparison.....	47
6. MODELLING OF THIN-FILM OUTDOOR PERFORMANCE.....	56
6.1 Basic equations	57
6.2 Spectral modelling	59
6.3 Loss factor analysis	61
6.4 Simplified model with aggregate inputs.....	66
6.5 Extension of the model to other geographical locations.....	73
7. CONCLUSIONS & FUTURE PERSPECTIVES	78
References	81
Annex 1: List of publications.....	83
Annex 2: Module table.....	85

1. FOREWORD

The *Swiss PV Module Test Centre* - part of the Institute of Applied Sustainability to the Built Environment (ISAAC) of the University of Applied Sciences and Arts of Southern Switzerland (SUPSI) and formerly known as TISO (Ticino Solare), founded in 1982 - offers a wide range of services and research collaborations in the field of PV module and system testing for the Swiss and international industry, being ISO 17025 accredited for more than 30 test procedures for PV modules.

The measurement capabilities and accuracies for the electrical characterization of PV modules have been continuously improved over recent years, also supported by the Swiss Federal Office of Energy (SFOE). The period from 2007-2010 (contract no. 153027) focused on the extension of the existing test equipment for the characterization of PV modules with solar simulators under conditions different from the standard test conditions (STC) (via variation of temperature, irradiance and spectrum) and on correlating these data to performance data measured in the field. The outdoor test facilities and related data evaluation procedures were therefore upgraded to reach the highest levels of reliability and accuracy.

With the boom of thin film (TF) module manufacturers in 2009/2010 and the strong position of Swiss research institutes and industries in these technologies, a new project named **PM-THIN (contract no. 500691-01)** was started in order to meet some of the major measurement challenges associated with thin film modules and to intensify the study of their performance under real operating conditions.

Over the last several years the combined effect of decreasing cost and increasing efficiency of c-Si has posed a severe challenge to most thin film modules, so that now many thin TF PV manufacturers are facing serious problems in maintaining their position in the market. The trend observed in 2009 has been reverting significantly in the last 3-4 years (i.e. the market share for TF PV is shrinking). Presently, CdTe is in fact the only technology competing with c-Si on a price level, and CIS-based devices are, among all TF technologies, the ones exhibiting the highest efficiencies, with still many players extensively working at these compounds. At the same time, new interest has risen in novel materials, most of all perovskite solar cells, which, in combination with first or second generation PV to form novel multi-junction structures, promise efficiencies well above 20-22%, which seems to be the practical limit of high-efficiency c-Si modules. These novel multi-junction modules will soon be available in R&D and may be on the market in the next 5-10 years, thus proposing new challenges in PV testing, while also offering new opportunities for the know-how acquired at SUPSI within PM-THIN.

The activities and achievements of the PM-THIN project '*Optimization of Thin Film Module Testing and PV Module Energy Rating at SUPSI*' are summarized in this report. The document is divided into four chapters, the first of which (Chapter 3) presents the novel upgrades of our solar simulators for the purpose of **PV module characterization of thin film modules** and its impact on the accuracy of indoor measurement. Chapter 4 presents the results of a detailed analysis of meta-stabilities observable in new and outdoor-exposed polycrystalline thin film modules (i.e. II-VI and I-III-VI), and of different **pre-conditioning procedures**, which can be applied in order to stabilize the module before performing a power rating. Chapter 5 presents the novelties introduced in our outdoor test facility and the results of a 4-year **thin film outdoor measurement campaign**, together with the indoor-measured data of all modules and their stability analysis. Chapter 6 links the outdoor performance figures with the indoor data by means of **module performance models**, allowing us to differentiate between the four significant aspects of thin film technologies (temperature, irradiance, spectrum and seasonal variations) and to better understand the different behaviours observed.

2. ABSTRACT

For the PM-THIN project, the indoor and outdoor testing facilities and test procedures available at SUPSI were upgraded in order to improve the accuracy of thin film module measurements and to analyze their performance under controlled laboratory and real operating conditions. The focus of the project was on the characterization of multi-junction devices and procedures for the pre-conditioning of polycrystalline thin film modules, which needed to be improved in order to guarantee a higher degree of comparability and repeatability of their power measurements. The progress in module characterization, in combination with long-term outdoor monitoring data and modelling activities, led to an increase in the understanding of thin film performance in comparison with that of crystalline silicon technologies. The technologies analyzed within the project included a-Si, a-Si/a-Si, a-Si/ μ c-Si, CdTe, CIS, CIGS and CIGSS. Crystalline silicon was taken as a reference technology.

In particular, the spectral response system available at SUPSI was improved and extended for the characterization of multi-junction devices, and a LED bias light system was added for the tuning of the solar simulator spectrum. Improvements in the equipment and spectral mismatch correction procedure decreased the uncertainty of P_{\max} of all single-junction thin film modules from $\pm 3.4\%$ down to $\pm 1.9\%$ and to 2.0% for multi-junction modules, thereby being comparable to that of single junction devices, which was one of the milestones of the project. The Swiss PV Module Test Centre is now one of the few testing centres with measurement capabilities for multi-junction commercial size modules. Furthermore, based on the outcome of this project and collaborations with other testing laboratories, a new pre-conditioning procedure for the stabilization of CIS and CdTe modules was introduced, also taking into account short-term meta-stabilities in the range of minutes, seconds and milliseconds. Besides these indoor activities, a 4-year outdoor measurement campaign on eleven different thin film technologies was concluded, demonstrating differences in the annual energy production of up to $\pm 10\%$ within the different technologies. CIS and a-Si/ μ c-Si modules slightly underperformed or performed very close to c-Si, whereas CdTe and a-Si tended to overperform, due to their much better temperature coefficients. The introduction of loss-parameter models allowed us to distinguish between different contributions affecting the energy performance of modules in operation (i.e. temperature, spectral, low-irradiance and reflection losses). Spectral and angle of incidence losses were added to the more straightforward modelling of thermal and irradiance losses, and a new approach was implemented for the modelling of the Staebler-Wronsky effect in amorphous silicon in different climates and was validated for Lugano. The approach takes into account the accumulated irradiance and temperatures reached by the module to predict the seasonal variations of a-Si modules, and thereafter can be applied to any climate. The outdoor data were also shared at the international level, within the framework of the International Energy Agency's Photovoltaic Power System Programme (IEA PVPS) Task 13, and a new approach for the representation and analysis of PV module field data was developed. The approach allows the comparison of data measured in different climates and conditions, as well as of data acquired during different test periods, and correction for spectral effects, thus allowing the extraction of the thermal performance under real operating conditions and the comparison of this with the indoor-measured temperature coefficients.

Along with the many achievements, some new challenges were also identified during the project. Limitations in current spectral irradiance measurements were highlighted, as well as the need for a common effort among testing laboratories to improve temperature coefficient measurements, in particular of thin film technologies, as well as the stabilization of CIGS and CdTe modules, whose effectiveness still has to be demonstrated. As was done for indoor testing, also outdoor testing facilities and the related testing procedures should in future be harmonized so as to increase the comparability of outdoor data. The proposed performance models must be extended to multi-junction devices, as well as the description of degradations occurring in PV modules.

3. CHARACTERIZATION OF THIN FILM MODULES

Background:

Thin-film PV modules generally show peculiarities that require new methods of measurement for their characterization. One of the most significant differences with crystalline silicon (c-Si) PV modules is the wide range of spectral responsivities available on thin-film modules, which may show either narrow band (a-Si, CdTe) or multiple band responses (a-Si/a-Si, a-Si/ μ c-Si, a-Si/a-Si/a-Si multi-junction PV modules). When the spectral responsivity of the testing module varies significantly with the reference c-Si cell used to detect the total irradiance, large spectral mismatch uncertainties may arise in the indoor electrical characterization, even on Class AAA solar simulators.

Scope of the project:

- To upgrade the spectral responsivity (SR) measurement setup to multi-junction modules;
- To develop new procedures for SR measurement of multi-junction modules and spectral mismatch correction;
- To upgrade the class A+A+A+ solar simulator and allow spectral tuning;
- To target the uncertainty of maximum power measurement of multi-junction modules at 3-4%, in line with single-junction modules.
- To prepare a dedicated measurement procedure and uncertainty calculation for multi-junction modules;
- To submit all the new documentation to SAS for ISO 17025 accreditation;
- To confirm the reputation of SUPSI as a centre of reference for electrical characterization of first and second generation PV, via dissemination and participation in international normative activity.

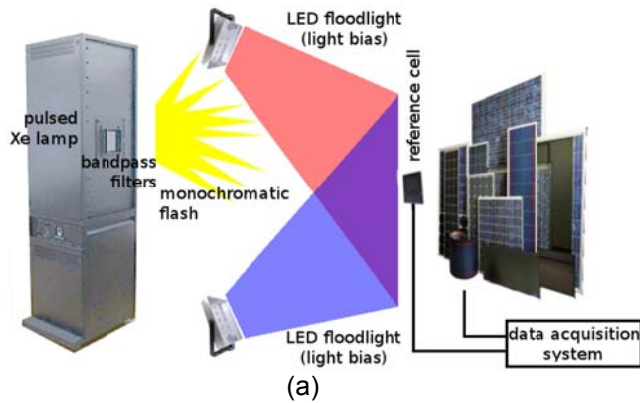
Results:

- The SR measurement setup was redesigned, upgraded and ISO 17025 accredited;
- The effect of the spectral mismatch to the electrical parameters was quantified;
- Measurement uncertainty on P_{max} was lowered to 1.6% for c-Si, to 1.9% for single-junction thin-film modules and 2.0% for multi-junction ones;
- New procedures were prepared and submitted for ISO 17025 accreditation;
- Active participation in IEA dissemination work and IEC preparation of dedicated international standards for multi-junction PV modules;
- Publications in peer-reviewed journals and conference proceedings.

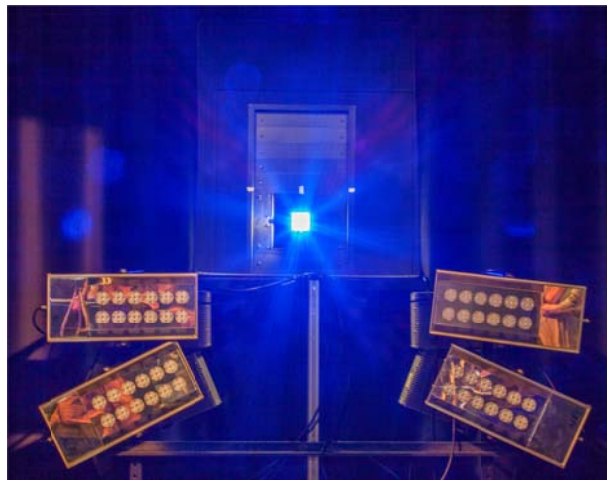
3.1 Spectral responsivity (SR) measurement

3.1.1 Test facility

At the beginning of the project, a spectral responsivity (SR) measurement setup for the characterization of single-junction modules was available at SUPSI, being designed as an optional tool of the A+A+A+ Pasan IIIb pulsed solar simulator. In the first year of the project (2012), the equipment was further upgraded by means of a set of coloured LED floodlights by AEON Ltd. [PMTHIN 1], with peak wavelengths at 475, 630 and 850 nm, thus allowing first measurements of multi-junction devices (the a-Si compounds: a-Si:H/ μ c-Si, a-Si:H/a-Si:H and a-Si:H/a-Si:H/a-Si:H), according to the standard procedure available [REF 3.1].



(b)



(c)

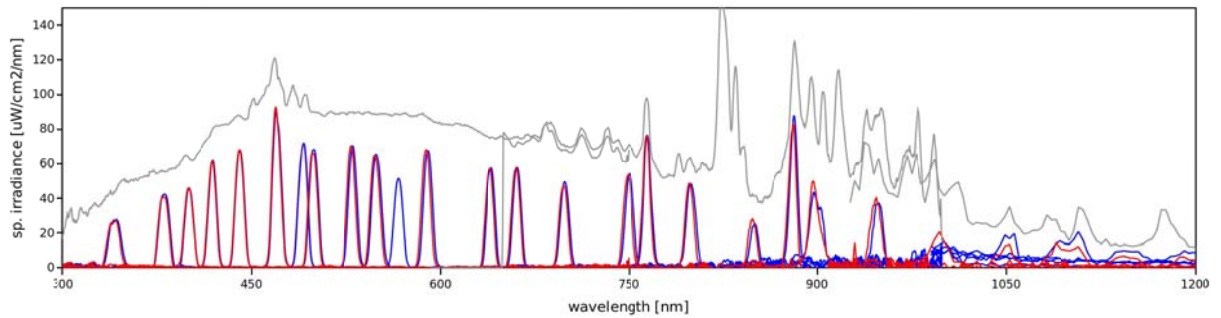


Figure 3.1: The new and final setup for SR measurements on Pasan IIIa available at the end of the project: (a) the scheme; (b) detail of the lamp filtering system; (c) photo showing the LED bias light system; (d) transmittance of the new bandpass filters.

The Pasan IIIb is a 4-lamp pulsed simulator and therefore requires a complex combination of band-pass filters to produce quasi-monochromatic light. As a consequence, the original setup showed some unexpected experimental artifacts over the first years of use (arising from non-uniformity and stray-light) which needed to be solved. The system was therefore re-designed on a single source pulsed simulator (Pasan IIIa) available at SUPSI (see Figure 3.1). The upgrade resulted in a simplification of the opto-mechanical system and a separation of the current-voltage characterization (Pasan IIIb) and SR measurement (Pasan IIIa). The new setup was also equipped with additional bandpass filters (28 instead of the original 18 filters) with a narrower bandpass (11 nm on most filters, instead of the original 25 nm). The spatial uniformity was improved, leading to a further optimization of the SR measurement uncertainty.

The new system was validated and ISO 17025 was accredited in October 2014.

3.1.2 Theory and results (multi-junction modules)

The measurement principle for single-junction PV modules is straightforward (see [REF 3.2]):

- 1) a large-area monochromatic beam is produced via filtering the flash of a solar simulator with up to 28 bandpass filters of peak-wavelength λ ;
- 2) the short-circuit current given by the module under testing and by the reference detector (an unfiltered c-Si reference cell with calibrated SR) is measured with two trans-impedance amplifiers;
- 3) the SR of the test device is given by

$$SR_{test}(\lambda) = \frac{A_{ref} \cdot I_{sc,test}}{N_{par} \cdot A_{test} \cdot I_{sc,ref}} SR_{ref}(\lambda) \quad (\text{equation 3.1})$$

where A_{ref} and A_{test} are the areas of the reference cell and the module to be tested; N_{par} is the number of cells in parallel in the test device; $I_{sc,test}$ and $I_{sc,ref}$ are the measured short-circuit currents of the test device and the reference cell respectively, and $SR_{ref}(\lambda)$ is the SR of the reference cell at wavelength λ .

In multi-junction modules the series connection between junctions inhibits SR measurements. In fact, the photo-generated current from a given junction under a monochromatic beam at a given wavelength is blocked by the junction(s) that is (are) not responding at that wavelength. As a result, the basic procedure for single-junction devices described above generally gives the minimum of the SRs of the component junctions (the black dashed line in Figure 3.2a).

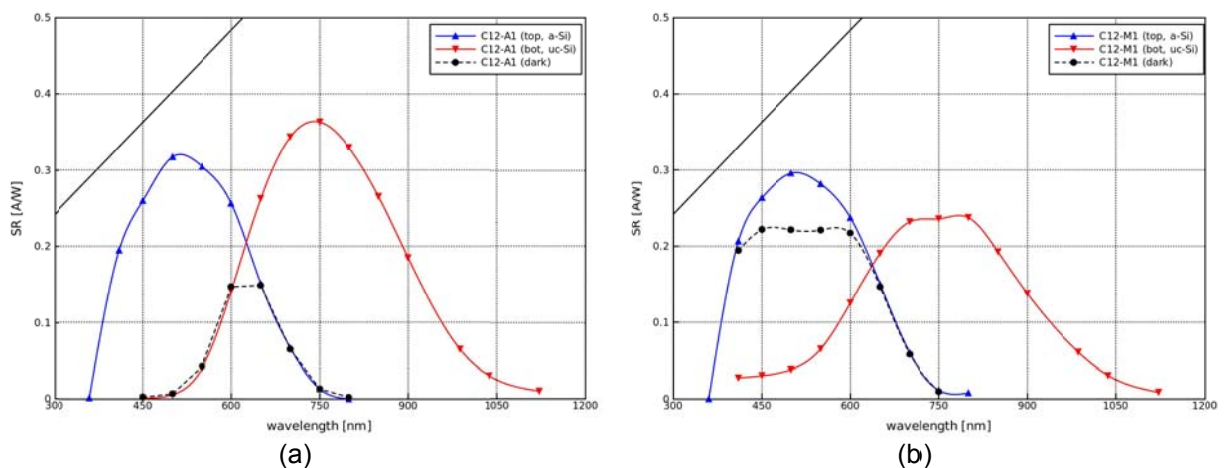


Figure 3.2: Examples of SR measurements at SUPSI: (a) a-Si:H/ μ c-Si module (the black dashed line shows the SR measurement without coloured bias light: current-limitation between junctions gives the minimum of the SRs of the component junctions); (b) a-Si:H/ μ c-Si module, with current-leakage through a shunt resistance in the bottom junction.

Moreover, current leakage from component junctions in multi-junction PV devices causes non-zero SR in wavelength regions where a junction is not expected to respond (Figure 3.2b, [REF 3.3]). In both cases the real SR of the top and bottom junction(s) (blue and red curves in Figure 3.2) are not measured and an alternative procedure must be applied.

In order to avoid current-limitation and to measure the SR of multi-junction PV devices, coloured bias light is used. In the experimental setup developed at SUPSI, bias light is provided by LED floodlight. Additionally, voltage bias may also be applied to limit current leakage through shunts, as described in the cited ASTM standard: a review of these methods with an innovative theoretical approach has been published in some papers during the project [PMTHIN 2 - PMTHIN 6]. The results of this work were used as input for the preparation of the new draft international standard [REF 3.4] for SR measurement of multi-junction devices.

3.2 Spectral mismatch (MM) error calculation

3.2.1 Methodology

Standard Test Conditions (STC) give a common basis for indoor electrical measurement inter-comparison of PV devices. For terrestrial, non-concentrating modules, they refer to 25°C cell temperature, 1000 W/m² total irradiance and AM1.5g spectral irradiance. The first two conditions may be measured with a calibrated temperature probe and a reference cell. Linear correction to the electrical parameters can easily be applied when indoor measurements are performed in a controlled environment. On the other hand, indoor measurements on solar simulators are generally affected by a spectral mismatch error arising from the difference between the spectral irradiance of the solar simulator in use and the standard AM1.5g spectrum, as well as from the differences between the SRs of the testing device and of the reference cell in use. In fact, when the reference cell responds in a different spectral range than the testing module, differences in the total irradiance "seen" by the testing module may not be recorded by the reference cell and vice versa, thus directly overestimating or underestimating the current measurement and therefore the maximum power of the testing module.

The following term quantifies the spectral mismatch factor *MMF*, according to the international standard IEC 60904-7 [REF 3.5],

$$MMF = \frac{\int SR_{test} E_{AM1.5g} d\lambda}{\int SR_{test} E_{solsim} d\lambda} \cdot \frac{\int SR_{ref} E_{solsim} d\lambda}{\int SR_{ref} E_{AM1.5g} d\lambda} \quad (\text{equation 3.2})$$

and needs to be applied to current and power to correct for spectral mismatch error. Significantly, *MMF* equals 1 (i.e. no correction to be applied) when:

- $SR_{test} = SR_{ref}$, which means the testing module and the reference cell "see" the same fraction of the spectral irradiance;
- $E_{solsim} = E_{AM1.5g}$, which means there is no mismatch between the solar simulator and the standard spectrum.

3.2.2. Results: single junction modules

The spectral mismatch factor *MMF* on single-junction PV devices may be close to 1, i.e. within a few percentage points, on a high-quality solar simulator and when using a filtered reference cell with SR well matched to the SR of the testing device.

There are two approaches to take into account for the spectral mismatch on single-junction modules:

1. Statistical approach: quantify the worst possible *MMF* on a given solar simulator for the widest possible range of commercial PV modules and take it as a source of measurement uncertainty, thus completely avoiding the calculation of *MMF*.
2. Quantitative approach: calculate *MMF* and apply it to the measured short-circuit current and maximum power via estimation of the uncertainty of the *MMF* value itself.

The statistical approach is the only possible one in the absence of a SR measurement setup. On the other hand, this relies on the known spectral irradiance of the solar simulator in use and on the choice of the range of commercial PV modules. Furthermore, this approach may contribute greatly to budget uncertainty, and can thus limit any enhancement of measurement precision.

The quantitative approach relies on knowing the SRs of the testing module and of the reference cell, as well as on the uncertainty of measurements of the spectral irradiance of the simulator in use, which may be either large or unknown.

Once the SR setup had been developed and accredited at SUPSI, the quantitative approach was introduced into the quality system, with a significant enhancement of the overall uncertainty of single-junction modules, both c-Si and thin-film, as shown in the following section 3.5.

3.2.3 Results: multi-junction modules and effect on the open-circuit voltage

In multi-junction modules, the spectral mismatch generally has a different effect on various junctions, so a spectral mismatch factor must be calculated for each junction. Furthermore, even a solar simulator with Class A+ spectral irradiance may exhibit MMF values as high as 1.1, thus giving a $\pm 10\%$ uncertainty contribution to current and maximum power, as discussed by the authors in Ref. [PMTHIN 8]. The project demonstrated that for multi-junction modules the open-circuit voltage is also influenced by spectral mismatch [PMTHIN 3].

Consider for example a 2-junction PV module in which the two junctions are perfectly current-matched at AM1.5g: in this case, the measured current at AM1.5g clearly equals the photogenerated current of both the top and the bottom junction (Figure 3.3a) and at AM1.5g $MMF_{top,AM1.5g} = MMF_{bot,AM1.5g} = 1$ with any reference cell. If we now consider the same 2-junction PV module under a Class A+ solar simulator, which is 5% red-shifted (i.e. it has 5% more irradiance in the bottom junction SR band than in the top junction SR band), which is quite common on Xe-based solar simulators, then a broadband reference cell (e.g. an unfiltered c-Si reference cell, responding within the whole band where both the top and the bottom junctions respond) will "see" 1000 W/m^2 total irradiance over the entire band. As a result, the top junction will "see" less (say, 5% less) irradiance than will the bottom junction due to the 5% red-shift in the spectrum of the simulator and therefore:

1. the module will be top limited;
2. the measured short-circuit current will be underestimated by 5% with respect to the measurement at AM1.5g (which could be corrected by applying the correct MMF value, calculated from the top junction SR);
3. the measured open-circuit voltage will most probably be correct, being the sum of the underestimated voltage contribution from the top junction and the overestimated voltage contribution from the bottom (Figure 3.3b).

On the other hand, a filtered reference cell which is spectrally matched to the top junction will "see" 1000 W/m^2 on the short-wavelength band, while forcing the simulator to deliver up to 10% more irradiance over the bottom junction. As a result:

1. the module will still be top-limited, with the same current imbalance as before (the spectrum of the simulator itself will not really change significantly);
2. the measured short-circuit current will be close to the one measured at AM1.5g (and therefore the MMF value, calculated from the top junction, will be close to 1);
3. *but* the measured open-circuit voltage will be overestimated, due to the larger voltage contribution from the bottom junction (Figure 3.3c).

Similarly, under the same conditions as above and with a filtered reference cell spectrally matched to the bottom junction:

1. the module will still be top-limited, with the same current imbalance as before;
2. the measured short-circuit current will be approximately 10% less than at AM1.5g (and therefore the MMF value, calculated from the top junction, will be close to 1.1);
3. the measured open-circuit voltage will be underestimated, due to the smaller voltage contribution from the top junction (Figure 3.3d).

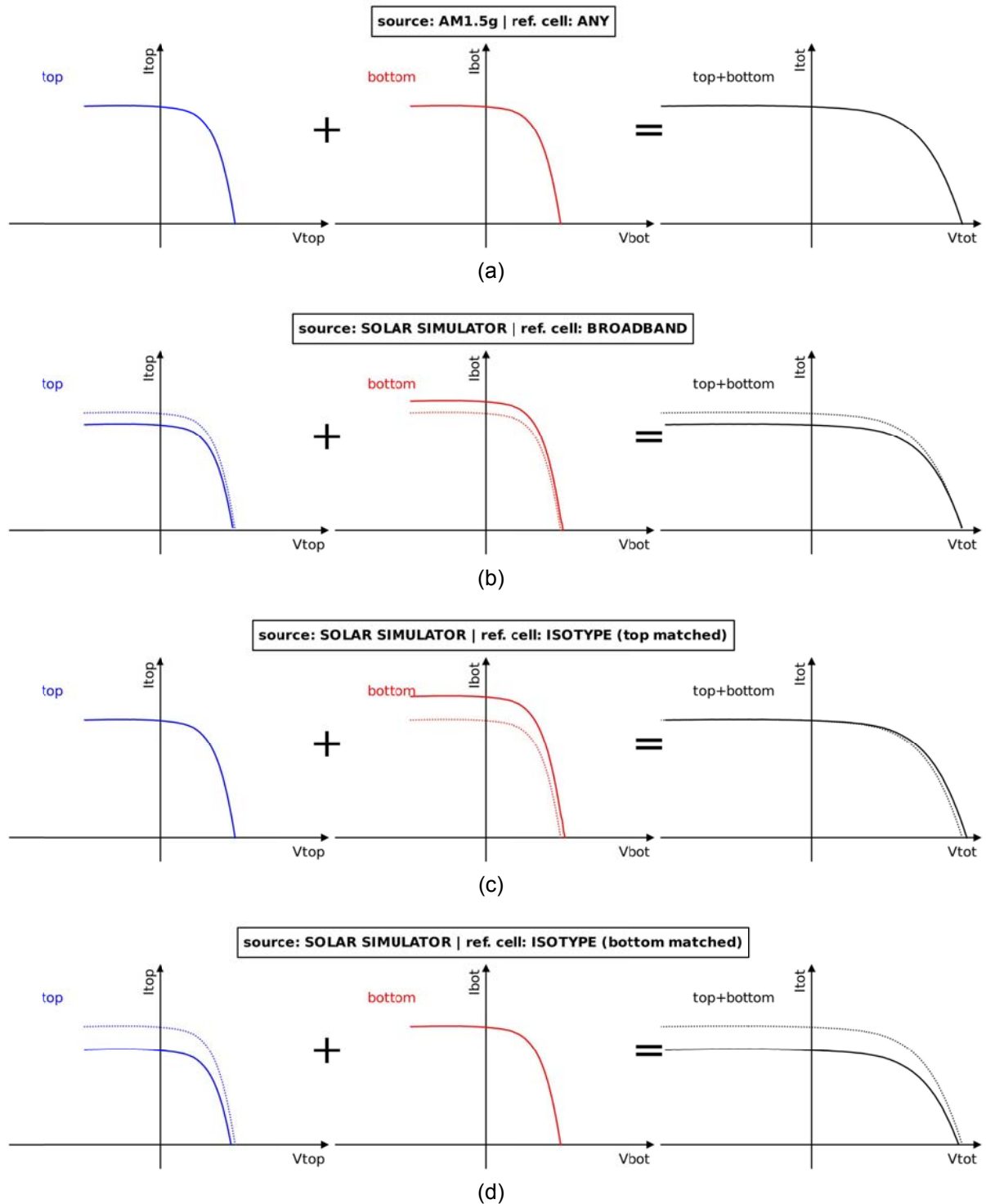


Figure 3.3: Effect of the spectral mismatch on the electrical parameters (case scenario: 2-junction PV device perfectly matched at AM1.5g): (a) reference case (AM1.5g); (b) on a red-shifted solar simulator, with a broadband reference cell (the device is top-limited: underestimated I_{sc} , correct V_{oc}); (c) same simulator, with a top-matched reference cell (top-limited: correct I_{sc} , underestimated V_{oc}); (d) same simulator, with a bottom-matched reference cell (top-limited: underestimated I_{sc} , underestimated V_{oc}).

The results from a measurement intercomparison campaign published in [PMTHIN 3] confirmed this theoretical approach: an a-Si:H/ μ c-Si module measured at SUPSI (Lab1 in the charts of Figure 3.4) on a Class A+, non-spectrally-adjustable and red-shifted solar simulator with a two-filtered and one unfiltered reference cell, was compared with the same module measured at TEL Solar (Lab2) on a spectrally-adjustable Class A+ solar simulator. The intercomparison showed that:

1. on the spectrally adjustable solar simulator, the deviations between short-circuit current and open-circuit voltage measurements with different reference cells are minimized;
2. on the red-shifted, non-spectrally adjustable simulator the short-circuit current measured with a broadband reference cell (PRC212) is underestimated by roughly 10% with respect to the measurement with a spectrally matched reference cell (ISE088), due to the spectral mismatch (Figure 3.4a);
3. on the other hand, the spectral mismatch leads V_{oc} to be overestimated with the spectrally-matched reference cell on the same spectrally non-adjustable simulator (Figure 3.4b).

Such differences may be largely above the assessed uncertainty for the electrical characterization of single-junction PV modules, both c-Si and thin-film. A reduction of the measurement uncertainty to 3-4% in P_{max} (the goal of this project) could be obtained on multi-junction devices only with an upgrade of the measurement setup so as to allow spectral tuning. Furthermore, improvements in the data acquisition system and in the measurement setup led to a decreased uncertainty budget on both single-junction c-Si and thin-film modules. This enhancement is discussed in the next two sections.

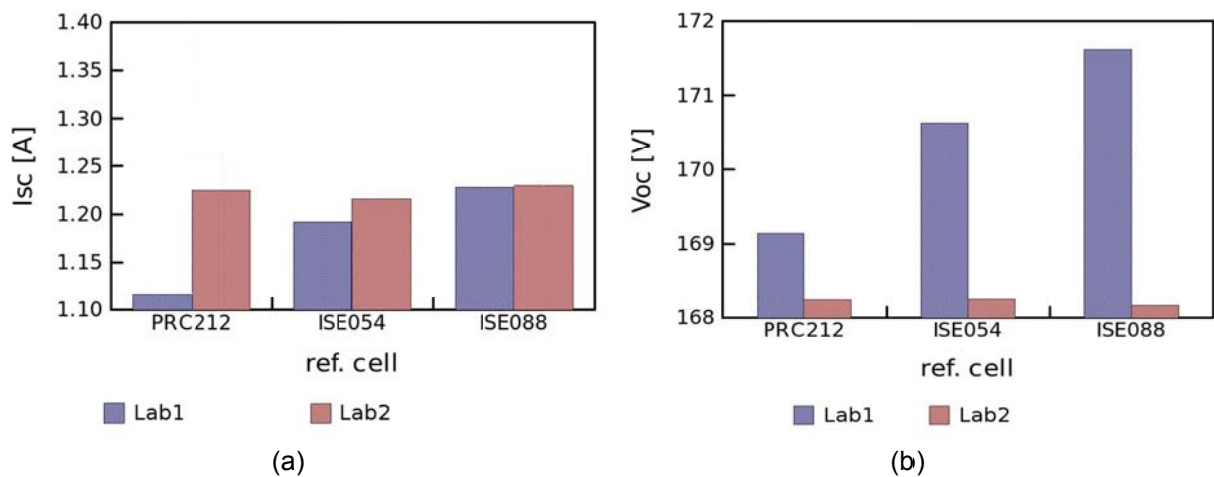


Figure 3.4: Experimental verification of the theoretical argument of Figure 3. Lab1 has a non-spectrally adjustable, red-shifted solar simulator; Lab2 has a spectrally adjustable simulator (reference cells: PRC212 broadband; ISE054 poorly matched; ISE088 best matched): (a) underestimation of the I_{sc} with the broadband reference cell in Lab1; (b) overestimation of the V_{oc} with the spectrally matched reference cell.

3.3 Current-voltage (IV) measurements

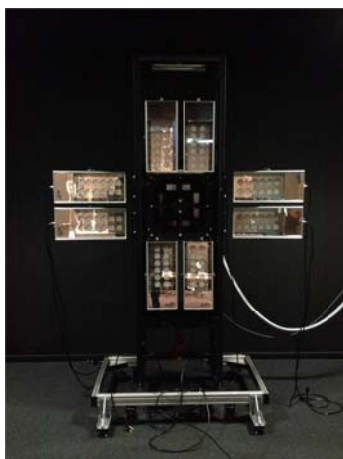
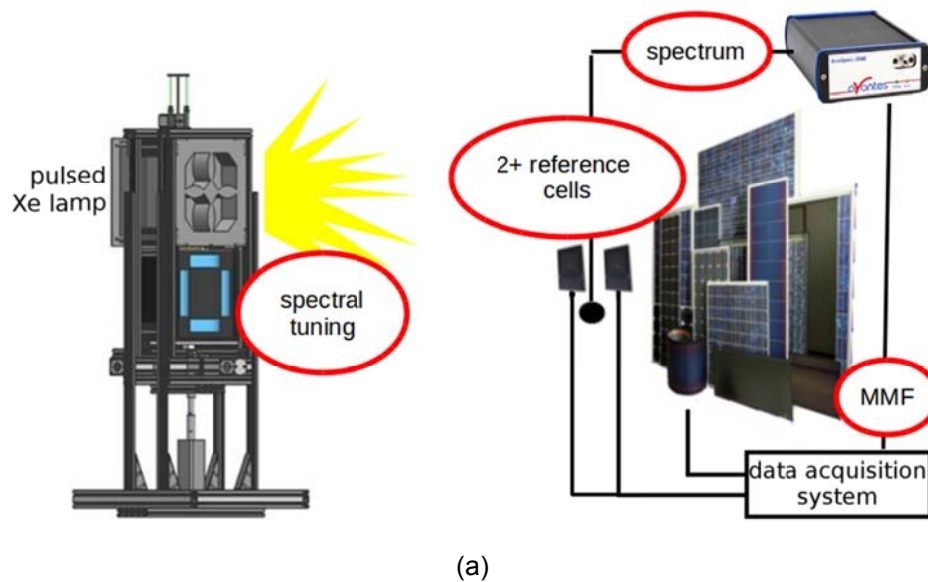
3.3.1 Test facility

The Class A+A+A+ solar simulator Pasan IIIb, available at SUPSI, was moved to a larger darkroom at the Swiss PV Module Test Centre, with improvements in the spatial uniformity. In 2012 the system was upgraded with a new electronic load HighLight[®] developed by PASAN in collaboration with SUPSI (CTI project: 9626.1 PFIW-IW). The new electronic load allowed us to significantly reduce the measurement uncertainty contribution of data acquisition. The new electronic load is also equipped with a multi-channel input for irradiance, thus allowing for up to 4 reference cells to be measured at the same time.

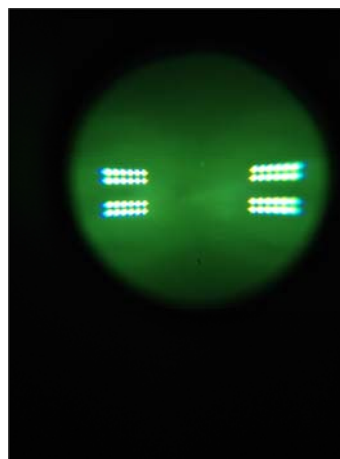
The experimental setup was further upgraded with a dedicated fast spectroradiometer (Figure 3.5a) for the real time measurement of spectral irradiance, which allowed us to better control the spectral mismatch error.

Finally, a set of commercial LED floodlights (blue 475 nm, red 640 nm and NIR 850 nm) was mounted close to the lamp, to allow spectral tuning (Figure 3.5b-d). The new configuration was capable of checking that the Class A+A+A+ requirement was still fulfilled in all possible configurations.

The new setup was presented in the visual session of the 2015 Swiss PV Tagung, where it was awarded second prize. It has also been presented as one of many possible new applications of the use of powerful LEDs in PV testing in Ref. [PMTHIN 7].



(b)



(c)



(d)

Figure 3.5: Upgrade of Pasan IIIb solar simulator: (a) the framework, with spectral irradiance equipment; (b) a picture of the new LED bias light system; (c) near infrared (850 nm) LEDs, on a IR camera; (d) blue (475 nm) LEDs, side view. Additional red (640 nm) LEDs are also available.

3.3.2 Test procedure (multi-junction modules)

A new testing procedure was developed, in line with the new standard IEC 60904-1-1 *Measurement of current-voltage characteristics of multi-junction photovoltaic (PV) devices* ([REF 3.6] (in draft at the time of writing)). This new international standard follows the experimental practice already in use in testing laboratories, especially those working on concentrating PV (see [REF 3.7]).

The procedure was submitted for ISO 17025 accreditation as follows:

- 1) Measurement of the SR and determination of the current-limiting junction on Pasan IIIb
- 2) Reference cell selection

Choose one reference cell spectrally matched to the current-limiting junction selected in point 1) and one reference cell for each of the other junctions (Figure 3.6 shows the SR of the calibrated reference cells available).

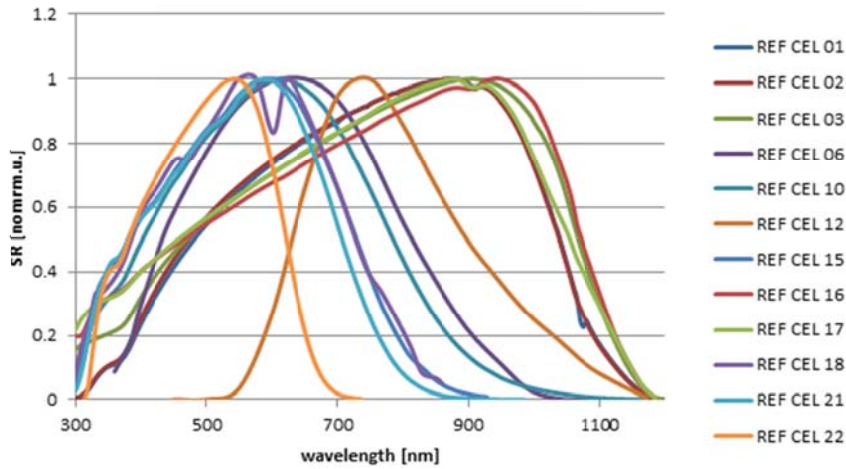


Figure 3.6: SR of the 12 reference cells available at the Swiss PV Module Test Centre.

3) Current-voltage characterization with the selected reference cells on Pasan IIIb

The electrical parameters are recorded, together with the following parameters for each i -th junction and for the corresponding i -th reference cell:

- the *spectral mismatch*: MMF_i (calculated as in section 3.3, for the i -th junction and with respect to the corresponding i -th reference cell)

- the *matching factor*: $Z_i = \frac{1000}{G_{i,meas} \cdot MMF_i}$
(where $G_{i,meas}$ is the total irradiance measured by the i -th junction)

- the *current imbalances*: $Bal_{i/j}^{test} = \frac{\int SR_i(\lambda) E_{test}(\lambda) d\lambda}{\int SR_j(\lambda) E_{test}(\lambda) d\lambda}$ (with $i \neq j$)

$Bal_{i/j}^{AM1.5g} = \frac{\int SR_i(\lambda) E_{AM1.5g} d\lambda}{\int SR_j(\lambda) E_{AM1.5g} d\lambda}$ (with $i \neq j$)

$Bal_{lim}^{test/AM1.5g} = \frac{\int SR_{lim}(\lambda) E_{test}(\lambda) d\lambda}{\int SR_{lim}(\lambda) E_{AM1.5g}(\lambda) d\lambda}$

(where: $SR_i(\lambda)$, $SR_j(\lambda)$ are SRs of the i -th and j -th junction; $SR_{lim}(\lambda)$ is the SR of the current-limiting junction; $E_{test}(\lambda)$ is the spectral irradiance of the solar simulator and $E_{AM1.5g}$ is the standard AM1.5g spectrum)

4) Spectral tuning

Repeat point 3, via adjusting the simulator's spectral irradiance with LED floodlight and measuring the new spectral irradiance $E_{test}(\lambda)$.

5) Spectrometric characterization and spectral mismatch correction

Plot the electrical parameters as a function of the corresponding $Bal_{lim}^{test/AM1.5g}$.

Select the measurement results with Z_i and $Bal_{lim}^{test/AM1.5g}$ closest to 1 (typically Z_i should be within 1.00 ± 0.03).

6) Report of the selected results

Apply spectral mismatch correction to short-circuit current and maximum power. All parameters (Z_i , MMF_i , $G_{i,meas}$, $Bal_{i/j}^{test}$, $Bal_{i/j}^{AM1.5g}$, $Bal_{lim}^{test/AM1.5g}$) and the adjusted spectral irradiance $E_{test}(\lambda)$ are reported.

3.3.3 Example: spectrometric characterization of a multi-junction a-Si:H/a-Si:H module

An example is shown here of the spectrometric characterization of a double-junction a-Si:H/a-Si:H module (cell area: 192 cm²; number of cells in parallel: 3). The procedure described in the previous section runs as follows:

1) Measurement of the SR and determination of the current-limiting junction on Pasan IIIb

Figure 3.7a shows the SR of the top and bottom junctions. The calculated photo-generated currents from the top and bottom junctions give:

$$I_{sc,top} = N \cdot A \int_{300}^{900} SR_{top}(\lambda) E_{Pasan}(\lambda) d\lambda = 3.58 \text{ A}$$

$$I_{sc,bot} = N \cdot A \int_{300}^{900} SR_{bot}(\lambda) E_{Pasan}(\lambda) d\lambda = 4.28 \text{ A}$$

and the module is therefore top-limited on Pasan IIIb.

2) Reference cell selection

The following filtered reference cells were selected (Figure 3.7b), as those minimizing the spectral mismatch factor MMF_i with respect to the i-th junction and on Pasan IIIb (with no bias light): ISE088 for the top junction ($MMF_{top} = 1.008$); ISE069 for the bottom junction ($MMF_{bot} = 0.963$).

3) Current-voltage characterization with the selected reference cells on Pasan IIIb

Current-voltage characterization gives the following results:

$$I_{sc} = 4.177 \text{ A}$$

$$V_{oc} = 40.70 \text{ V}$$

$$P_{max} = 109.7 \text{ W}$$

$$FF = 0.6452$$

Furthermore:

$$MMF_{top} = 1.008, MMF_{bot} = 0.963$$

$$Z_{top} = 0.993, Z_{bot} = 1.014$$

$$Bal_{top/bot}^{test} = 0.838$$

$$Bal_{top/bot}^{AM1.5g} = 0.898$$

$$Bal_{top}^{test/AM1.5g} = 0.993$$

4) Spectral tuning

Figure 3.7c shows a comparison between the standard AM1.5g, Pasan IIIb and adjusted PasanIIIb spectra. Spectral adjustment was performed with three different configurations: with blue LED bias on (475 nm); with red LED bias on (640 nm); with both blue and red LEDs on. Table 3.1 reports the electrical and spectral match parameters in the three different cases, compared to the unadjusted case of point 3 (NO LED), in decreasing order of red spectral content:

	I_{sc}	V_{oc}	P_{max}	FF	MMF_{top}	MMF_{bot}	Z_{top}	Z_{bot}	$Bal_{top/bot}^{test}$	$Bal_{top}^{test/AM1.5g}$
R LED	4.172	40.66	110.0	0.6485	1.008	0.953	0.992	1.012	0.819	0.992
NO LED	4.177	40.70	109.7	0.6452	1.008	0.963	0.993	1.014	0.838	0.993
B+R LED	4.199	40.62	110.0	0.6447	1.003	0.964	0.997	1.011	0.842	0.997
B LED	4.203	40.61	109.6	0.6420	1.001	0.974	0.999	1.008	0.858	0.999

Table 3.1: Spectral mismatch factors (MMF) with different spectral adjustments (red LED, no LED, blue+red LED and blue LED)

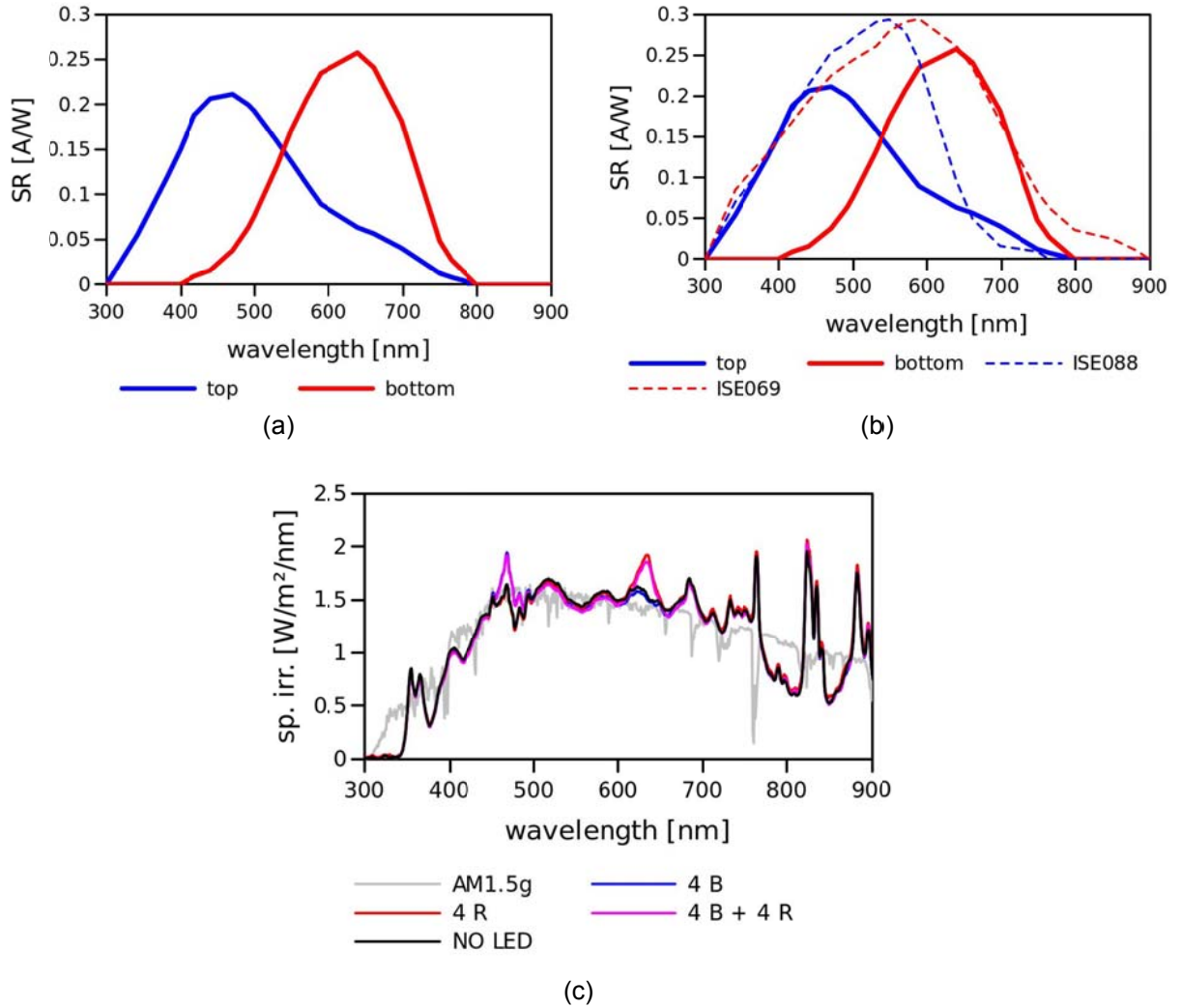


Figure 3.7: Example of spectrometric characterization of an a-Si:H/a-Si:H PV module: (a) SR of top and bottom junctions; (b) selected reference cells (ISE088, top matched, in blue dashed line; ISE069, bottom matched, in red dashed line); (c) spectral tuning with blue and red LEDs (AM1.5g reference spectrum in grey; Pasan IIIb unadjusted spectrum in black; B, R and B+R adjusted spectra in blue, red and magenta, respectively).

5) Spectrometric characterization and spectral mismatch correction

The best adjusted spectral irradiance is the one highlighted in bold in the previous table (B LED), leading to the minimum deviations from 1 of the matching factors Z_i and of $Bal_{top}^{test/AM1.5g}$, and with $Bal_{top/bot}^{test} = 0.858$ closest to $Bal_{top/bot}^{AM1.5g} = 0.898$. Figure 3.8a shows all the electrical parameters as a function of $Bal_{top}^{test/AM1.5g}$.

6) Report of the selected results

The measured short-circuit current and maximum power of the best adjusted spectral irradiance are spectrally corrected with the spectral mismatch factor $MMF_{top} = 1.001$, giving the final values:

$$\begin{aligned} I_{sc} &= 4.207 \text{ A} \\ V_{oc} &= 40.61 \text{ V} \\ P_{max} &= 109.7 \text{ W} \\ FF &= 0.6420 \end{aligned}$$

The following parameters are also reported:

$$\begin{aligned} MMF_{top} &= 1.001, MMF_{bot} = 0.974 \\ Z_{top} &= 0.999, Z_{bot} = 1.008 \\ Bal_{top/bot}^{test} &= 0.858 \\ Bal_{top/bot}^{AM1.5g} &= 0.898 \\ Bal_{top}^{test/AM1.5g} &= 0.999 \end{aligned}$$

The red dots of Figure 3.8b are the spectrally-corrected electrical parameters. The red crosses are the electrical parameters that would have been reported with the original procedure, with spectral mismatch correction and no spectral tuning. While the short-circuit current is corrected to the same value, V_{oc} is overestimated by the spectral mismatch, and as a consequence P_{max} and FF are also overestimated, giving confirmation of the theoretical approach described above.

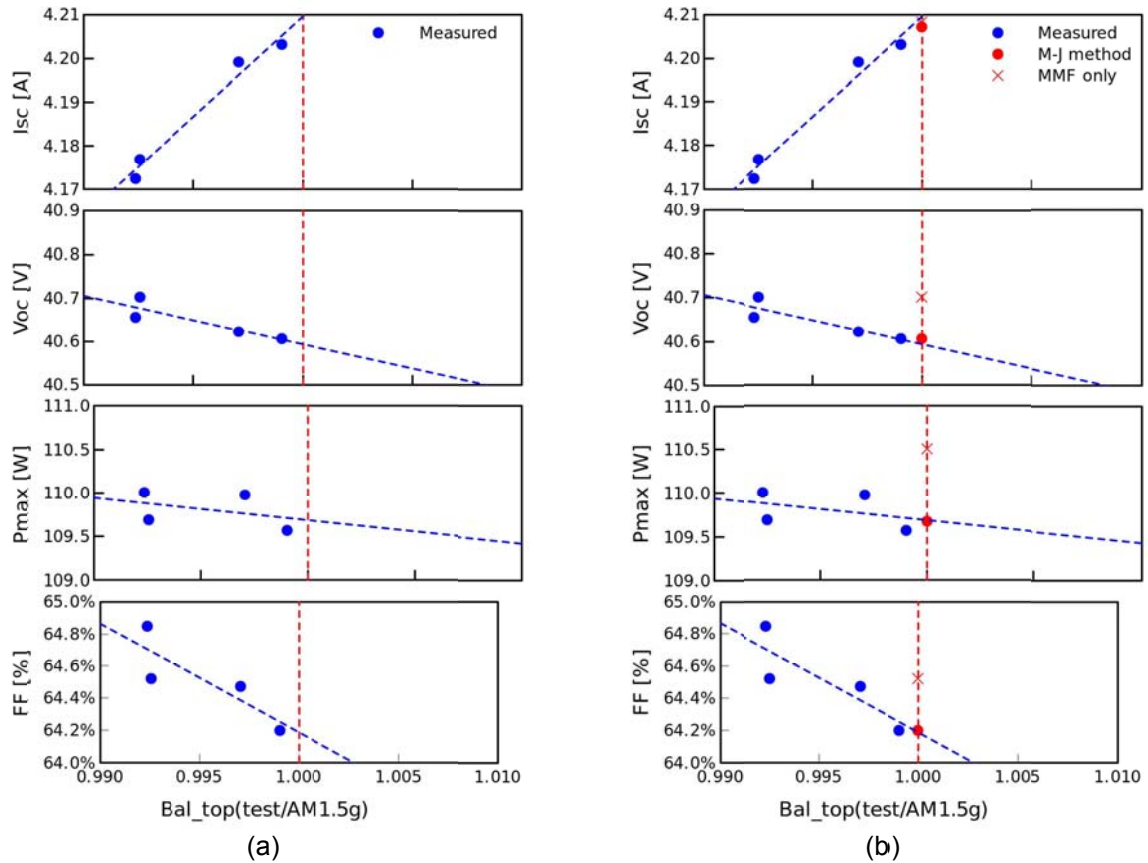


Figure 3.8: Spectrometric characterization: (a) measured electrical parameters as a function of $Bal_{top}^{test/AM1.5g}$; (b) reported results (in red dots). The red crosses show the electrical parameters obtained with the original procedure (spectral mismatch correction, without spectral tuning).

3.4 Measurement uncertainties

3.4.1 Methodology

A measurement without uncertainty does not exist: emphasis on uncertainty in measurements is among the requirements of an ISO 17025 accredited laboratory, where the uncertainty contributions in all measurements must be recognized and quantified. The official document describing how to quantify measurement uncertainty is the *ISO Guide to the Expression of Uncertainty in Measurement* (JCGM 100:2008) [REF 3.8]. The work by Müllejans et al. [REF 3.9] gives important hints on measurement uncertainty calculation for measurements of PV devices for terrestrial applications at STC.

One of the objectives of this project was to target the uncertainty of maximum power measurement of multi-junction modules at 3-4%, in line with thin film single-junction modules. Improvements in the measurement techniques and in data acquisition during the project led to the outstanding result of having nearly halved the target on all technologies. Table 3.2 table summarizes the results, as a comparison between the expanded measurement uncertainty of P_{max} at the start of the PM-Thin project and at the end of the project, as well as the three groups of technologies: c-Si, single-junction thin-film and multi-junction thin-film ("expanded" uncertainty is based on a standard uncertainty multiplied by a coverage factor $k = 2$, providing a 95% confidence in the measurement results).

	Expanded uncertainty on the measurement of P_{max}		
	c-Si	thin-film (single-j)	thin-film (multi-j)
Before PM-Thin	± 2.4%	± 3.4%	-
After PM-Thin	± 1.6%	± 1.9%	± 2.0%*

*ISO 17025 accreditation pending

Table 3.2: Expanded measurement uncertainty of P_{max} before and after the project PM-Thin for three groups of technologies (c-Si, single junction thin film technologies and multi-junction technologies).

In the current-voltage characterization of PV modules, only voltage and current are measured directly, while the maximum power is given by

$$P_{max} = I_{sc} \cdot V_{oc} \cdot FF \quad (\text{equation 3.3})$$

Thereafter, the standard uncertainty of P_{max} (u_P) depends on the standard uncertainties of I_{sc} , V_{oc} and FF (u_I , u_V and u_{FF} , respectively), as the root of the sum of their squares:

$$u_P = \sqrt{u_I^2 + u_V^2 + u_{FF}^2}. \quad (\text{equation 3.4})$$

According to the ISO 17025 requirements, uncertainty contributions are:

- *Type A:* when the contribution is based on a statistical method for treating data (for example as the average deviation of a series of observations);
- *Type B:* when the contribution is not Type A, i.e. when it is based on previous measurement data, on experience or general knowledge, on the manufacturer's specifications (datasheet), on a calibration report, on the literature or on experimental practice.

Also, the uncertainty of a measurement $x = X \pm u_X$ follows a distribution that generally can be:

- *Uniform (or Rectangular):* when any value for x within $\pm u_X$ around X is equally probable (and the probability is zero outside $X \pm u_X$);
- *Linear (or Triangular):* when the probability of a value different from X decreases linearly and is zero outside $X \pm u_X$;
- *Normal (or Gaussian):* when the probability of a value different from X decreases exponentially as a Gaussian distribution (but in principle is non-zero anywhere).

To combine several contributions, it is useful to treat all contributions as percentage uncertainties. They should also be converted into standard uncertainties (usually referred to as $u_X(1\sigma)$), depending on the distribution, as follows:

Rectangular (R) uncertainty: u_X	→	Standard uncertainty: $u_X(1\sigma) = \frac{u_X}{\sqrt{3}}$
Triangular (T) uncertainty: u_X	→	Standard uncertainty: $u_X(1\sigma) = \frac{u_X}{\sqrt{6}}$
Gaussian (G) uncertainty: u_X	→	Standard uncertainty: $u_X(1\sigma) = u_X$

In general, a divisor k (the *coverage factor*) applies to the uncertainty u_X with a given distribution to give the standard uncertainty component $u_X(1\sigma)$

$$u_X(1\sigma) = \frac{u_X}{k} \quad (\text{equation 3.5})$$

where $k = \sqrt{3}$ for rectangular distributions, $k = \sqrt{6}$ for triangular ones. Uncertainties with Gaussian distributions may be stated either as standard uncertainties ($k = 1$), by directly stating the coverage factor k , or by stating the level of confidence, i.e. the probability that x is within $X \pm u_X$:

- 68.0% confidence: $k = 1$ ("standard" uncertainty)
- 95.0% confidence: $k = 2$ ("expanded" uncertainty)
- 99.0% confidence: $k = 2.576$
- 99.7% confidence: $k = 3$

In this section the sources of uncertainties are presented, while the single contributions and the final budget are listed in the next sections, in comparison with the uncertainty contributions that were taken into consideration before PM-Thin.

The uncertainty contributions in current-voltage measurements of PV modules are grouped as follows:

1) Electrical uncertainty

This is the uncertainty in data acquisition of current and voltage and is stated in the calibration certificate of the data acquisition boards (Type B). Typically different uncertainties are given for different ranges: in general, the worst case is chosen.

2) Temperature uncertainties

Temperature uncertainties affect both current and voltages, depending on the temperature coefficients of the testing device: a typical choice is $0.06\%/^{\circ}\text{C}$ for current and $-0.33\%/^{\circ}\text{C}$ for voltage (approximately equal to the temperature coefficients of c-Si). It can be shown that variations in the choice of the coefficients give negligible variations to the calculated uncertainties.

Temperature uncertainty contributions may arise from:

Indicators

This is the uncertainty in the temperature values given by the data acquisition system and is usually stated in the manufacturer datasheet (Type B).

Probe calibration

Probes are usually calibrated, and the calibration certificate states the uncertainty of the calibration (Type B), usually as Gaussian $k = 2$ uncertainty.

Temperature setting

Electrical characterization at STC is performed close to 25°C , typically with rectangular uncertainty (e.g. at any temperature within $(25.0 \pm 0.5^{\circ}\text{C})$, meaning that no measurement is performed when the indicator shows temperatures below 24.5°C or above 25.5°C). This uncertainty is set by the experimental practice (Type B).

Temperature non-uniformity

This is how uniform temperature is over all of the testing module, and takes into account any difference in the module with respect to the temperature read by the probe. It is usually assumed based on previous measurements and on the quality of the air conditioning system of the laboratory and of the storage rooms (Type B).

3) Optical uncertainties

The optical uncertainties linearly affect current measurements and logarithmically affect voltage measurements. In order to calculate the uncertainty contribution to the voltage, a diode factor D is assumed. It can be shown that variations in the choice of D give negligible variations to the calculated uncertainty of voltage.

Spatial non-uniformity

Spatial non-uniformity of the beam is usually stated by the manufacturer of the solar simulator (Type B) and controlled periodically in order to verify the classification of the simulator. It is usually considered as a rectangular distribution, due to the variability of module size, positioning and target area.

Orientation of the testing module and the reference detector

Typically, incident irradiance is not collimated, and therefore reaches the target plane at various angles: the orientation uncertainty component takes into account the maximum possible cosine effect due to non-collimation. The maximum deviation and the uncertainty contribution can be calculated from the geometry of the simulator (Type B), and the distribution can be treated as triangular, assuming that it is less probable that the testing module and the reference cell will be placed at the widest angle of incidence rather than at the normal incidence.

Alignment

This contribution takes into account any misalignment between the testing module and the reference cell and the consequent cosine error. It can be estimated by the geometry of the rack and of the reference cell holder (Type B), and is usually a rectangular distribution.

Spectral mismatch (current)

This contribution was discussed in sections 3.3.2-3.3.3 and can be evaluated in two ways:

- *Statistically* (Type A) as the maximum possible spectral mismatch error on the widest possible range of technologies and reference cells available. This was the approach followed at SUPSI in the uncertainty calculation before this project. Figure 3.9a shows the distribution of the calculated mismatch factors *MMF* after 10,000 random variations of the spectrum of the simulator, of the SRs of 10 different c-Si testing modules and of a set of unfiltered reference cells (random variations within their stated uncertainties).
- *Quantitatively*, as the uncertainty of the calculated spectral mismatch factor *MMF*. This is also evaluated statistically (Type A), via Monte Carlo modelling: Figure 3.9b shows the distribution of the calculation of a single *MMF* on a typical module, via random variation of its SR, of the SR of the reference cell and of the testing spectral irradiance, within their stated uncertainties. This is the approach followed at SUPSI in the uncertainty calculation after this project.

The first approach of Figure 3.9a assumes that the measurement data are not spectrally corrected, and the uncertainty shown ($\pm 2.7\%$, 99% confidence) takes the mismatch error into account. The second approach of Figure 3.9b instead assumes that data are spectrally corrected with a factor that is itself affected by the uncertainty shown ($\pm 0.5\%$, 99% confidence).

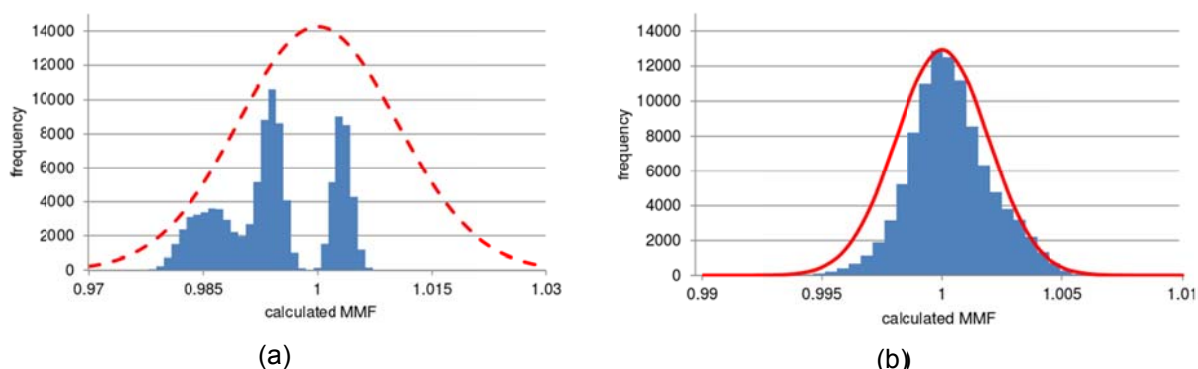


Figure 3.9: Uncertainty contribution of the spectral mismatch for c-Si modules: (a) before PM-Thin (largest possible *MMF* value among a set of commercial modules and of unfiltered reference cells); (b) after PM-Thin (largest possible *MMF* value among the calculated *MMF* values of a single commercial module, an unfiltered reference cell and the testing spectral irradiance, after random variations of these functions within their uncertainties). The approach of Figure (a) assumes that measurement data are not spectrally corrected, and the uncertainty shown ($\pm 2.7\%$, 99% confidence) takes the mismatch error into account; the approach of Figure (b) assumes that data are spectrally-corrected with a factor that is itself affected by the uncertainty shown ($\pm 0.5\%$, 99% confidence).

Spectral mismatch (voltage)

As discussed in section 3.3.3, in multi-junction PV devices the spectral mismatch also affects the voltage, due to the excess of irradiance on the saturated junction(s): this additional amount does not contribute to the current of the multi-junction modules (which is limited by the current-limiting junction), but does contribute to its voltage (due to the series connections of the junctions). This contribution is assumed based on previous measurements (Type B) and is distributed uniformly.

4) Reference cell uncertainties

These uncertainty contributions directly affect the measurement of irradiance and therefore linearly affect the correction of current to 1000 W/m^2 and logarithmically affect the measurement of voltage.

Calibration

The uncertainty in the reference cell calibration value is stated in the calibration certificate (Type B) and usually as a Gaussian distribution with 95% confidence. It may be larger for unfiltered reference cells.

Drift

Even if reference cells are quite stable, the calibration value may change with time due to ageing: a calibration drift is therefore taken into consideration, based on the history of previous calibrations (Type B, rectangular distribution).

Shunt calibration

The short-circuit current produced by the reference cell is usually measured as a voltage across a calibrated shunt, whose calibration uncertainty and drift are usually grouped in a Type B, rectangular uncertainty contribution based on the history of previous calibrations.

5) *Fill factor uncertainties*

All previous uncertainty contributions do not directly affect the fill factor. Apparently the fill factor is only affected by electrical connection and the uncertainty of *FF* for single-junction modules arises only from the repeatability.

Spectral mismatch (fill factor)

As discussed in section 3.2.3, in multi-junction PV devices the spectral mismatch also affects the fill factor. This contribution is assumed based on previous measurements (Type B) and is distributed uniformly.

6) *Repeatability*

Repeatability (*random errors*) is the variation in measurements taken by a single person, on a single instrument, while measuring a single module and under the same conditions. The measurement is said to be repeatable when this variation is smaller than an agreed limit, which is taken as the standard deviation of a series of repeated measurements and represents the uncertainty contribution of repeatability. This contribution is calculated as the standard deviation of all repeatability measurements (Type A, Gaussian distribution) and included in the uncertainty budget for both current, voltage and the fill factor.

3.4.2 Uncertainty tables (single junction thin-film)

In the summary tables in the next pages, each standard uncertainty $u_i(1\sigma)$ contribution is stated in %, but the single contribution u_i can originally be reported in other units (e.g. in the datasheet). Therefore, a conversion factor c_i applies. Furthermore, the divisor k must also be applied, depending on the distribution of the single uncertainty contribution: the i -th standard uncertainty contribution is thus given by

$$u_i(1\sigma) = \pm \frac{u_i}{k} \cdot c_i [\%] \quad (\text{equation 3.6})$$

Uncertainty contributions are grouped into: current, voltage, fill factor and maximum power. The bars indicate the percentage contribution to the total combined standard uncertainty. (For simplicity, the \pm symbol is omitted).

The tables in page 23 shows, the uncertainties of the electrical parameters of single-junction thin film are discussed and compared with the values stated at SUPSI before the project started. The coloured bullets near each contribution indicate where the uncertainty calculation has been enhanced (green: decreased uncertainty; red: increased uncertainty; yellow: no change).

Uncertainty of current measurements

Description	After PM/Thin							Before PM/Thin	
	Type	u_i	Unit	Distribution	k	c_i	$u_i(1\sigma)$	$u_i(1\sigma)$	
Electrical uncertainties									
Data acquisition (irradiance)	B	0.012	%	G	2	1	0.006	0.194	
Data acquisition (current)	B	0.046	%	G	2	1	0.023	0.194	
Temperature uncertainties									
Indicators	B	0.5	°C	G	2.576	0.085	0.016	0.016	
Probes	B	0.1	°C	G	2	0.085	0.004	0.013	
Temperature setting	B	0.5	°C	R	1.732	0.085	0.025	0.049	
Temperature non-uniformity	B	0.5	°C	R	1.732	0.060	0.017	0.017	
Optical uncertainties									
Spatial non-uniformity	B	1.0	%	R	1.732	1	0.577	0.635	
Orientation	B	5.36	deg	T	2.449	$1-\cos(x)$	0.073	0.293	
Alignment	B	3	deg	R	1.732	$1-\cos(x)$	0.046	0.046	
Spectral mismatch	A	0.8	%	G	2.576	1	0.311	1.4	
Reference cell uncertainties									
Calibration	B	0.97	%	G	2	1	0.485	0.25	
Drift	B	0.29	%	R	1.732	1	0.167	0.058	
Shunt	B	0.1	%	R	1.732	1	0.058	0.058	
Repeatability									
Repeatability	A	0.24	%	G	1	1	0.240		
Combined standard uncertainty									
							0.874	1.62	
Combined expanded uncertainty									
				G	2			1.75	3.24

Uncertainty of voltage measurements

Description	After PM/Thin							Before PM/Thin	
	Type	u_i	Unit	Distribution	k	c_i	$u_i(1\sigma)$	$u_i(1\sigma)$	
Electrical uncertainties									
Data acquisition	B	0.002	%	G	2	1	0.001	0.194	
Temperature uncertainties									
Indicators	B	0.5	°C	G	2.576	0.33	0.064	0.064	
Probes	B	0.1	°C	G	2	0.33	0.017	0.051	
Temperature setting	B	0.5	°C	R	1.732	0.33	0.095	0.191	
Temperature non-uniformity	B	0.5	°C	R	1.732	0.330	0.095	0.095	
Optical uncertainties									
Spatial non-uniformity	B	1.0	%	R	1.732	$0.053 \log(1-x)$	0.031	0.034	
Orientation	B	5.36	deg	T	2.449	$0.053 \log(2-\cos(x))$	0.004	0.016	
Alignment	B	3	deg	R	1.732	$0.053 \log(2-\cos(x))$	0.002	0.002	
Spectral mismatch	A	0.8	%	G	2.576	$0.053 \log(1-x)$	0.016	0.074	
Reference cell uncertainties									
Calibration	B	0.97	%	G	2	$0.053 \log(1-x)$	0.026	0.013	
Drift	B	0.29	%	R	1.732	$0.053 \log(1-x)$	0.009	0.003	
Shunt	B	0.1	%	R	1.732	$0.053 \log(1-x)$	0.003	0.003	
Repeatability									
Repeatability	A	0.08	%	G	1	1	0.081		
Combined standard uncertainty									
							0.176	0.31	
Combined expanded uncertainty									
				G	2			0.35	0.62

Uncertainty of the fill factor

Description	After PM/Thin							Before PM/Thin	
	Type	u_i	Unit	Distribution	k	c_i	$u_i(1\sigma)$	$u_i(1\sigma)$	
Fill factor uncertainties									
Repeatability	A	0.06	%	G	1	1	0.061	0.49	
Combined standard uncertainty									
							0.061	0.49	
Combined expanded uncertainty									
				G	2			0.12	0.98

Uncertainty of maximum power measurements

Description	After PM/Thin							Before PM/Thin	
	Type	u_i	Unit	Distribution	k	c_i	$u_i(1\sigma)$	$u_i(1\sigma)$	
Uncertainty on current									
Combined standard uncertainty	A	0.874	%	G	1	1	0.874	1.62	
Uncertainty on voltage									
Combined standard uncertainty	A	0.176	%	G	1	1	0.176	0.31	
Uncertainty on fill factor									
Combined standard uncertainty	A	0.1	%	G	1	1	0.061	0.49	
Repeatability									
Repeatability	A	0.26	%	G	1	1	0.260		
Combined standard uncertainty									
							0.931	1.72	
Combined expanded uncertainty									
				G	2			1.9	3.4

Table 3.3: Uncertainty calculation tables for thin film single junction technologies and single contributions (current, voltage, fill factor and power)

3.4.3 Uncertainty tables (multi-junction thin-film)

In this section, the uncertainties of the electrical parameters of multi-junction thin-film are discussed. The additional uncertainty contribution due to spectral mismatch affects only voltage and fill factor.

Uncertainty of voltage measurements

	After PVThin							Before PV Thin	
Description	Type	u_i	Unit	Distribution	k	c_i	$u_i(1\sigma)$	$u_i(1\sigma)$	
Electrical uncertainties									
Data acquisition	B	0.002	%	G	2	1	0.001	0.194	●
Temperature uncertainties									
Indicators	B	0.5	°C	G	2.576	0.33	0.064	0.064	●
Probes	B	0.1	°C	G	2	0.33	0.017	0.051	●
Temperature setting	B	0.5	°C	R	1.732	0.33	0.095	0.191	●
Temperature non-uniformity	B	0.5	°C	R	1.732	0.330	0.095	0.095	●
Optical uncertainties									
Spatial non-uniformity	B	1.0	%	R	1.732	$0.053 \log(1-x)$	0.031	0.034	●
Orientation	B	5.36	deg	T	2.449	$0.053 \log(2-\cos(x))$	0.004	0.016	●
Alignment	B	3	deg	R	1.732	$0.053 \log(2-\cos(x))$	0.002	0.002	●
Spectral mismatch (current)	A	0.8	%	G	2.576	$0.053 \log(1-x)$	0.016	0.074	●
Spectral mismatch (voltage)	B	0.1	%	R	1.732	1	0.058		●
Reference cell uncertainties									
Calibration	B	0.97	%	G	2	$0.053 \log(1-x)$	0.026	0.013	●
Drift	B	0.29	%	R	1.732	$0.053 \log(1-x)$	0.009	0.003	●
Shunt	B	0.1	%	R	1.732	$0.053 \log(1-x)$	0.003	0.003	●
Repeatability									
Repeatability	A	0.08	%	G	1	1	0.081		●
Combined standard uncertainty				G	1		0.186	0.31	●
Combined expanded uncertainty				G	2		0.37	0.62	

Uncertainty of the fill factor

	After PVThin							Before PV Thin	
Description	Type	u_i	Unit	Distribution	k	c_i	$u_i(1\sigma)$	$u_i(1\sigma)$	
Fill factor uncertainties									
Repeatability	A	0.06	%	G	1	1	0.061	0.49	●
Spectral mismatch	B	0.50	%	R	1.732	1	0.289		●
Combined standard uncertainty				convolved	1		0.295	0.49	●
Combined expanded uncertainty				G	1.67		0.49	0.98	

Uncertainty of maximum power measurements

	After PVThin							Before PV Thin	
Description	Type	u_i	Unit	Distribution	k	c_i	$u_i(1\sigma)$	$u_i(1\sigma)$	
Uncertainty on current									
Combined standard uncertainty	A	0.874	%	G	1	1	0.874	1.62	●
Uncertainty on voltage									
Combined standard uncertainty	A	0.186	%	G	1	1	0.186	0.31	●
Uncertainty on fill factor									
Combined standard uncertainty	A	0.49	%	G	1.67	1	0.293	0.49	●
Repeatability									
Repeatability	A	0.26	%	G	1	1	0.260		●
Combined standard uncertainty				G	1		0.976	1.72	●
Combined expanded uncertainty				G	2		2.0	3.4	

Table 3.4: Uncertainty calculation tables for multi-junction technologies and single contributions (voltage, fill factor and power)

The additional contribution arising from the spectral mismatch on multi-junction devices is a dominant non-Gaussian type B uncertainty. When a rectangular distribution and a Gaussian distribution are convolved, the coverage factor for a coverage probability of 95% is not $k = 2$, but depends on the ratio between the Gaussian and the rectangular uncertainty: in our case, this ratio is $\frac{u_i(G)}{u_i(R)} = \frac{0.06}{0.50} = 0.12$, giving $k = 1.67$ (see [REF 3.10]).

4. PRE-CONDITIONING OF THIN FILM MODULES

Background

It is well known that polycrystalline thin film PV modules such as CIS and CdTe can be influenced by internal meta-stabilities, which may in some cases strongly influence their performance, even after very short exposure times to light (seconds, hours) [REF 4.1]. If the devices are stored in the dark, their performance may decrease considerably, though the time scale of the phenomenon varies considerably for different devices. Furthermore, the metastable behaviour of these materials can vary strongly from device to device, even when they come from the same manufacturer.

Scope of the project:

- Improvement of preconditioning facility and data processing
- Investigation of dark storage and light soaking effects for different thin film technologies
- Sufficient stabilization procedure for polycrystalline thin film modules such as CdTe and CIS/CIGS

Results:

- During the project the light soaking facility was improved in terms of light and temperature uniformity, extension of measurement setup (MPPT) and upgrade of software with graphic interface.
- Based on the outcomes of this work, a draft preconditioning procedure was defined for polycrystalline thin film modules, combining indoor light soaking with dark current soaking.
- Indoor preconditioning proved to be the preferred treatment for polycrystalline thin film modules due the higher reproducibility of the testing conditions and the shorter treatment time.
- Outdoor and indoor preconditioning approaches proved to be comparable within a limited uncertainty of $\pm 2\%$.
- A stabilization criterion of $\pm 1\%$ for indoor preconditioning with a class CCB sun simulator was defined in order to be certain that modules with slow changes are also actually stabilized.
- CIS and CdTe modules exhibited different responses, showing transient effects that can be reduced with a short current soaking treatment.
- It is suggested that the time period between the removal of the module from artificial light or sunlight and the performance measurement (including cool-down time) should be kept to a minimum, possibly not exceeding 20 minutes.
- In dark current soaking (CS) sensitive modules, long term CS in the range of hours (e.g. 3 hours) generally leads to a higher power compared to the first measurement after transfer into the laboratory. The losses due to dark storage are fully recovered.

4.1 Meta-stability of polycrystalline thin film modules

Existing international standards (e.g. IEC 61646 [REF 4.2]) address the issue of the long-term stabilization of these devices, but not that of short-term variations which are necessary for drafting a proper pre-conditioning procedure required for a correct power rating. Therefore, manufactures of polycrystalline thin film modules generally provide their own recommendation for light soaking and stabilization procedures for their products [REF 4.3].

There is a general assumption that CdTe and CIS (including alloys) PV devices are not affected by capacitive or sweep-time effects [REF 4.4]. Nevertheless, they may be affected by other types of transient effects which are referred to by some authors as being in a "pre-measurement state" and which may also lead to an incorrect power estimation. This refers to the state in which the device is kept for a very short time [ms, s, min] just before the measurement, i.e. exposure to light or to a forward bias if the module is not in a stable state [REF 4.5].

Figure 4.1 provides an example of I-V measurements for a CIS module before and after 10 days of dark storage, as shown by the green and light green curves respectively. The change in P_m and FF is clearly visible. The blue line represents the test with a short current soaking treatment (I_{CS}) of only 5 seconds before the I-V measurement. As a result of the current treatment, the modules' power and FF increase, here +6% in P_m and +5.3% in FF. Other modules show different behaviours. Some CIS and CdTe show a power increase of between 1 and 6%, while other CIS modules do not show any response to the short I_{CS} treatment. However, for these devices forward biasing (current soaking) in the dark has long been known to be a valid alternative to more traditional light soaking preconditioning approaches, potentially reducing the size of testing facilities and electricity costs, improving control of the module temperature during the preconditioning and operating much faster.

The following paragraph describes the problems of meta-stabilities of dark storage and an approach to overcoming those effects with current-soaking.

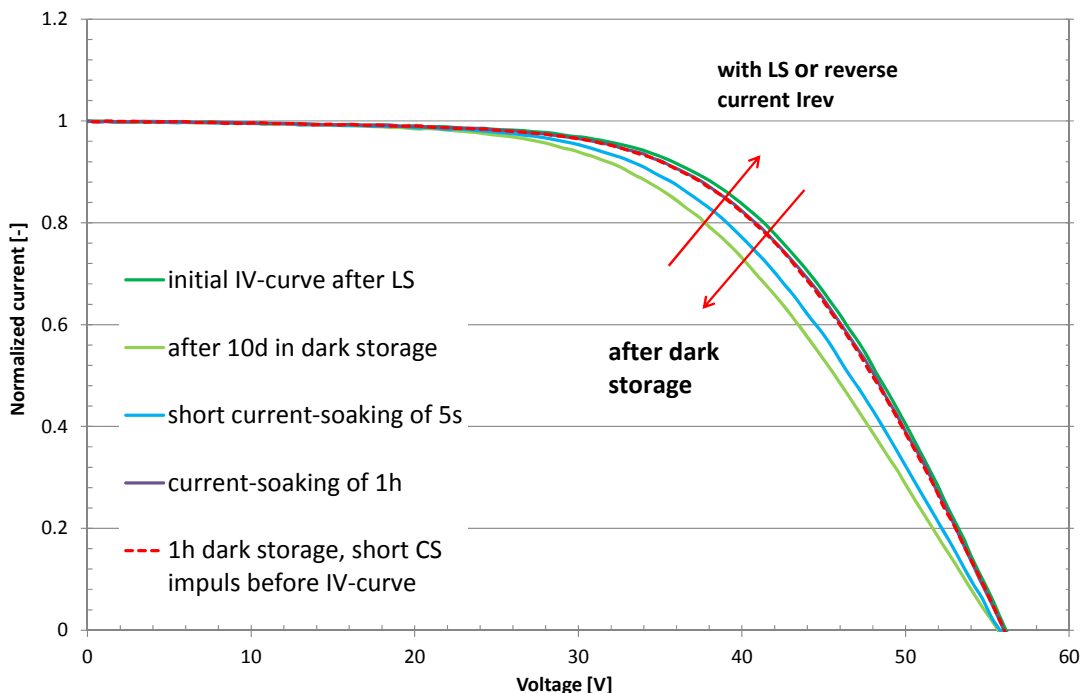


Figure 4.1: I-V curves of a CIS module: initial measurement after outdoor exposure (LS) of 3 years (green); measurement after dark storage of 10 days (light green); measurement after dark storage of 10 days with a short current soaking treatment of 5 seconds before I-V measurement (blue); measurement after 1 hour of current soaking (purple) and measurement after 1 hour of dark storage with a short current soaking treatment of 5 seconds before I-V measurement (dotted red).

4.2 Preconditioning of thin film PV modules with light

4.2.1 Light soaking facility

Since 2010, the Swiss PV Module Test Centre has used a Mitronic CCB (IEC classification for uniformity, spectral match, temporal stability) steady-state sun simulator for preconditioning and light soaking applications such as LID (light-introduced degradation) for c-Si modules. The simulator is equipped with 12 metal halide lamps in a fixed-frame structure, and the entire testing plane is 3.0 x 2.2 metres. The irradiance level can be regulated to between 600 and 1200 W/m². Preconditioning can be done in open-circuit voltage (V_{oc}) or in maximum power point (P_{mpp}). The parameters of the modules, such as short-circuit current (I_{sc}), V_{oc} , temperature and a full I-V curve, are recorded with the MPP-Tracker developed at SUPSI in combination with dedicated software. Data can be recorded with a minimum resolution of one minute.

During the project the light soaking setup and the software were continuously improved. The following enumeration summarizes the improvements achieved:

- The **uniformity** was improved by painting the simulator's structure black so as to avoid reflections. Reflections occurred mainly in the corners of the testing plane due to the simulator's structure itself. Figure 4.2 (a) shows the structure of the simulator and (b) the light-uniformity measurement results on the testing plane. The uniformity is 9.4% on a testing plane of 225 x 240 cm, which matches the IEC requirements of a class C simulator.
- To meet the IEC requirements for **temperature uniformity and stabilization** of modules, six large fans were installed between the lamps to create a continuous airflow around the device under testing. In this way, the temperatures of the modules could be controlled within a range of $50 \pm 5^\circ\text{C}$.
- The measurement setup was extended with two additional **MPP-Trackers** with different voltage- and current-measurement ranges suitable for thin film PV technologies. Furthermore, two temperature sensors for each DUT were used to control the uniformity of the temperature of the modules.
- The dedicated **software** was upgraded in terms of: management of the MPPT measurements, data acquisition and analysis, graphic interface with visualization of the measurement data and the implementation of different tools, which allowed tests according to the relevant IEC testing procedures such as IEC 61646 (i.e. MQT 19 - stabilization of thin film modules).

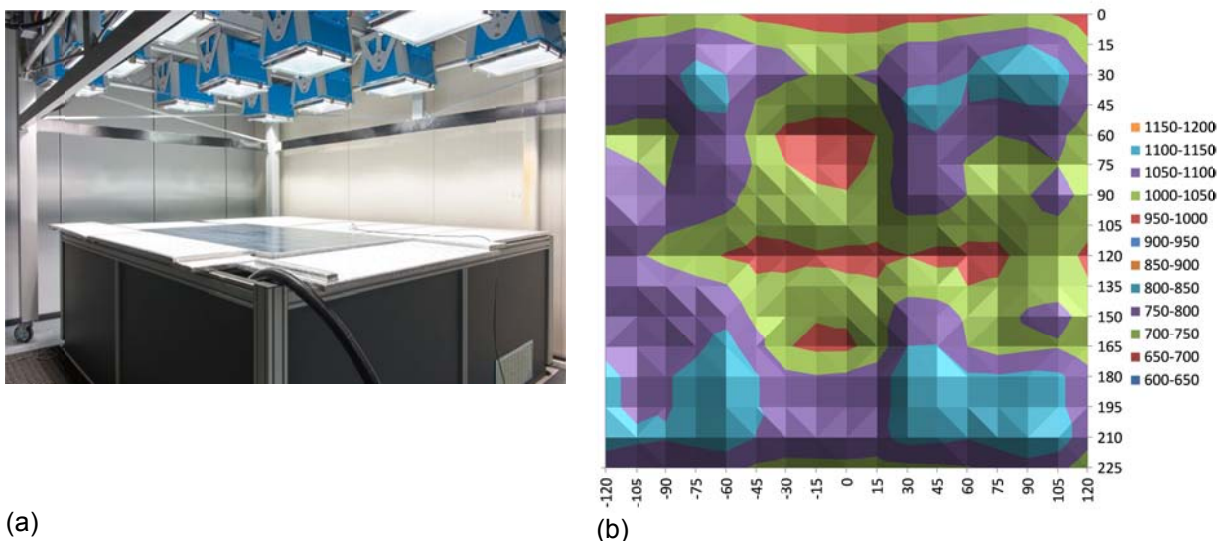


Figure 4.2: Improved light soaking setup: (a) results of uniformity measurement on the test plane (b) The uniformity is 9.4% on 225 x 240 cm, matching the IEC requirements for a class C simulator.

4.2.2 Comparison of indoor and outdoor preconditioning

Figure 4.3 shows the stabilization curves of three different TF technologies (three CIS modules, one CdTe and one a-Si single junction). The modules were new, purchased in 2014, and belong to the latest manufactured generations. The modules were all exposed to simulated sunlight to an irradiance of 1000 W/m^2 (class CCB simulator) and a temperature of $50 \pm 5^\circ\text{C}$. The modules' power was measured every minute by means of a MPP-Tracker and corrected to a temperature of 50°C . The power of the modules was considered as stable if the difference between the three consecutive measurements of P_m , separated by 20 kWh/m^2 of irradiation, was less than $\pm 1\%$.

Different technologies exhibit highly different stabilization times even if the modules are of the same family (e.g. CIS). The a-Si module decreases quickly in the first hours of light exposure and then stabilizes slowly after 275 hours, while the CdTe 2 module decreases in the first 20 hours and then continuously increases. The module reaches stabilization after 250 hours. The three CIS modules show different behaviours. CIS 6 and CIS 4 require at least 25 hours before the power remains stable within the chosen criteria of $\pm 1\%$. Instead, module CIS 5 seems stable from the beginning, but it increases slightly by less than 1% over the preconditioning time. However, the power measurements at STC which were performed before and after light exposure showed a decrease of -4.2% , which could indicate that the modules' power was changing very rapidly within the first seconds or minutes of light exposure.

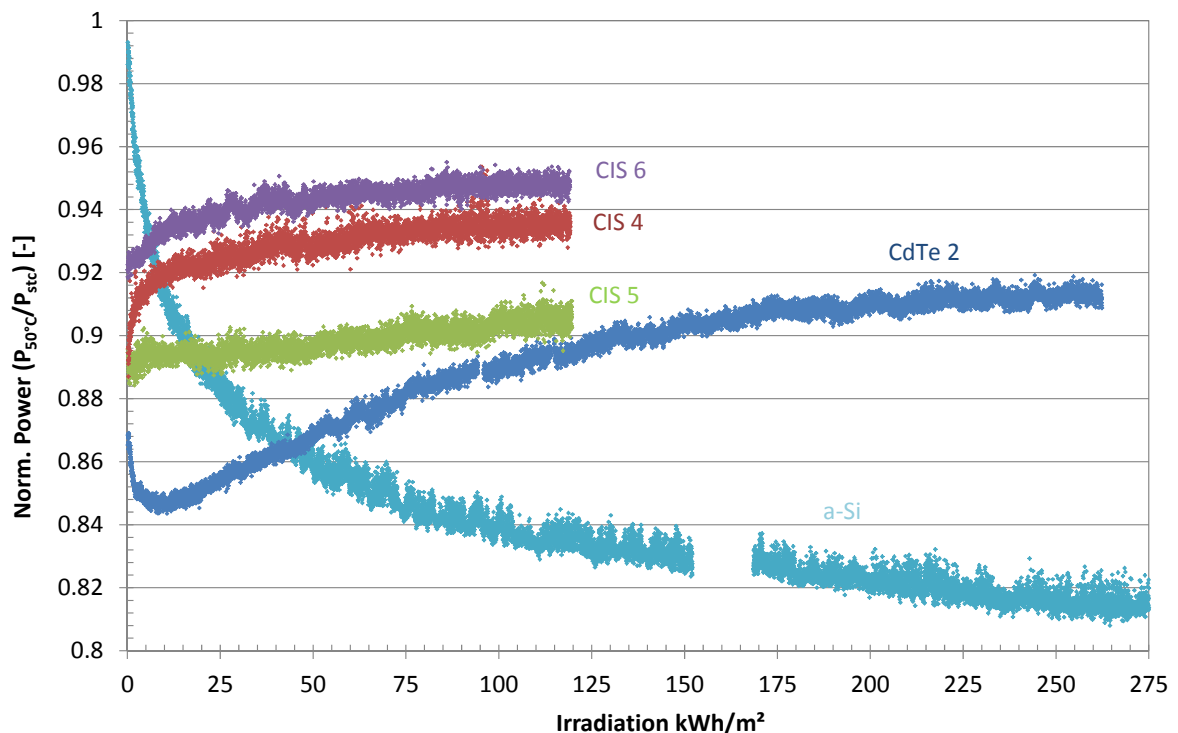


Figure 4.3: Example of stabilization curves of three different TF technologies (three CIS modules, one CdTe and one a-Si single junction). The modules' power is measured every minute during the indoor preconditioning campaign. P_{max} values are corrected to 50°C ($P_{50^\circ\text{C}}$) and normalized to the power at STC measured with a class AAA simulator after preconditioning.

Figure 4.4 shows the results of an outdoor and indoor preconditioning campaign on modules CdTe 2 and CIS 4. Both modules were new and had not been exposed to light before. The initial power of the modules (P_0) had been previously measured. The modules were first exposed to natural sunlight in open-circuit conditions with an irradiation of approximately 30 kWh/m^2 . The modules were then measured again indoors at STC, followed by a dark storage period of at least four weeks. Afterwards, an indoor preconditioning campaign was performed under simulated sunlight.

The power of the CIS module increased by 11.5% after a light exposure of 28 kWh/m². In this period (late summer) the meteorological conditions ranged from clear to cloudy days. The module's temperature was at maximum 40°C. During the dark storage period of four days the power decreased by about -5%. The following indoor preconditioning campaign of 45 kWh/m² again showed an increase in power of 7.2%, with respect to the initial value. The difference between the outdoor and indoor preconditions was 1.9%.

After 30 kWh/m² outdoor exposure (late summer), the investigated CdTe module showed a decrease in power of -1.1%. During this period the meteorological conditions were mostly cloudy days and the module's temperature was at maximum 40°C. The outdoor exposure was therefore extended to 120 kWh/m². The power then increased to 5.7% with respect to the initial value P₀. During the dark storage period the power decreased by 3.2%. However, in the following indoor preconditioning campaign under simulated sunlight, a similar behaviour of power changes could be observed. First the power decreased after approximately 45 kWh/m² and then increased with increasing light exposure time - also see Figure 4.3 (dark blue curve). The difference between outdoor and indoor preconditioning is -0.7%. Due to the fact that the power of the CdTe module decreased for both short outdoor and indoor light exposure (<45 kWh/m²), it is assumed that this behaviour is related to the technology of the module and not to the meteorological conditions such as day types or ambient temperature. In order to have a sufficient preconditioning and to be certain that the CdTe module is stabilized, an indoor preconditioning campaign is recommended.

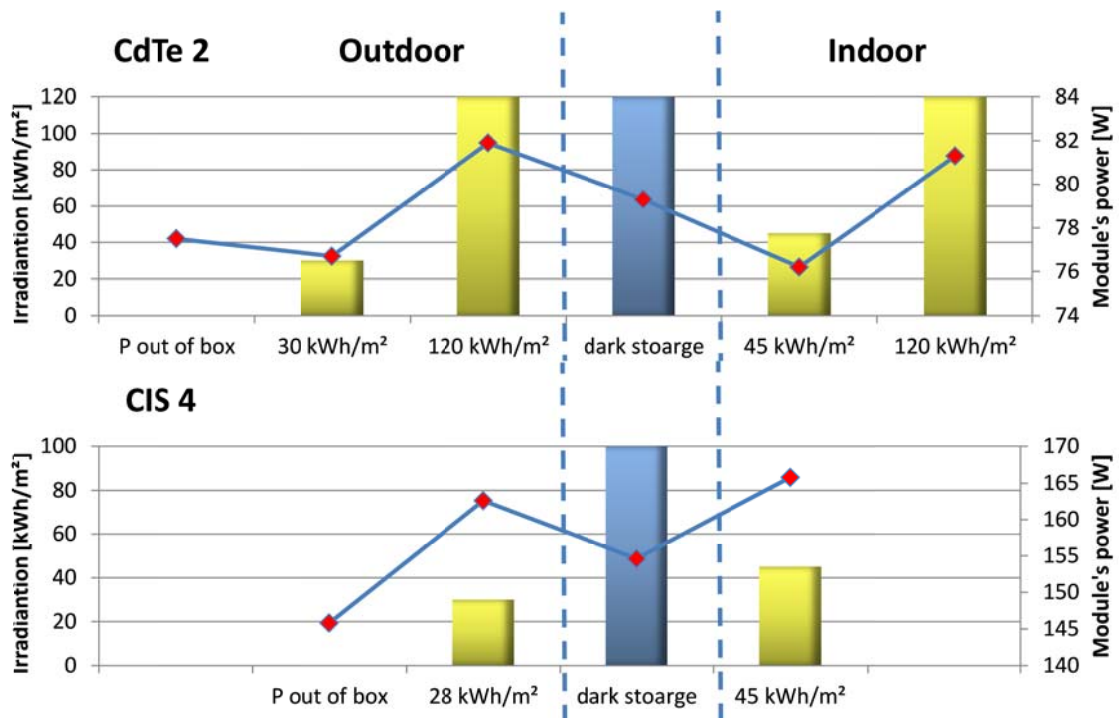


Figure 4.4: Outdoor and indoor preconditioning of a CdTe and a CIS module. The red squares are the measurement with a class AAA simulator; P_{out of box} is the measured power before the outdoor and indoor preconditioning campaign; the yellow bars are the light dose of the outdoor and indoor preconditioning, and the blue bars represent the dark storage period of at least four weeks.

4.2.3 Dark storage effects after long term outdoor exposure

In order to investigate meta-stabilities occurring after dark storage, commercial CIS, CIGS and CdTe modules from different manufactures were taken from the ongoing outdoor measurement campaign (test cycle 12), discussed in Chapter 5, in which the modules were exposed outdoors for more than 4 years.

The outdoor-exposed modules (3 CIS/CIGS, 2 CdTe) were disconnected and transported to the laboratory. After temperature stabilization to 25°C, continuous I-V measurements with increasing steps from 1 to 5 to 10 minutes were performed during the first hour of dark storage. The time between

removing the modules from the light and their first indoor I-V measurement was kept to under 15 minutes. Following the initial measurement, the modules were then stored in darkness at 25°C and I-V measurements were performed every 24 hours until their power became stable within $\pm 0.5\%$ over three days. All indoor measurements were performed with a pulsed sun simulator (class A+A+A+) with a flash duration of 10 ms.

Figure 4.5 (a) shows the change in power and (b) in fill factor for all five tested modules. Both technologies CIS and CdTe show only slight changes in P_m in the first five minutes of the initial measurement. After 1 hour the difference is about -1.7% for CIS 3 and CIS 1 and -0.5% for the CdTe modules. Module CIS 3 and CIS 1 show the strongest degradation with up to -7.5% after 24 hours of dark storage. Stabilization of module CIS 3 was reached after 9 days of dark storage, while this took CIS 1 only 6 days. The difference from the initial I-V measurement for both is -11%. Module CIS 2 and the two CdTe modules instead show a lower degradation of -1% in the first 24 hours. The stabilization of P_m in darkness is reached after 10 days. The difference from the initial measurement is about -2.2%.

It was also observed that the short circuit current (I_{sc}) was stable during dark storage for all tested modules. However, the open-circuit voltage (V_{oc}) decreased over time, and with it the fill factor (FF).

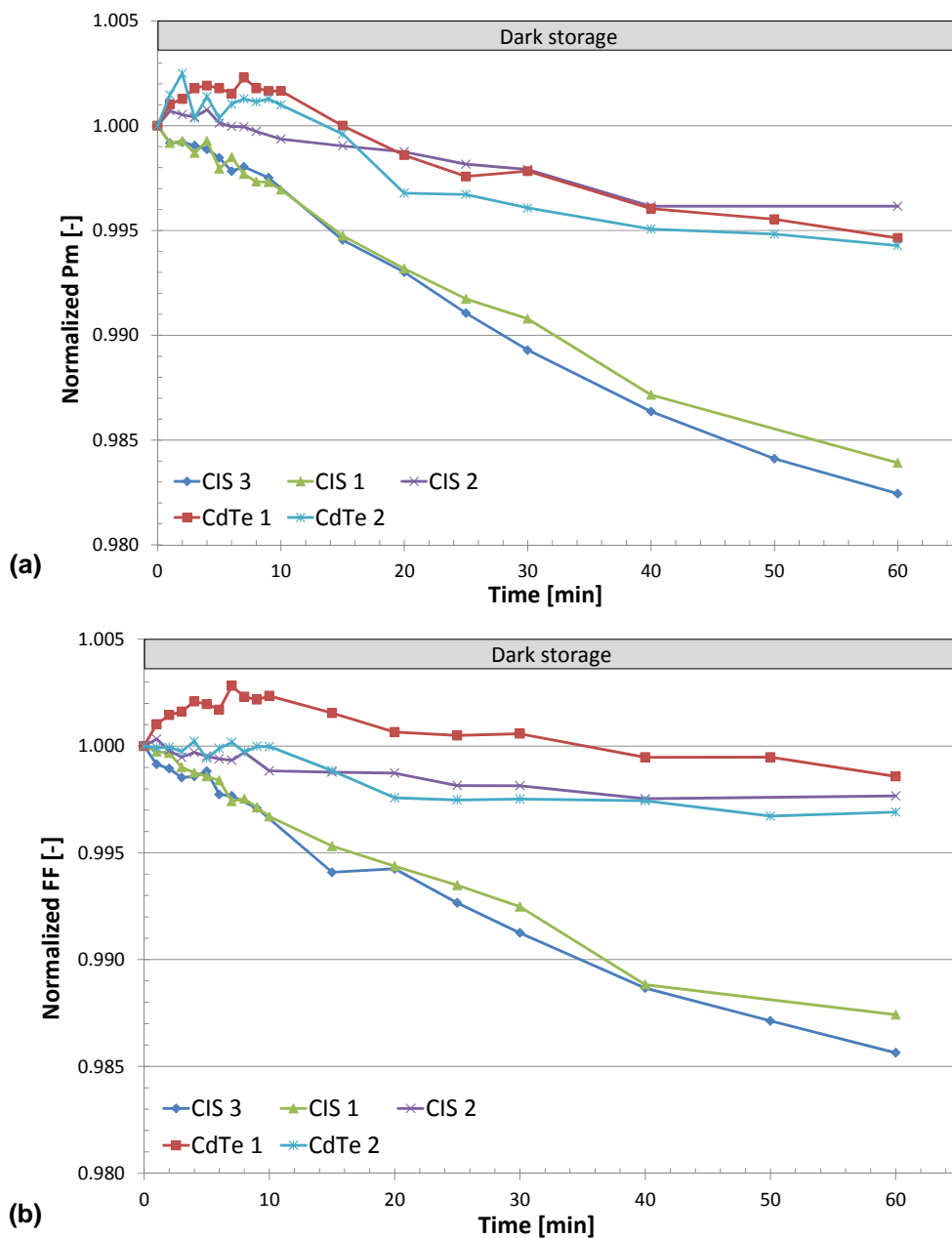


Figure 4.5: Changes in module power (a) and fill factor (b) in the first hour of dark storage. Values are normalized to the initial indoor measurement after temperature stabilization.

4.3 Dark current soaking (CS)

For polycrystalline thin film modules, current-soaking in the dark has long been known to be a valid alternative to more traditional light-soaking preconditioning approaches, potentially reducing the size of testing facilities and electricity costs, improving the control of the module temperature during preconditioning and being much faster [REF 4.6]. However, CdTe and CIS modules may be affected by so-called transient effects which contribute to incorrect power estimations.

To investigate the effect of current-soaking and transient effects, it is necessary to keep the time between the current treatment and the actual I-V measurement as short as possible. Therefore, a dedicated setup was built. A constant current source was used to provide the bias current. The current flow could be stabilized to an exact value of interest. The modules were connected via an electromagnetic relay to the constant current source and the electronic load of the solar simulator. Due to this set-up, the time between switching the module from the current source to the I-V measurement was less than 2 seconds.

Indoor measurements were performed with a pulsed sun simulator (class A+A+A+) with a flash duration of 10 ms. I-V curves were measured in forward sweep from short circuit current (I_{sc}) to open circuit voltage (V_{oc}).

The following paragraphs describe the transient effects due to the use of a short-pulsed sun simulator (10 ms) and current soaking as a preconditioning method on CdTe and CIS modules.

4.3.1 Transient effects

Pulsed sun simulators with a short pulse duration, e.g. 10 ms, are often used in production lines as well as in testing laboratories. For standard crystalline silicon modules, the measurement results agree well with measurements under steady state conditions such as natural sunlight. Besides the well-known discrepancies between outdoor measurements and measurements with a pulsed sun simulator, such as the spectral match to the standard spectrum AM1.5 and capacitive effects due to sweep duration, the CdTe and CIS modules are mainly affected by transient effects, such as light soaking. These effects can occur on a very short time scale of milliseconds. By using pulse durations which are too short, the modules' power, and in some cases their open circuit voltage, is underestimated. The size of the error depends on the measurement setup and the module type. Underestimations of up to 5% in power have been reported [REF 4.1]. Therefore, manufacturers of CIS modules in general recommend the use of long-pulse simulators.

CdTe and CIS modules from different manufacturers were tested to observe if such effects occur by using a pulse simulator with a flash duration of 10 ms and whether this could be minimized through the use of a short current soaking treatment. All modules were measured in forward or direct sweep (I_{sc} to V_{oc}) and in backward or reverse sweep (V_{oc} to I_{sc}) after a dark storage period of at least four days. The modules were then connected to the power supply and to a current (abbreviated as I_{CS}) corresponding to I_{sc} of the module flow for 5 seconds before each the I-V measurement. In a second test the modules' current at a stable voltage during the 10 ms flash was measured before and after the I_{CS} treatment.

Figure 4.6 (a) and (b) shows the direct and reverse I-V measurement of a CIGS (CIS5) module without and with I_{CS} treatment of 5 seconds before the I-V measurements, respectively. The difference, or hysteresis, between direct and reverse sweep is 1.2%. As a result of the I_{CS} treatment, Figure 4.6 (b), the hysteresis is clearly reduced to 0.47% and the module's power, FF and V_{oc} increase, here +3.2% in P_m , +1.1% in FF and +1.2% in V_{oc} . I_{sc} is not affected due to the I_{CS} treatment. As discussed in the reference [REF 4.4], the measurements are not influenced by a capacitive effect. Figure 4.6 (c) shows the change in current over the flash duration of 10 ms. The measurement with the I_{CS} treatment (green) shows a much faster stabilization during the flash. If the (I_{CS}) treatment is increased to two minutes, no changes can be observed compared with the 5-second I_{CS} treatment. On this module, this effect is reversible. If the module is stored in darkness for at least 2 minutes, the same differences as in Figure 4.6 can be observed.

However, the other tested modules show different behaviours under the short lcs treatment. We observed increases in power of between 1 and 6%, while one CIS (CIS 2) module does not show any response to the lcs treatment.

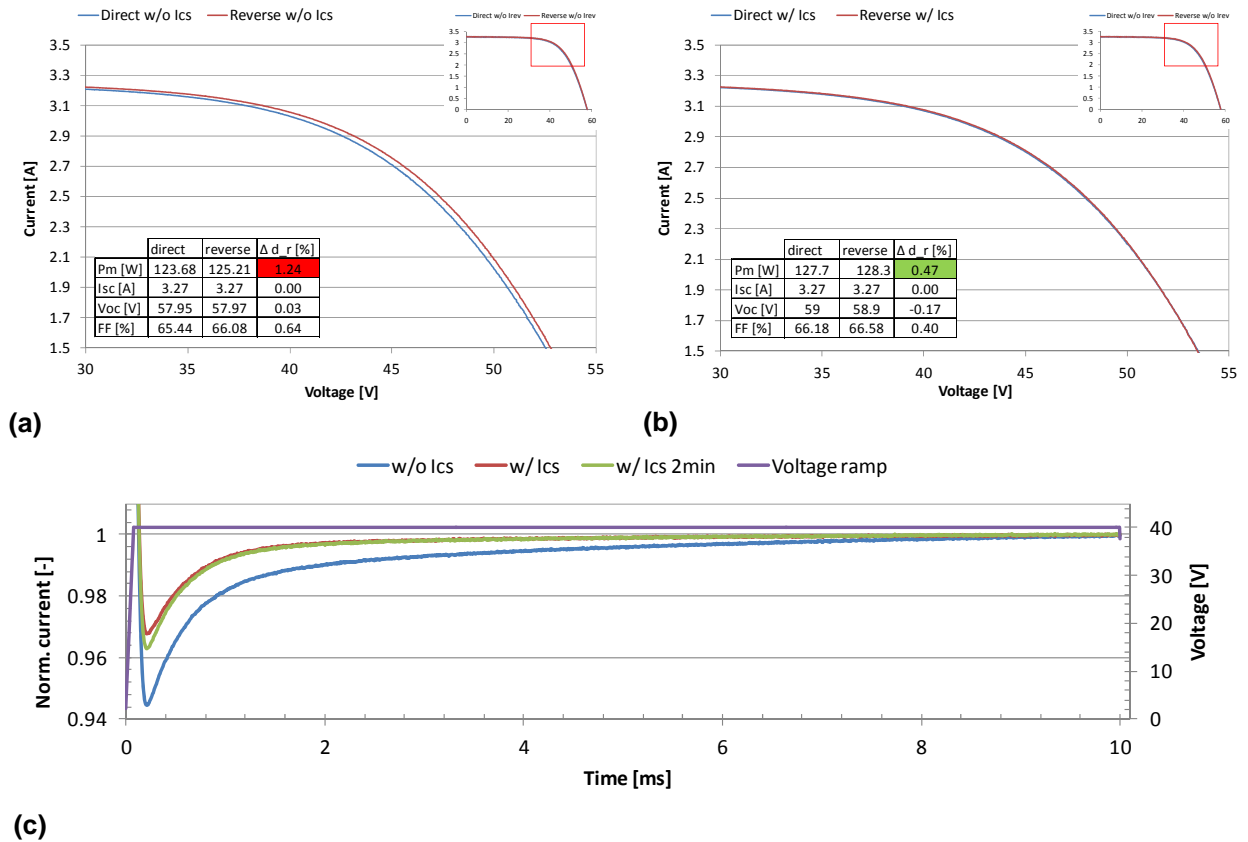


Figure 4.6: Transient effects: (a) direct (blue) and reverse (red) I-V measurement of a CIGS (CIS 5) module after a dark storage period of four days, (b) direct (blue) and reverse (red) I-V measurement with a lcs treatment of 5 seconds before each I-V measurement, (c) modules' current at a stable voltage during 10 ms flash duration (blue), after dark storage (red), with 5s lcs treatment and (green) with 2-minute lcs treatment.

4.3.2 Dark current soaking

The preconditioning with current soaking in darkness was carried out with three CIS modules, purchased in 2011, and two CdTe modules, purchased in 2013 (CIS 3; CIS 1; CIS 2; CdTe 1 and 2). The modules were exposed outdoors for at least 2 years. In order to investigate the maximum changes in the modules' power and to determine whether saturation occurred during the current soaking, lcs was applied to the module for 3 hours. I-V measurements were performed every 15 minutes. All modules were stored in the dark for at least four weeks before the measurement campaign.

Figure 4.7 presents the results of current soaking over 3 hours in order to observe the maximum power reached by this approach. The power was normalized to the initial indoor measurement after outdoor exposure. The yellow dots indicate measurements after 5 seconds, 30 minutes, 1 hour, 2 hours, and the final measurement after 3 hours.

Module CIS 2 does not respond to the current soaking, while Pm remains within $\pm 0.2\%$ over 3 hours. The difference from the initial measurement is -2.4% . On the other hand, the power of modules CIS 3 and CIS 1 rises continuously and reaches its maximum after three hours. However, with the increase of time, the increase of power becomes slower. The maximum power is $+3.7\%$ higher than the initial measurement after outdoor exposure.

Both module CdTe 1 and CdTe 2 show the same behaviours. The power increases very quickly in the first minutes and reaches its maximum after 30 minutes. The difference from the initial measurement is +3.2% for module CdTe 1 and +4.8% for module CdTe 2. After 30 minutes, a slight decrease was detected. The stabilized power after three hours of current-soaking for CdTe is 1 +2.6% higher than the initial measurement and for CdTe this is 2 +3.8%.

However, the higher power after current soaking could indicate that the degradation in the first seconds or minutes of dark storage is much higher or that some other metastable mechanism in the module technology plays a role, and that current soaking pushes the module into a partially different state as compared with the light soaking approach.

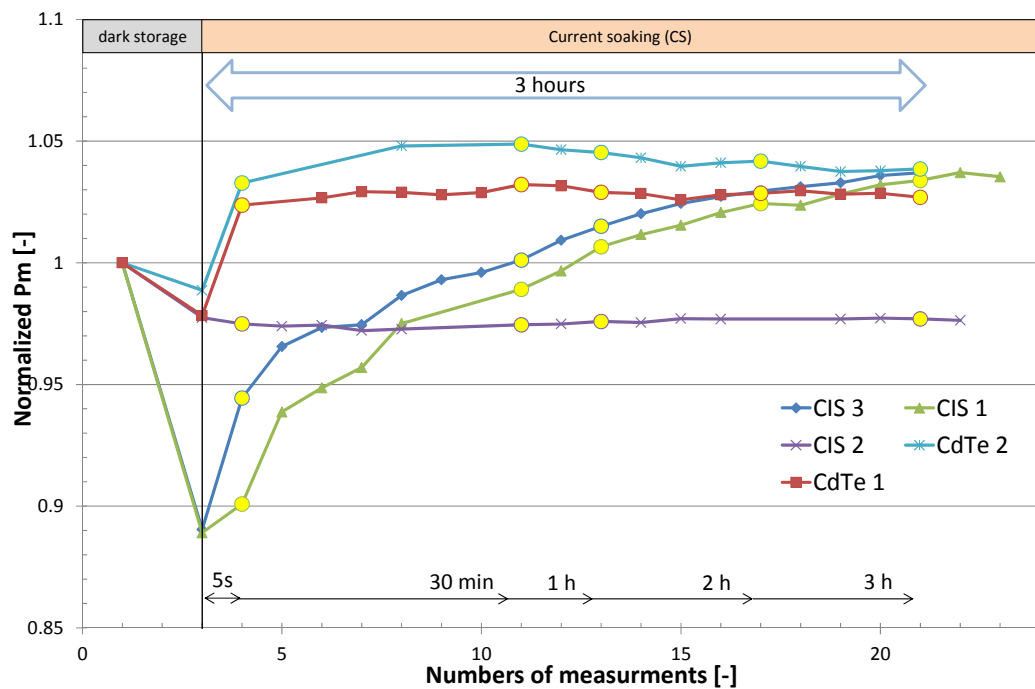


Figure 4.7: Results of current soaking over three hours: Measurements are carried out continuously with steps of 15 minutes. The yellow dots indicate measurements at 5 seconds, 30 minutes, 1 hour, 2 hours and 3 hours. All values are normalized to the initial indoor measurement after outdoor exposure. (CIS 3; CIS 1; CIS 2; CdTe1 and 2)

4.4 CIGS and CdTe preconditioning procedure

The preconditioning procedure for polycrystalline thin film modules such as CdTe, CIS, CIGS is based on the outcomes of observations made during the project, along with collaboration with other testing laboratories. This procedure is divided into three parts: (1) verification of transient effects, (2) preconditioning of newly manufactured modules ("out-of-box"), and (3) pre-conditioning of modules coming from the field (i.e. operating PV systems or PV outdoor test facilities). In this procedure a preconditioning treatment with simulated sunlight - and a continuous record of the modules' power - is preferred, due to the more repeatable testing conditions and shorter treatment times.

1. Current-soaking impulse test (verification of transient effects)

- Connection to current-soaking setup
- First measurement without bias current
- I_{CS} corresponding to the modules' I_{sc} for 5 seconds before I-V measurement. Time between bias current and I-V measurement should be less than 2 seconds.
- Report differences between performed measurements and consider these in the uncertainty budget
- If >2%, measurement shall be performed with I_{cs} treatment

2. Initial light exposure for **new modules** or modules with dark storage time > 3 hours:

- a) Expose the module to simulated sunlight with the following requirements:
 - Class CCC or better sun simulator
 - Irradiance of between 950 - 1100 W/m²
 - Back-of-module temperature of between 50°C ±10°C
 - Active maximum power point tracker
 - Report temperature-corrected power of modules over time; (P_m corrected to 50°C)
 - Stabilization occurs when measurements from two consecutive periods of minimum 20 kWh/m² meet the criteria $(P_{\max} - P_{\min}) / P_{\text{average}} < 1\%$.
- b) Maximum power determination:
 - Measurement requirements according to ISAAC's testing procedure for performance measurements (TP02)
 - Cool module down to 25°C
 - Performance measurement must be done within **20 minutes** after the initial light exposure

3. **Modules coming from the field** with outdoor exposure time > 3 months and dark storage time shorter than 3 hours:

- c) Expose the module to simulated sunlight with the following requirements:
 - Class CCC or better sun simulator
 - Irradiance between 950-1100 W/m²
 - Back-of-module temperature of between 50°C ±10°C
 - Open circuit voltage or passive load
 - Light exposure must last for at least 5 hours
- d) Maximum power determination:
 - Measurement requirements according to ISAAC's testing procedure for performance measurements (TP02)
 - Cool module down to 25°C
 - Performance measurement must be done within **20 minutes** after the initial light exposure

5. OUTDOOR PERFORMANCE OF THIN FILM MODULES

Background:

The performance of thin film modules under real operating conditions is far from being understood as well as that of crystalline silicon modules. Each single technology behaves differently and depends on the manufacturing process. Even samples coming from the same production line can behave differently due to variations in production. Depending on the climatic conditions, the performance can vary and technologies which perform well under warm climates can be disadvantaged in other climates. The standard approach for module benchmarking is to mount selected modules on the same outdoor test facility and to monitor them for at least a year in one or more locations. Optimally, each module is characterized before being installed and is checked at regular intervals.

Scope of the project:

- Continuous upgrade of the outdoor testing facility and data handling procedures.
- Demonstration of technological differences (module benchmarking).
- Investigation of the stability/variation of module parameters during outdoor exposure.
- Comparison of modules exposed under different climatic conditions.

Results:

- The quality control procedures available at SUPSI have been continuously improved by implementing a calibration procedure for the testing equipment (MPPT3000) and by implementing a real-time control of all pyranometers.
- 4 years of outdoor measurements have been concluded successfully, demonstrating differences in annual energy production of up to $\pm 10\%$ with different thin film technologies. CIS and a-Si/ $\mu\text{c-Si}$ modules slightly underperformed or performed very closely to c-Si, whereas CdTe and a-Si tended to overperform, due to their much better temperature coefficient.
- The crystalline-silicon-reference technology was demonstrated to be stable in all of its parameters (STC power, low irradiance performance and temperature coefficient).
- Degradation and/or meta stabilities seemed instead to be an issue in many of the investigated thin film technologies, making the measurement of a unique value, as needed for energy predictions, very difficult.
- For the three investigated CIGS modules, very different low irradiance performances and temperature coefficients were measured, and differences were also observed in modules coming from the same manufacturer.
- The micromorph technology is characterized by a much lower seasonal variation of PR as compared to amorphous silicon modules.
- The temperature coefficient measurements were shown to be strongly influenced by meta stabilities and by spectral effects which must be analyzed further, as these constitute one of the major input parameters for simulations.
- A new approach to the representation and analysis of PV module field data was defined in the framework of the International Agency's Photovoltaic Power System Programme (IEA PVPS) Task 13. The method allows a separation of spectral effects from thermal effects and a comparison of data measured under different conditions and in different testing periods.

5.1 Outdoor test facility

Test facility

SUPSI started the first outdoor tests in 1991. Since then more than 150 different modules have been tested. Whereas in the past the majority of the tested modules were of crystalline silicon technology [REF 5.1], in 2011 a new outdoor measurement campaign (also referred to as "test cycle 12"), focusing only on thin film module performance, was started. A selection of 11 thin film technologies, including a-Si, a-Si/a-Si, a-Si/ μ c-Si, CdTe, CIS, CIGS and CIGSS, were exposed outdoors for over 4 years, together with a c-Si module. Two modules of each type were mounted on the outdoor facility (Figure 5.1), and a third one was stored in the dark as a reference. All modules were purchased anonymously on the market.

Note: Due to the small sample set and the continuous progress in the manufacturing processes, the results cannot be considered to have statistical relevance or to be representative of the modules available on the market. The purpose here is purely research-oriented and to demonstrate technological trends.



Figure 5.1: Picture of the outdoor testing facility at ISAAC with the 11 different thin film technologies and 2 c-Si modules for inter-comparison.

For the outdoor measurements, each module was connected to a maximum power point tracker (MPPT3000) developed by SUPSI [REF 5.2]. In addition to the monitoring of the maximum power point parameters (I_m , V_m) and module temperature (T_{mod}) at minute intervals, the cumulative energy (as given by the maximum power tracker) and the full I-V curves were recorded at intervals of five minutes. Simultaneously with the module parameters, the following irradiance values were monitored: horizontal global and diffuse irradiance, in-plane global irradiance and spectral irradiance. The irradiance stability was measured separately with a reference cell which was monitored at 1-second intervals. The in-plane irradiance was measured with a Kipp&Zone CMP21 pyranometer and the spectrum with a EKO MS-710/712 (350-1700nm) spectroradiometer installed in July 2012. Wind speed and direction, ambient temperature and humidity were monitored separately through the weather tower located in close proximity to the energy yield test stand.

The main parameters extracted from measurements are the Specific Yield (E_{rel}) and the Performance Ratio (PR):

$$E_{rel} = \Sigma P_{meas} / P_{stc} \quad (\text{equation 5.1})$$

$$PR = \Sigma P_{meas} * 1000W/m^2 / \Sigma G * P_{stc} \quad (\text{equation 5.2})$$

where P_{meas} is the instantaneous power measured under real operating conditions, G is the irradiance measured with the pyranometer and P_{stc} is the Power measured at standard test conditions (STC). The STC power can either be taken from the nameplate or measured with a solar simulator. Nameplate values are not considered here.

Except for in-plane irradiance (G), the other meteorological parameters and module temperature (T_{mod}) are not really required for module benchmarking, although they are of importance to a better understanding of the differences in energy output or for the validation of energy prediction models.

Quality control and calibration procedures

One of the greatest uncertainties in the determination of the PR of a module is the in-plane global irradiance measurement. The largest uncertainty contribution here comes from the calibration and the drift of the pyranometer, as well as from maintenance-related issues such as soiling or misalignment of the sensor. Good quality control procedures help to reduce some of these uncertainties. Annual recalibrations against a secondary standard pyranometer calibrated at PMOD/WRC-Davos and the measurement of multiple sensors, up to 3 sensors for each test row, are the rule at SUPSI. All pyranometer data from sensors mounted on the test facility or close to it are analyzed continuously following the procedure for the calibration of pyranometers (ISO 9847). This allows to detect very soon any drifts due to aging, soiling or any misalignment caused by external factors (dismounting of modules, wind, etc).

Another contribution to the uncertainty of PR arises from the hardware used for the modules' current-voltage measurement. The MPPT3000s were calibrated and controlled before being installed. In order to avoid long interruptions to data acquisition, the MPPTs were re-calibrated only once during the full measurement campaign. Any drifts or malfunctions occurring during the test period were detected by means of the quality control algorithms described in the next paragraph. Malfunctions occurring during the 4 years of outdoor exposure were mainly related to the failure of some components, which in some cases required the complete replacement of the MPPT. The stability of the instruments proved to be very high. A calibration procedure was written and new software was created in order to automatize and document the calibration of the MPPTs. Calibrations were performed with ISO 17025 calibrated equipment and a solar array simulator (AGILENT E4360A). The following diagram shows the configuration of the calibration setup. The graphs in Figure 5.3 show the results of a MPPT voltage and current calibration. All values must be within the declared tolerance range of $\pm 0.2\%$ at full scale.

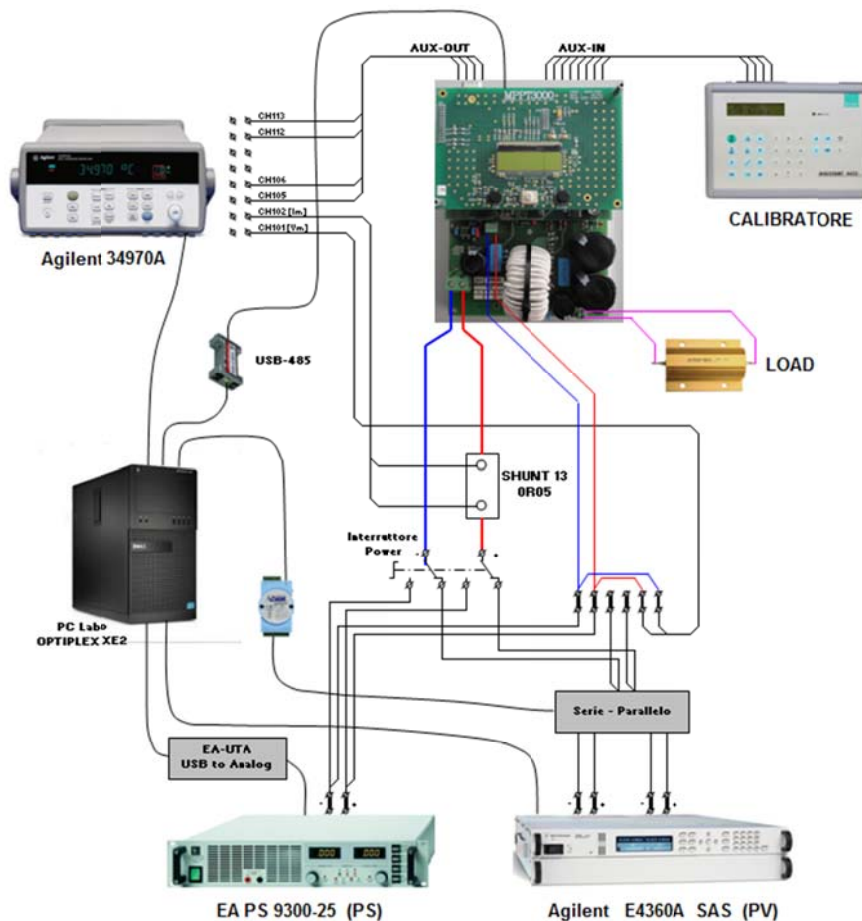


Figure 5.2: Test configuration for the calibration of a MPPT3000.

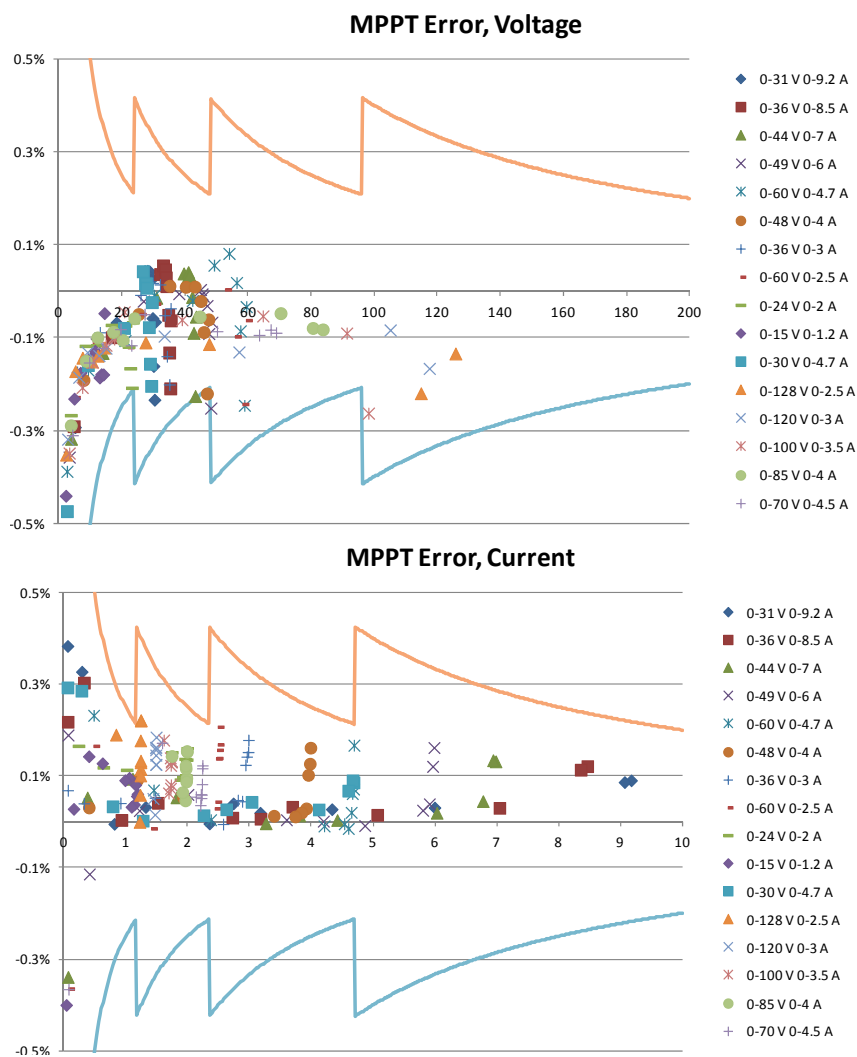


Figure 5.3: Example of a current/voltage calibration of a MPPT3000.

The spectroradiometer EKO MS-710/712 used in the outdoor field is calibrated every year in a spectroradiometric inter-comparison campaign which has taken place every year since 2011 with several European partners, both research centres and those from within the industry. Results from the inter-comparison have been published in a series of conference proceedings and peer-review papers [PMTHIN 9 - PMTHIN 12].

Data pre-processing (quality/error markers)

The experience of over 20 years in the monitoring of our own data and the analysis of data coming from other testing facilities has allowed us to develop a sophisticated data control system, based on a number of algorithms, which permits the detection of a number of very different malfunctions or anomalies which can affect the reliability of PV module inter-comparisons [REP 01, PMTHIN 14]. The number of error markers, introduced mainly for the control of current and voltage measurements, was also extended and refined during the project in order to improve the reliability of irradiance and temperature measurements.

The control of the module temperature data was significantly improved so as to very quickly detect any problems of detachment of the sensor from the back of the module. As discussed at the beginning of this chapter, a new approach for the control of irradiance data was also introduced, which basically consists of a continuous calibration of multiple pyranometers one against the other. Moreover, a new algorithm for the detection of noise was introduced. The spectrum data, which have been obtained at SUPSI since 2012, are controlled by means of a plausibility check against the AM1.5 spectrum with a defined tolerance. Table 5.1 shows the updated table with the current available error markers and a short description.

FLAG	DESCRIPTION
-999	Missing data
-888	Out-of-range
-777	Negative values
-666	Blocked signal
-222	Disconnected module
-444	MPPT/module drift
-555	Singular MPPT errors (e.g. peaks)
-557	Shadow, MPPT error over periods >15 minutes
-778	Signal below MPPT switching threshold
-111	Detached Tbom sensor (method1)
-112	Detached Tbom sensor (method2)
-113	Temperature outliers
-333	Irradiance sensor drift
-669	Noise on pyranometer
-445	Pyranometer stability check
-180	Correlation of measured spectrum with AM1.5
-223	Snow (manual setting)

Table 5.1: List of errors for which a check is made at SUPSI (status in January 2015).

5.2 Module characterization

Before their installation on the outdoor test facility, all modules, including the dark-stored reference modules, underwent a set of preliminary laboratory tests (electro-luminescence, visual inspection, insulation test and wet-leakage test). The modules passed all of these tests. After this, the modules underwent a full electrical characterization with a class A+A+A+ solar simulator. The initial electrical performance was measured under standard testing conditions (STC), different irradiance levels (100-1000W/m²), temperatures (25-65°C) and spectral wavelengths (360-1170 nm). The modules were dismantled 1 or 2 times a year and measured again together with the dark-stored modules in order to detect any changes having occurred during outdoor exposure.

5.2.1 Performance at Standard Test Conditions (STC)

The first I-V curve at STC was measured at the beginning on the as-purchased modules (out-of-box), without any pre-conditioning or exposure to light. The modules were installed on the test facility in January 2011 and dismantled for the first time in September/October 2011. The indoor measurements were then repeated at intervals of 6 months to 1 year. In order to maintain comparability over time, the data reported here were all measured according to the same testing procedure and without changing the equipment or the reference cell. A simplified approach without any pre-conditioning or spectral mismatch correction had to be used, as the improved testing procedures and testing equipment developed during this project, and described in the two preceding chapters, were not available from the beginning of the project. In order to minimize uncertainty due to spectral mismatch, the best reference cell was chosen for each technology (from the devices available at SUPSI as shown in Figure 3.6), by applying the procedure described in the 'Guidelines for PV Power Measurement in Industry' [REF 5.3]. The procedure suggested measuring the short-circuit current versus spectral irradiance and choosing the cell with the lowest deviation. The best-identified reference cells are summarized in Table 5.5, together with the mismatch errors which were calculated later.

The following approach was taken for the different technologies throughout the entire outdoor measurement campaign:

- CIS and CdTe modules were all measured within 1-3 hours after the dismantling of the module (the time required to transport the module to the laboratory and to cool down the module to $25\pm 0.5^\circ\text{C}$). The measurements were all done without any pre-conditioning (LS and/or CS).
- a-Si and μ -Si modules were measured either at the end of the cold season or after the summer so as to be close to the seasonal minimum or maximum due to the equilibrium between light-induced degradation and thermal annealing. The modules were measured as they came from the field without any pre-conditioning (light soaking accord IEC61646).

Stability figures

Figure 5.4 and Table 5.3 show how the P_{\max} of the thin film modules tends to change over time. The changes can be attributed to one effect or a combination of effects, such as: initial stabilization, metastabilities and irreversible degradation effects.

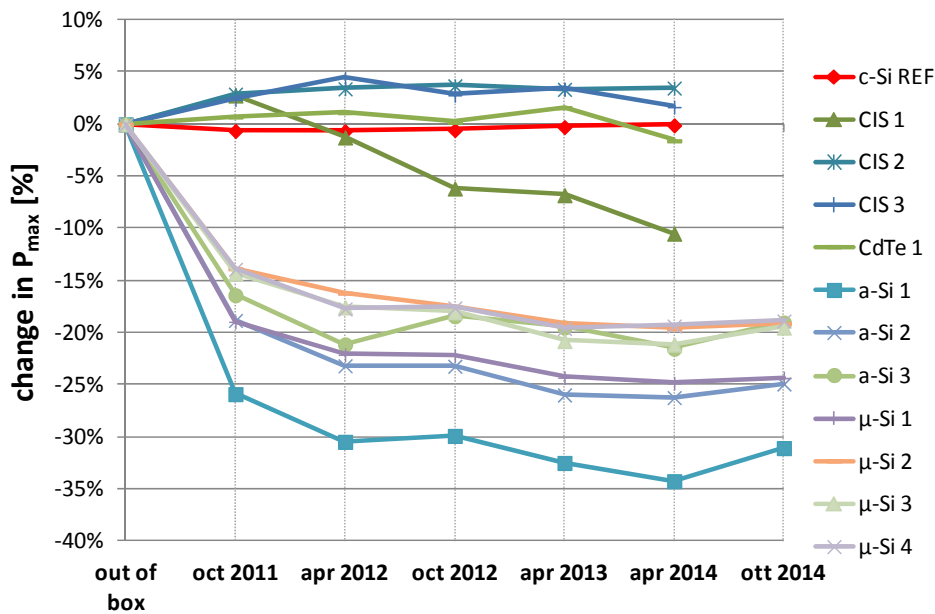


Figure 5.4: Change of P_{\max} in [%] with respect to the first value measured out-of-box (as purchased).

	initial degradation	long term outdoor stability		long term indoor stability	
c-Si REF	-0.6%	0.3%	++	0.1%	++
CIS 1	2.8%	6.1%	--	0.4%	++
CIS 2	2.9%	0.3%	++	0.3%	++
CIS 3	2.4%	1.2%	+	0.3%	++
CdTe 1	0.7%	1.4%	+	0.6%	++
a-Si 1	-30.4%	5.2%	-	0.8%	++
a-Si 2	-23.1%	4.5%	-	1.0%	+
a-Si 3	-21.1%	2.9%	-	1.3%	+
μ -Si 1	-22.1%	3.4%	-	0.6%	++
μ -Si 2	-16.2%	3.2%	-	1.1%	+
μ -Si 3	-17.5%	3.9%	-	1.0%	+
μ -Si 4	-17.7%	3.2%	-	2.0%	-

Table 5.2: Table with: (1) initial degradation after the first year of outdoor exposure, (2) long-term stability of the modules exposed outdoors and (3) long-term stability of the reference modules stored in the dark. (Note: The stability is calculated as the relative standard deviation of all measurements except the first one.)

Initial degradation/recovery

Most technologies are affected by an initial degradation or increase in power when exposed to light for the first time. Each technology is characterized by a different type of initial stabilization process: (1) c-Si by a first-light-induced degradation (LID), (2) CIS and CdTe by a first-positive-light soaking effect and (3) a-Si and μ -Si by the Staebler-Wronski degradation, which is later partially recovered by thermal annealing. The time scales in which this stabilization occurs vary widely among the technologies. Whereas the first two are quite fast, within a range of days to weeks, the last can be much longer, with a duration of more than 1 year. Table 5.2 summarizes the change in STC power between the first indoor measurement (brand-new never-exposed modules) and the second measurement in October 2011 for the CIS and CdTe modules, and the third measurement in April 2012 for all a-Si and μ -Si technologies. For these latter technologies, the first measurement after the cold season is used as a reference, in order to ensure that most of the Staebler-Wronski degradation has occurred and that the recovery by thermal annealing is minimal.

The **c-Si module** shows a drop in power of 0.6%, which is attributed to LID. The measurement of the reference module remained unvaried within 0.1%.

The **CIS and CdTe modules** showed an increase in power (2-3% for CIS and 0.7% for CdTe) which occurred in the very first days to weeks of outdoor exposure.

As expected, all **a-Si based modules** demonstrated the typical initial degradation, which ranged from approximately 30% for the single-junction technology to around 20% for double-junction a-Si (a-Si/a-Si) and down to 16% for micromorph (a-Si/ μ -Si) modules.

Long-term stability

The long-term stability is shown in Figure 5.4 and quantified in Table 5.2. The stability is expressed here as relative standard deviation (%RSD) calculated as absolute standard deviation (SD) divided by the average values (excluding the first measurement). A comparison can be done with the stability of the dark-stored reference modules.

Once stabilized (after LID), the outdoor-exposed **c-Si module**, used here as reference technology, proved to be very stable, without any visible degradation or variation in power over time.

Except for one CIS technology (CIS 1) which continuously degraded over the years, the other **CIS and CdTe modules**, after the initial gain previously described, demonstrated a slightly higher variability in P_{max} as compared to c-Si, although below 1.5%. For one of the CIS technologies (CIS 2), the measurements were very stable over the entire 4 years, whereas the other two technologies (CIS 3 and CdTe 1) showed a small variation within the range of ± 1 -1.5%. However, the variations observed here must be put into relation to the meta-stabilities described in Chapter 4.2.3 (dark-storage effects after long-term outdoor exposure). The module CIS 2 is characterized here by a lower variability, also shown to be less affected by dark storage, making it easier to measure after dismantling it from the test field. The variations of the module technology CIS 3 and CdTe 1 are probably influenced by the meta-stabilities, which are well described in Chapter 4.2.3. The module CIS 1 is instead influenced by both meta stabilities and degradation, which is also clearly visible in the outdoor data.

The **a-Si-based modules** show a higher variability (± 2.3 -4.1%), caused by a partial recovery during the warm season, counteracting the light-induced degradation. The effect is more pronounced in a-Si1 and a-Si2 and, as expected, less pronounced in all micromorph modules. The separation of seasonal variations from long-term degradations is difficult to quantify here, but a slight negative trend is visible, which could be explained by only a partial recovery, which leads to an accumulation of defects with an effective efficiency loss over time.

Dark-stored modules and measurement repeatability

The **modules stored in the dark** should give some more feedback on the repeatability of the measurements for each technology, but the output of these measurements is not always transferable to the outdoor-exposed modules and is technology-dependent. CIS and CdTe are influenced by the previously-described meta stabilities, which are again influenced by the history of the module. The modules stored in the dark over long periods without being exposed to the sun are less affected by meta stabi-

ties than a module exposed outdoors and then transferred to the dark. In general, all module technologies tested here, except for one of the micromorph modules, remained stable within a range of $\pm 1.2\%$ or better. The crystalline silicon module shows, as expected, the lowest variation of less than $\pm 0.2\%$, which corresponds to the typical repeatability of STC measurements of stable c-Si modules at SUPSI.

5.2.2 Irradiance dependency

The irradiance dependency of a module can be described by the relative efficiency curve

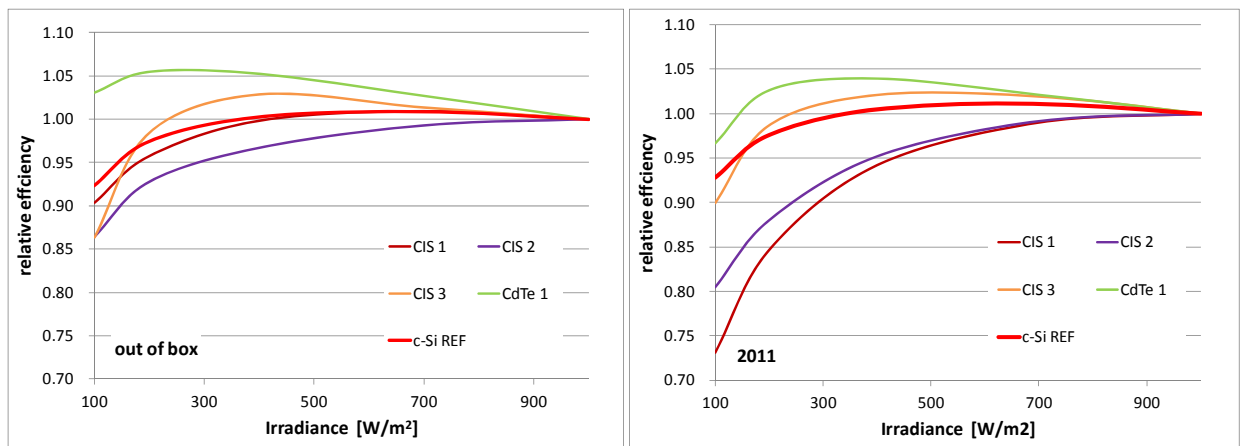
$$\eta_{rel}(G) = \eta(G) / \eta(1000\text{W/m}^2) \quad (\text{equation 5.3})$$

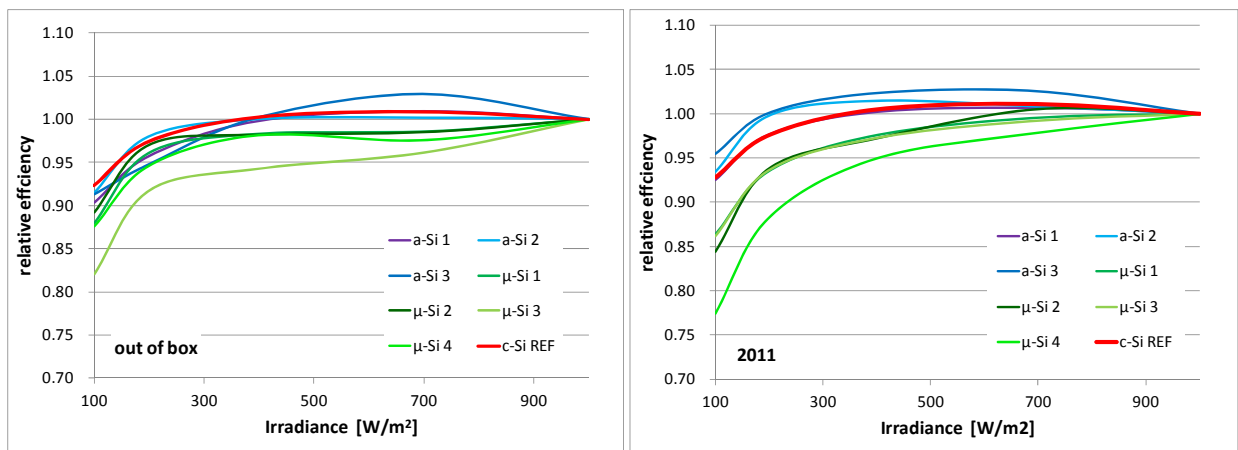
which is extracted from I-V measurements at different irradiance levels of from 100 to 1000 W/m², at 25°C module temperature and AM1.5g spectral irradiance.

The efficiency curve is a direct or indirect input of most simulation tools, and can have up to 10% influence on the final yield, depending on the environmental conditions [REF 5.4, REF 5.5]. The efficiency losses at various irradiance levels are a result of the two parasitic resistances of the module (the series resistance R_s and the shunt resistance R_{sh}), which result from the resistances of the cells and the module manufacturing process. The relative low-light performance is better for higher R_s , but its absolute STC efficiency is reduced. Lower shunt resistances reduce both low-light performance and STC efficiency. As long as no degradation or changes occur at the module level, which would be visible in a degradation or change of the parasitic resistances, low-light performance is also expected to remain stable.

Stability figures

The efficiency curves of the modules were measured after each STC measurement. Neutral density filters with an attenuation factor of 0.1, 0.2, 0.4 and 0.7 were therefore applied in front of the lamps of the PASAN IIIb. A description of the setup and measurement uncertainties is given in [REP 01]. Figure 20 shows the relative efficiency curves of all module types as measured at the beginning (out-of-box) and after 1 year of outdoor exposure (October 2011). The table gives the absolute change for each irradiance.





	c-Si REF	CIS 1	CIS 2	CIS 3	CdTe 1	a-Si 1	a-Si 2	a-Si 3	μ-Si 1	μ-Si 2	μ-Si 3	μ-Si 4
1000	0.0%	0.0%	0.0%	0.0%	0.0%	0.0%	0.0%	0.0%	0.0%	0.0%	0.0%	0.0%
700	0.2%	-1.9%	-0.4%	0.6%	-0.6%	-0.3%	0.7%	-0.4%	1.0%	2.8%	3.1%	0.3%
400	0.2%	-5.6%	-1.5%	-0.8%	-1.3%	0.4%	1.5%	2.1%	-0.7%	-0.4%	3.0%	-3.2%
200	0.2%	-11.1%	-5.0%	0.2%	-2.8%	1.9%	1.8%	5.3%	-2.6%	-1.8%	1.9%	-6.3%
100	0.5%	-17.2%	-6.8%	3.6%	-6.4%	2.2%	2.0%	4.2%	-1.7%	-2.4%	4.1%	-10.1%

Figure 5.5: Relative efficiency curve measured before (out-of-box) and after outdoor exposure (2011): in the upper graphs for CIS and CdTe and in the lower graphs for a-Si and μ-Si. The c-Si reference technology is shown in all graphs (red curve). The last table quantifies the changes.

Initial degradation/recovery

Compared to the thin film technologies, the relative efficiency curve of the **c-Si module** did not change when exposed to light for the first time (after LID).

As expected, the **CIS and CdTe modules** changed after outdoor exposure due to a variation of both series and shunt resistance. Table 5.3 shows the R_s and R_{sh} as measured before and after outdoor exposure. It is very difficult to come to a general conclusion for CIS or CdTe, as each technology behaves differently. Also, differences have been observed between modules of the same type. In any case, there is a general increase in losses in efficiency at low irradiances associated with the improvement in STC power within the first hours of exposure. Only module CIS3 has a gain at low irradiances associated with the increase of the shunt resistance.

	R_s out of box	R_s 2011	R_{sh} out of box	R_{sh} 2011
	[Ω]	[Ω]	[Ω]	[Ω]
CIS 1	5.3	4.9	399	368
CIS 2	5.6	5.1	3845	3089
CIS 3	5.5	4.6	367	523
CdTe 1	14.9	12.2	3160	1704

Table 5.3: Measured series and shunt resistances of CIS and CdTe before and after outdoor exposure. Note: Highlighted in green are the parasitic resistances which are affected positively by outdoor exposure, and in red are those affected negatively.

The efficiency curves of the two **a-Si based technologies**, a-Si and μ-Si, stabilized differently after their initial degradation. The a-Si single- and double-junction modules showed a slight improvement at low irradiances after exposure to the sun, with a performance similar to or slightly better than that of the c-Si module. The micromorph modules were instead characterized by a negative change at low irradiances, except for μ-Si3, which improved. All technologies, however, stabilized well below the c-Si reference curve, with μ-Si1, μ-Si2 and μ-Si3 at a similar level and μ-Si4 at a lower level.

Long-term stability

As expected, the efficiency curve of the **c-Si module** did not change over the entire 4 years, with a variation of loss at 200W/m², from -2.0% to a maximum of -2.6%, which is well within the measurement repeatability of low irradiance measurements ($u=\pm 3.4\%$ [k=2]).

The **CdTe module** showed a variation in loss at 200W/m² within the range of 1.9% to a maximum of 4.9%, always with positive values due to the typical high series-resistance values. It is very difficult to make a differentiation between degradation and meta stabilities.

The **CIS modules** are not comparable to each other, and again are difficult to interpret due to the meta stabilities. Module CIS2, which was stable under STC, showed a slight increase in efficiency loss at 200W/m², from -9.4% to -11.6%. The second of the two exposed modules is comparable to the first one, though with a slightly higher negative trend. The losses of module CIS3 at 200W/m² ranged from +1.3 to -2.8%, again suggesting the issue with meta stability and transient effects for this type of technology. As for STC performance, the performance at low irradiances of the module CIS1 was also characterized by a continuous degradation. The 3 samples are not comparable to each other, suggesting that the modules came from a non-optimized production batch with a high production inhomogeneity. In the worst case, the efficiency loss at 200W/m² was -25.6%.

After the initial degradation, the efficiency curves of the **a-Si based technologies** did not demonstrate large variations. After the first year the efficiency loss of the 3 a-Si modules at 200W/m² stabilized at around -3.7% for the single junction technology, around -1.0% for the double junction technologies and around -7.0% for μ -Si modules, except for one which stabilized at around -14.0% (μ -Si 4).

5.2.3 Temperature coefficients

The temperature coefficients (TC) α , β and δ describe the rate at which the module short-circuit current (I_{sc}), open-circuit voltage (V_{oc}) and peak power (P_{max}), respectively, change as a function of module temperature. The coefficients are determined through the measurement of I-V curves at different temperatures in the range of 15-75°C, a fixed irradiance and constant spectral conditions. Details about the setup can be found in [REP 01].

The temperature coefficients stated in the manufacturer datasheets are generally measured at 1000W/m². Although the relative temperature coefficients of crystalline silicon technologies do not change with irradiance, non-linear temperature coefficients are reported in the literature [REP 01, REF 5.6]. for thin film technologies. A second value measured at 200W/m² would be quite beneficial to improving the accuracy of present energy prediction models.

For c-Si modules, measurement accuracies of around $\pm 25\%$ (k=2) for α and $\pm 10\%$ (k=2) for δ are given by testing laboratories. However, international measurement inter-comparison campaigns have shown even large deviations from the median: -8% to +16% for δ and up to $\pm 35\%$ for α [PMTHIN 17]. Higher deviations have been observed for thin film modules. The results suggest that there is still room for improvement, which can only be achieved through a deeper understanding of the origin of these discrepancies. The impact on energy predictions is not as critical as expected for crystalline silicon modules [PMTHIN 18], but it is so for thin film modules.

Stability figures

Due to the difficulties described above and the time-intensive measurement procedure, the focus here was only on measurements at 1000W/m², and the measurements were repeated only once, except for a few modules which were measured more intensively.

Table 5.4 summarizes the primary temperature coefficients of P_{max} as measured over the duration of the project. For c-Si, CIS and CdTe the temperature coefficients were additionally extrapolated from outdoor data. The procedure of how this was done is explained in paragraph 5.3.1., and can be applied to all technologies which show no evidence of degradation or seasonal variations due to SWE.

The temperature coefficient (TC) measured for the **c-Si module** was -0.43 %/°C. The parameter was not affected by LID. The value is comparable to what was extracted from outdoor data.

CIS and CdTe modules are generally affected by meta stabilities which are difficult to control in a time frame of several hours, the typical time required to thermally stabilize a module during a temperature coefficient measurement. The CIS2 modules were the only technologies having stable temperature coefficients within $-0.36 \text{ } \%/^{\circ}\text{C}$ and $-0.37 \text{ } \%/^{\circ}\text{C}$ and values close to those extracted from outdoor data. The reason for this is again the fact that this technology seems to be less affected by meta stabilities. The degrading CIS1 module showed an increasing temperature coefficient over time and no conclusions could be made about the real initial temperature coefficient. The modules CIS3 and CdTe were strongly affected by meta stabilities, resulting in temperature coefficients which varied up to 100% and 60% respectively for the two modules. Due to practical reasons, the time of dark storage was not always the same, even reaching several days before measurements were made. Repetitions of the measurements (not shown here) and small variations in the testing procedure (e.g. cooling instead of heating the module) demonstrated a low reproducibility of the indoor measurements. The outdoor measurements instead resulted in values much closer to the nameplate values, but further investigations are required in order to quantify the uncertainty of the parameters determined in this way. There is a clear need for preconditioning procedures which can be applied to temperature coefficient measurements, and these should be implemented in the future and validated against outdoor data.

The temperature coefficient of **a-Si based technologies** changes after its initial degradation. The value is generally lower after exposure (better temperature coefficient). The effect is less pronounced in a-Si modules and more pronounced in μ -Si modules. The amorphous silicon single- or double-junction modules have a lower temperature coefficient compared to the micromorph modules.

	Pmax temp. coeff.				
	nominal	out of box	2011	after 2011	outdoor
	$\%/^{\circ}\text{C}$	$\%/^{\circ}\text{C}$	$\%/^{\circ}\text{C}$	$\%/^{\circ}\text{C}$	$\%/^{\circ}\text{C}$
c-Si REF	-0.45	-0.43	-0.41	-0.43	-0.43
CIS 1	-0.30	-0.29	-0.37	-0.55	/
CIS 2	-0.38	-0.37	-0.36	-0.36	-0.35
CIS 3	-0.45	-0.29	-0.30	-0.57	-0.44
CdTe 1	-0.25	-0.36	-0.32	-0.26	-0.24
a-Si 1	-0.20	-0.18	-0.12	/	/
a-Si 2	-0.20	-0.11	-0.11	/	/
a-Si 3	-0.19	-0.15	-0.14	/	/
μ-Si 1	-0.25	-0.42	-0.30	/	/
μ-Si 2	-0.25	-0.36	-0.30	/	/
μ-Si 3	-0.28	-0.29	-0.23	/	/
μ-Si 4	-0.29	-0.34	-0.31	/	/

Table 5.4: Nameplate and measured temperature coefficients: (1) initial measurement (out-of-box), (2) measurement after approximately 10 months of outdoor exposure (2011), (3) second repetition of the measurement (after 2011) and (4) extrapolation of the temperature coefficient from outdoor data.

5.2.4 Spectral response

It is well known that some technologies are more affected by spectral variations than others. Therefore, the spectral response (SR) of the module must be known. Once stabilized, the SR curves were measured for all technologies (one module per type). Figure 5.6 shows the SR curves for the single junction and for the multifunction modules, measured with the equipment and procedure described in Chapter 3.

Once measured, the spectral mismatch was also calculated for the different available reference cells, in order to validate the initial approach of selecting the reference cell by means of a I_{sc} versus irradiance measurement, as described in Chapter 5.2.1. Table 5.5 lists the calculated spectral mismatch errors (as a percentage deviation from the unity of the spectral mismatch factor defined in Chapter 3) of the testing module with respect to the set of reference cells in use with the approach of Chapter 5.2.1, Pasan IIIb spectral irradiance and the standard AM1.5g spectrum. The values in bold

indicate the reference cell with the minimum spectral mismatch, to be compared with the reference cell actually selected by the initial approach. As a result, the selected reference cell almost always corresponds to the cell with the minimum calculated spectral mismatch, thus validating the original approach. (The 1% deviations between the two approaches in μ -Si1 and μ -Si2 are within measurement uncertainties. In the CIS 3 case, the reference cell with the minimum calculated spectral mismatch was AK110, which was not in use when the measurements were performed).

Table 5.5 also indicates the current-limiting junction in multi-junction devices and the corresponding spectral mismatch errors. This is not used for spectral correction, but may result in the measurement artefacts discussed in section 3, which can now be clarified by spectral tuning and spectrometric characterization.

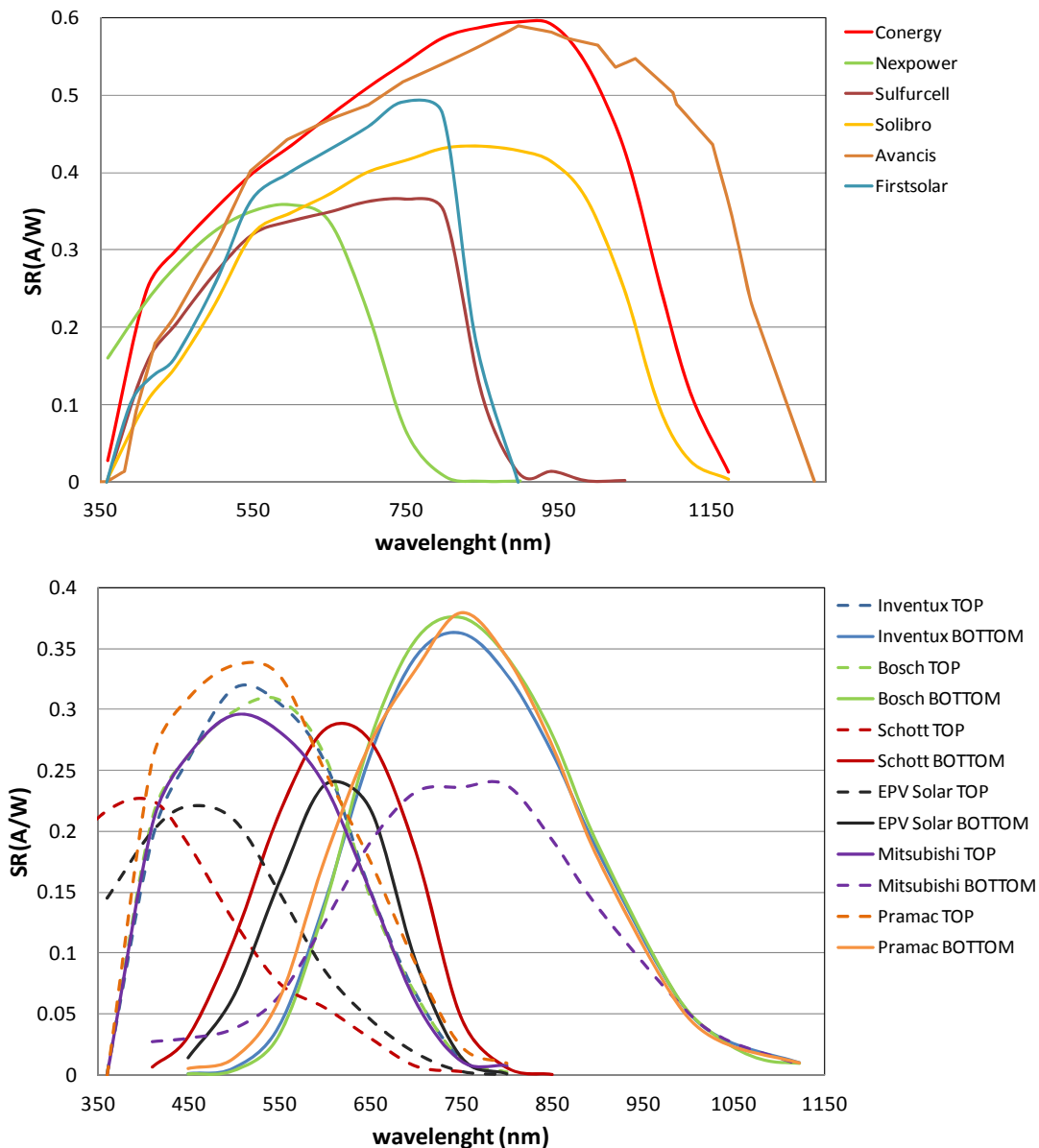


Figure 5.6: Measured spectral responsivity for (a) all single junction modules and (b) for all top and bottom cells of the multi-junction modules.

module	used ref cell	sub-cell	current imbalance	calc. spectral mismatch error [%]				
				VLSI365	MTFP	ISE054	ISE088	AK110
c-Si REF	VLSI365	-		0.2%	4.1%	6.7%	9.5%	1.7%
CIS 1	MTFP	-		4.5%	0.4%	2.4%	5.3%	6.4%
CIS 2	VLSI365	-		0.1%	4.0%	6.7%	9.5%	1.7%
CIS 3	VLSI365	-		2.7%	6.5%	9.0%	11.8%	0.8%
CdTe 1	MTFP	-		4.6%	0.5%	2.3%	5.2%	6.5%
a-Si1	ISE054	-		6.9%	2.7%	0.1%	3.1%	8.8%
a-Si2	ISE088	top	0.74	12.4%	8.1%	5.1%	1.9%	14.5%
		bottom		2.9%	1.1%	3.9%	6.7%	4.8%
a-Si3	MTFP	top	1.04	12.3%	7.9%	4.9%	1.8%	14.3%
		bottom		3.2%	0.8%	3.6%	6.5%	5.1%
μ -Si 1	ISE088	top	0.82	7.9%	3.7%	0.9%	2.1%	9.9%
		bottom		0.7%	4.6%	7.2%	10.0%	1.1%
μ -Si 2	ISE088	top	0.85	7.9%	3.7%	0.8%	2.2%	9.9%
		bottom		0.5%	4.4%	7.0%	9.8%	1.3%
μ -Si 3	ISE088	top	0.93	9.1%	4.9%	2.0%	1.1%	11.2%
		bottom		0.7%	4.6%	7.2%	10.0%	1.1%
μ -Si 4	ISE054	top	0.91	7.9%	3.7%	0.8%	2.2%	9.9%
		bottom		0.1%	4.0%	6.6%	9.4%	1.8%

Table 5.5: Validation of the reference cell selection approach of section 5.2.1: the second column indicates the selected reference cell; the fourth column indicates the current imbalance in multi-junction devices (i.e. the ratio between the photogenerated currents from the top and bottom junctions respectively: top-limitation when the imbalance is less than 1, bottom-limitation when it is greater than 1); the columns from five to nine show the calculated spectral mismatch errors (as a percentage deviation from the unity of the spectral mismatch factor as defined in Chapter 3). Except for CIS 3, μ -Si1 and μ -Si2, the selected reference cells always correspond to the minimum spectral mismatch error.

5.3 Energy yield (EY) inter-comparison

5.3.1 Measurements in Lugano (Switzerland)

The initial aims of an outdoor measurement campaign are to determine which module performs the best at a specific site, how stable the performance is over the years and what the reasons are for the level of its performance and its eventual degradation. The first step is to calculate the rankings and to put them into relation to the PR trends and the module parameters measured in the laboratory.

Note: The calculated specific yields (E_{rel}) and performance ratios (PR) always refer to the indoor-measured STC power (P_{ref}) done in April 2012 (the first indoor measurement according to which all thin film modules are stabilized). All data are grouped by technologies: (1) CIS and CdTe, (2) a-Si/ μ -Si and (3) a-Si single and multi-junction.

Module ranking

Figure 5.7 shows the module ranking as obtained for the last 3 years (2012-2014). Stabilization is assumed after the first year. The graph gives the difference of performance ratio of each thin film module with respect to the c-Si reference module ($\Delta PR=0\%$). Differences of up to $\pm 10\%$ were observed from one module to another. As previously reported, after the first year of operation (see annual report 2012) CIS and a-Si/ μ -Si modules slightly underperformed compared to c-Si, whereas CdTe and a-Si tended to overperform. Excluding the two extreme values (one due to a bad module), the spread is more than halved (8% rather than 20%).

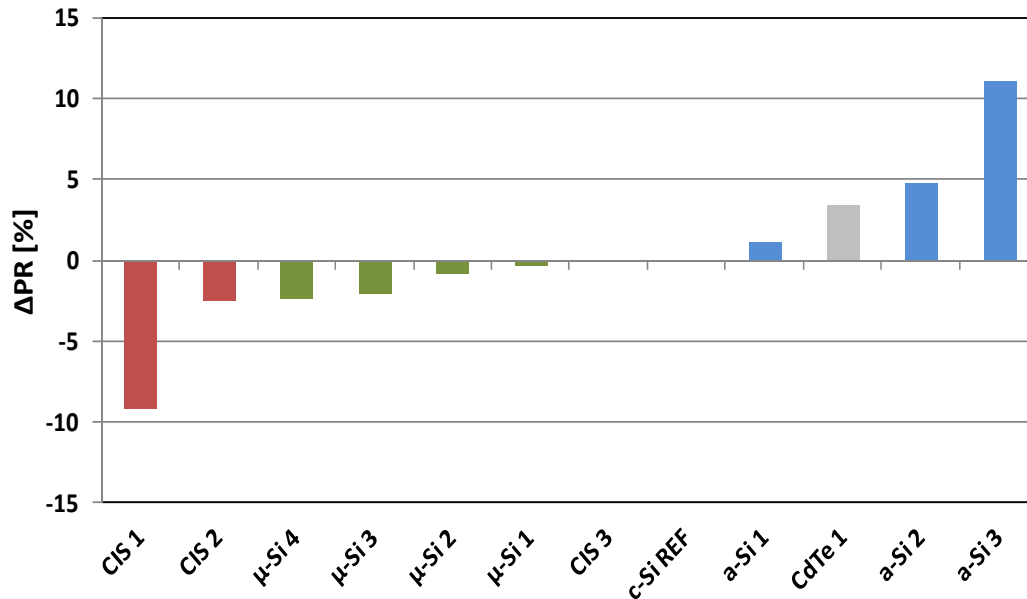


Figure 5.7: Thin film module ranking (2012-2014) expressed as difference of performance ratio $\Delta PR = (PR - PR_{c-Si}) / PR_{c-Si}$ for 11 different thin film technologies (CIS in red, CdTe in grey, μ -Si in green and a-Si in blue).

Note: The first year was not considered so as to allow all amorphous silicon-based technologies to stabilize.

The ranking shown here is of course strongly influenced by the reference power used for the calculation of the PR. When using the indoor-measured STC power, as done here, the ranking depends not only on the measurement accuracy of the kWh but also on the STC power and its stability over time. The contribution of the irradiance measurement can be ignored here as being almost the same for all modules. A different filtering of the data can have a small impact, but this can also be ignored. Whereas the measurement uncertainty of the kWh is well below $\pm 1\%$, considering all contributions by the testing facility (in-homogeneities) and equipment (calibration and MPPT accuracy), the uncertainty of the STC power of thin film technologies can vary here between $\pm 2-5\%$, depending on the technology and the period in which the module was taken from the field. A ranking with a higher precision will be achieved in the future by the full implementation of the new measurement procedures introduced in Chapters 3 and 4, along with a better definition of a reference power for a-Si modules.

PR figures

The pictures in Figure 5.8 show the 4 years of monitoring data, representing the daily performance ratio (PR) of each thin film technology in comparison to the PR of the c-Si reference module, here represented by a black line plot. Modules of the same class demonstrate similar trends (seasonal fluctuations), except for the module CIS1, which is affected by severe degradation.

CIS and CdTe show the same seasonal behaviour as c-Si (maximum PR in winter and minimum PR in summer) but with a different extension from minimum to maximum PR due to differences in temperature coefficients and spectral response (see Table 5.4).

As expected, all amorphous silicon-based technologies, meaning **a-Si and μ -Si**, show an increase in PR during the warm months (contrary to the c-Si module) due to thermal annealing, but with significant differences between the two module technologies. The 4 micromorph technologies demonstrate a very similar behaviour, with a much faster initial degradation, and compared to a-Si and c-Si, a much flatter seasonal PR variation (less than half that of the a-Si). The 3 amorphous silicon technologies took much longer for their initial degradation - a negative trend is still visible in the winter 2011/2012 - and the seasonal PR variations are close to those of the c-Si module (but opposite).

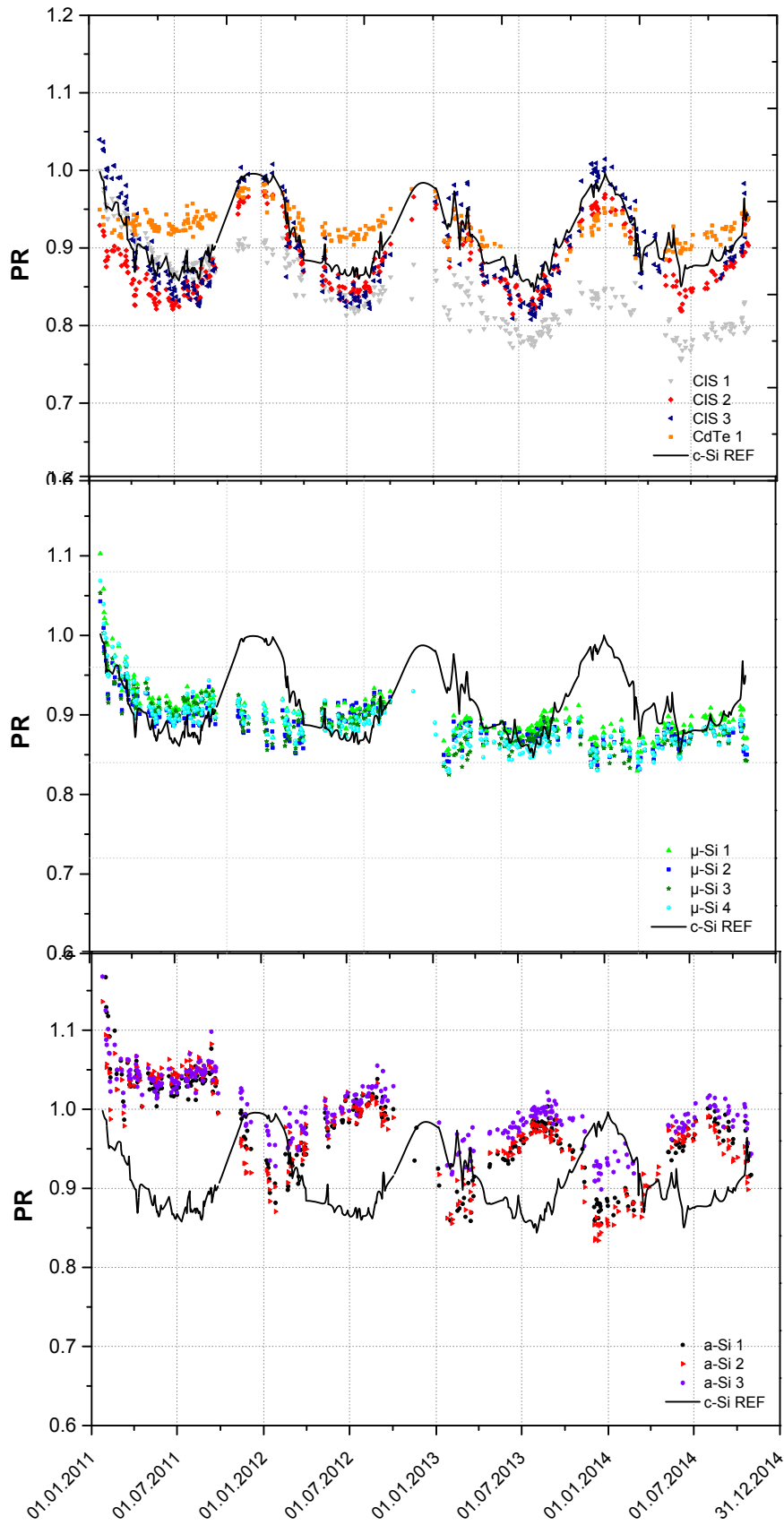


Figure 5.8: Daily performance ratio (PR) of thin film modules (coloured symbols) in comparison to the PR of the c-Si reference module (black line). Note: only clear days are depicted here.

Impact factors

Table 5.6 gives a summary of the stability and the module parameters extracted from the indoor measurements which have the highest impact on the energy output of a module (stability of STC power, P_{max} temperature coefficient, efficiency loss at low irradiances and spectral losses). As far as possible, only stabilized values are considered. In some cases the outdoor temperature coefficient was considered instead of the indoor one, as this was expected to be more reliable for modules affected by meta-stabilities.

The spectral dependency is determined here by plotting irradiance- and temperature-corrected power values of clear days against air mass, and by determining the slope of the linear trend. An alternative approach is described in Chapter 6.4.1.

The module parameters listed in Table 6 are later used for the calculation of losses or gains due to the different impact factors (temperature, irradiance, spectrum, etc.). This way of calculating loss factors helps us to better understand and predict the performance of different technologies. A detailed description of the calculation of loss factors is given in the next chapter (Chapter 6).

	STC	γ loss	$\eta_{loss,200}$	spec. loss	ΔPR
		%/°C	%	%/AM	%
CIS 1	--	-0.30*	-15.3	-1.50	-9.10
CIS 2	++	-0.36	-12.0	1.95	-2.40
μ -Si 4	-	-0.31	-14.0	-3.50	-2.30
μ -Si 3	-	-0.24	-7.1	-1.60	-1.90
μ -Si 2	-	-0.30	-7.4	-2.40	-0.80
μ -Si 1	-	-0.30	-7.0	-2.10	-0.20
c-Si REF	++	-0.43	-2.4	2.10	0.00
CIS 3	+	-0.44**	-1.3	3.23	0.00
a-Si 1	-	-0.10	-3.7	-7.80	1.10
CdTe 1	+	-0.24**	2.6	-0.48	3.40
a-Si 2	-	-0.11	-1.2	-6.10	4.80
a-Si 3	-	-0.14	-0.9	-3.00	11.00

Table 5.6: Summary of measured module parameters: STC power stability, temperature coefficient [γ], efficiency loss at 200W/m² [$\eta_{loss,200}$] and spectral AM coefficient together with outdoor-measured ΔPR as depicted in Fig.23. Legend: * initial value ** outdoor value

5.3.2 Measurements in different climates

The data acquired in the PmThin project were shared within the framework of the International Agency's Photovoltaic Power System Programme (IEA PVPS) Task 13, with the aim of comparing module data measured in different climates. SUPSI participated in the defining of a standard approach for the representation and analysis of PV module field data coming from different testing facilities and locations [REP 02]. Data including those from test cycle 12 were collected and analyzed. Figure 5.9 shows the meteorological data of all sites. More outdoor performance data from labs worldwide is being collected and will be analyzed in the future, while the methods for data evaluation and the result plots for the comparison of different PV module technologies will be further developed.

In order to compare the performance characteristics of the modules at the different sites, a common data format was defined. Table 5.7 gives a summary of the collected input parameters. The daily performance ratio of maximum power (PR(P_m)) and short-circuit current (PR(I_{sc})) are used as key parameters in characterizing the performance of the modules. The proposed approach is particularly useful when comparing thin film technologies and when a large number of modules from different locations measured during different time periods must be compared.

	Description	Formulas	Condition
Date			
Day type	clear/cloudy/very cloudy		
H_{poa}	daily in-plane (plane of array) irradiation	$\int G_{pyr} dt$	
avg. T_{bom}	daily avg. daylight ($G>0$) back of mod. temp.	$\sum T_{bom}/n$	$G>0$
avg. T_{amb}	daily avg. daylight ($G>0$) air temp.	$\sum T_{amb}/n$	$G>0$
$T_{bom,w}$	daily avg. irr.-weighted module temp.	$\sum T_{bom} \cdot G_{pyr} / \sum G_{pyr}$	$G>0$
PR (Pm)	daily performance ratio of Pmax	$(\sum Pm/Pm, stc) / (\sum G_{pyr}/1000)$	
PR (Isc)	daily performance ratio of Isc	$(\sum Isc/Isc, stc) / (\sum G_{pyr}/1000)$	
PR _{filt} (Pm)	daily performance ratio of filtered Pmax	$(\sum Pm/Pm, stc) / (\sum G_{pyr}/1000)$	$G>400W/m^2$ & $AOI<50^\circ$
PR _{filt} (Isc)	daily performance ratio of filtered Isc	$(\sum Isc/Isc, stc) / (\sum G_{pyr}/1000)$	$G>400W/m^2$ & $AOI<50^\circ$

Table 5.7: Parameters defined and used to perform common data analysis

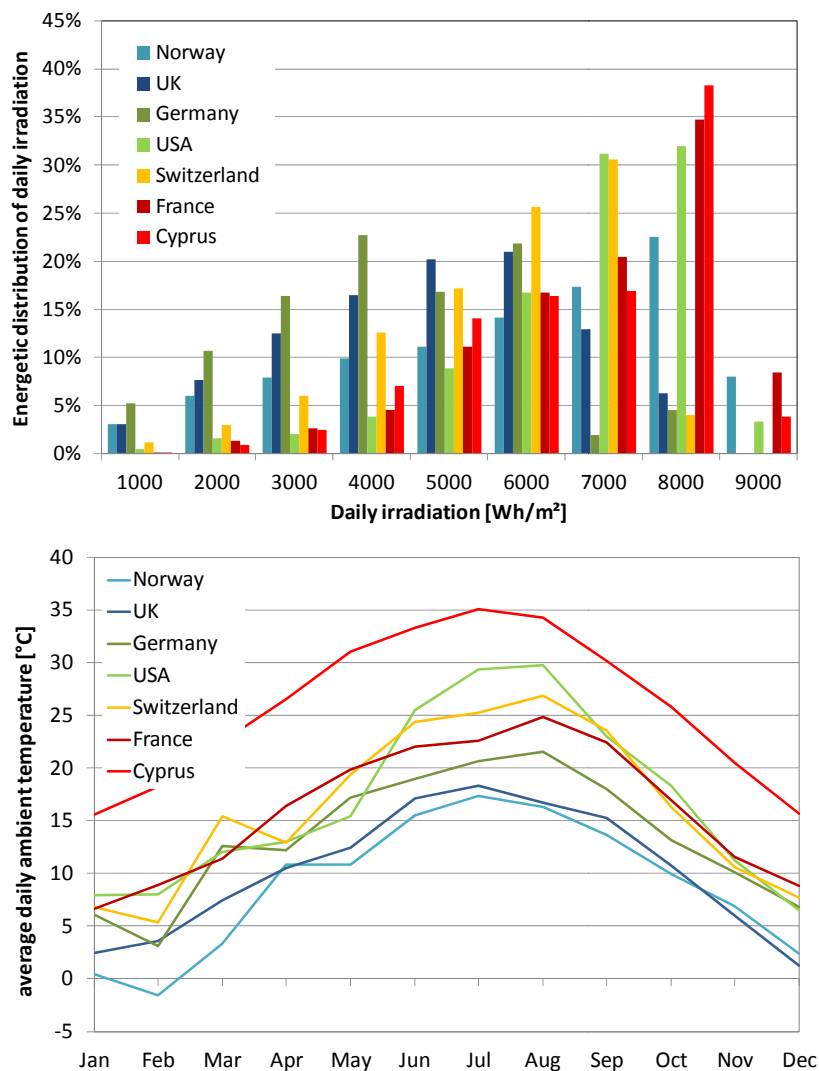


Figure 5.9: Meteorological data during monitoring period 2010-2012 at seven different sites. The upper figure shows the different distributions of daily irradiation sums, the lower figure shows the monthly average ambient temperatures measured at the sites.

Figure 5.10 shows an example of selected crystalline silicon and amorphous silicon modules measured at 7 different locations (Norway, UK, Germany, USA, Switzerland, France and Cyprus). The data show the typical opposite seasonal trends of performance ratio (PR) of the two technologies. The high spread for the a-Si modules is mainly due to differences in the approaches to the determination of STC power.

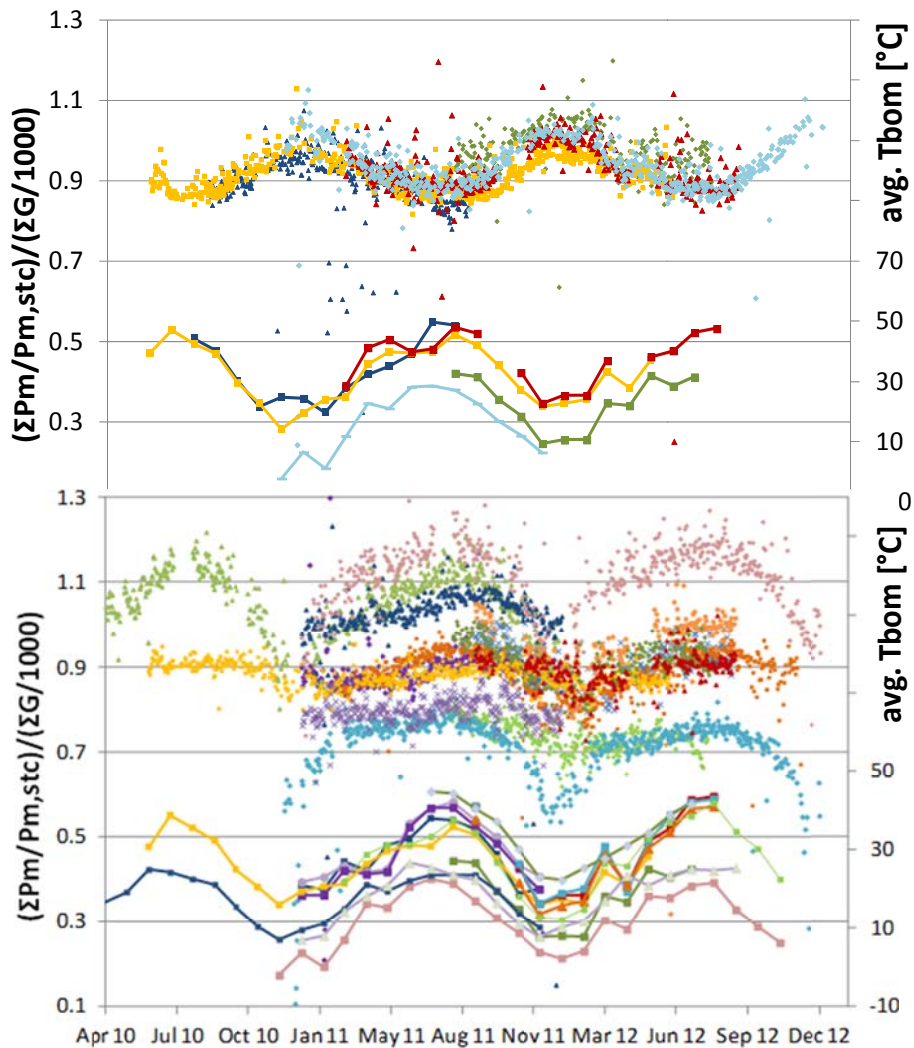


Figure 5.10: Average daylight back-of-module temperature (line plots) and daily PR of Pm (dot plots) for some c-Si- and a-Si-based modules measured at different locations during the period May 2010 to December 2012.

Methodology

First, the PR(Pm) and PR(Isc) performance ratios as defined in Table 5.7 were plotted into one-year plots. This was only done if no irreversible degradation was detected for the period investigated.

Figure 5.11 and 5.12 show the step-by-step approach of how data are analyzed for a set of crystalline and amorphous silicon technologies respectively. The basic idea behind the approach is to normalize the PR(Pm) figures with PR(Isc). In this way, the spread due to irradiance sensor calibration and spectral effects can be reduced, and irradiance and temperature dependencies can more easily be analyzed. The module temperature coefficient can be extracted by plotting the normalized clear day PR (P_{norm}) versus the irradiance-weighted module temperature ($T_{mod,w}$), and by applying a linear plot (see equation 5.4).

$$PR_{norm} = \frac{PR(Pm)}{PR(Isc)} = c + c \cdot \gamma \cdot T_{mod,w} \quad \text{(equation 5.4)}$$

In the case of the **c-Si technology** (Figure 5.11), the top right graph shows the typical seasonal variations of PR(Pm) due to module temperature, the left plot representing PR(Isc) being almost stable due to the very low spectral dependency of c-Si. The PR(Isc) variations are in the range of $\pm 5\%$, and they are mainly the sum of the uncertainties of irradiance measurement (pyranometer calibration), determination of I_{sc} at STC and very small spectral variations for c-Si modules. In order to exclude these uncertainties or influences from further analysis, the first step consists of a correction where PR(Isc) data are set equal to one, and applying the correction factor thereby obtained to the PR(Pm) performance ratio. The result of this normalization procedure is shown in plot 3 (middle graph), which then allows a more detailed analysis of the low-irradiance behaviour without spectral effects and the temperature behaviour, as shown in the two lower plots.

The graphs in Figure 5.12 show different **a-Si-based technologies** (a-Si, a-Si/ μ -Si, a-Si/a-Si, a-Si/a-Si/a-Si) monitored at 7 different sites. To reduce the high spread due to the uncertainty of STC power, the PR have first been normalized to match in the warm season. The first two plots at the top of the figure show how the performance ratio PR(Pm) and PR(Isc) display seasonal variations due to the spectrum, with increasing PR values in summer and decreasing values in winter months. In contrast to c-Si modules, the a-Si PV modules display an opposite PR(Pm) seasonal variation, and also demonstrate a seasonal variation of the PR(Isc) value. The spectrum has a significant impact on both the PR(Pm) and PR(Isc) plots. The normalization step leads to a correction of the spectral effects, so that thermal effects can be better analyzed. The two bottom graphs, obtained after the normalization, represent the typical low-irradiance and temperature behaviour of amorphous silicon modules. For the temperature dependency, low insolation days with $H < 1000 \text{Wh/m}^2$ and low temperatures of $T_{\text{bom,w}} < 20^\circ\text{C}$ were not considered, excluding mainly the cold months in which PR is changing due to SWE. The thermal behaviours of the different technologies are surprisingly close to one another, considering that single- and multi-junction modules (both a-Si and μ c-Si) are represented here and that they are operating under very different climatic conditions.

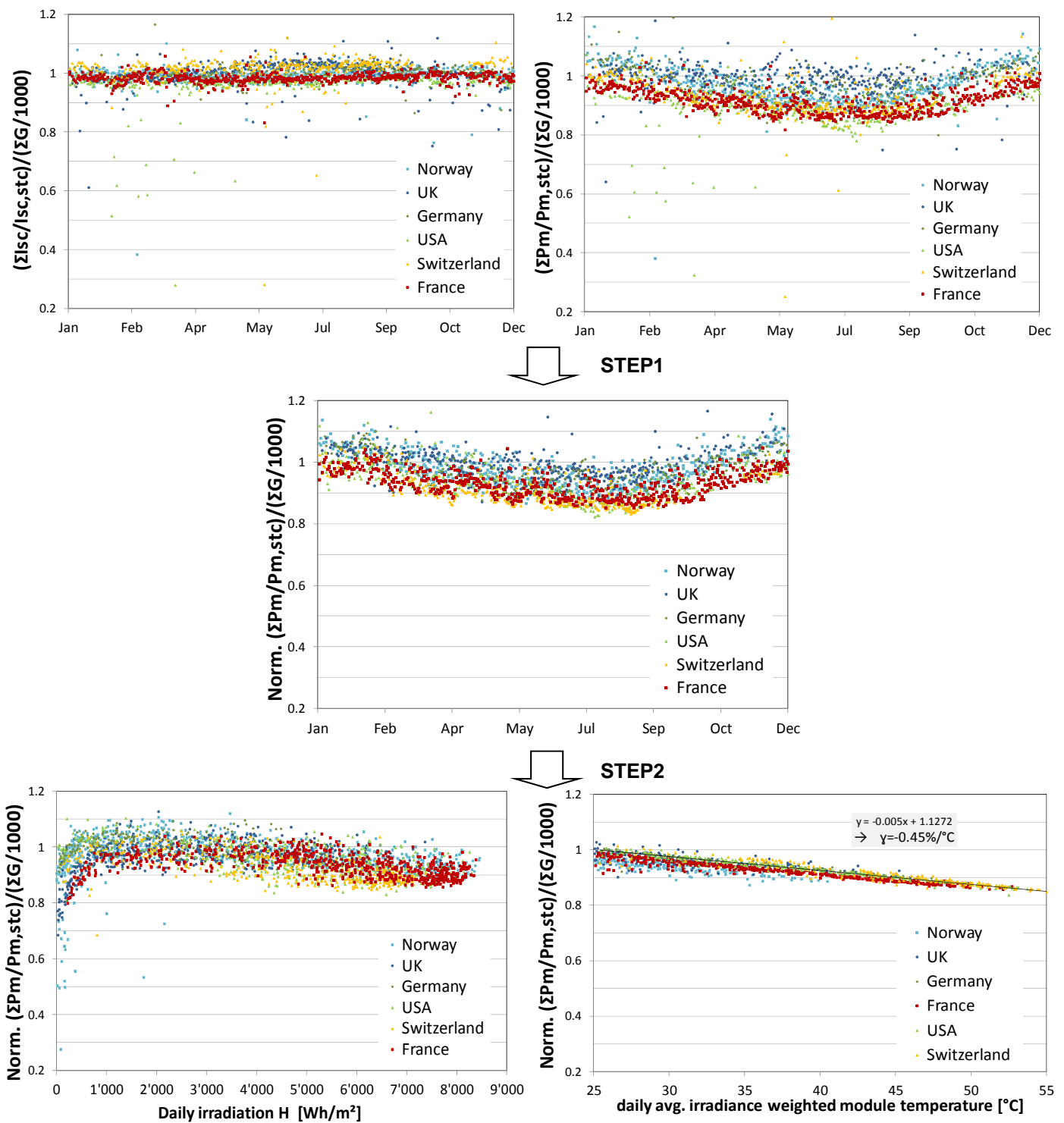


Figure 5.11: Example of analysis approach with daily performance ratio PR(Pm) (top/right) and PR(Isc) (top/left) of 6 different **c-Si modules** measured at different locations. Step 1: merge to normalized performance ratio norm. PR(Pm) and Step 2: plot in dependence of daily irradiation (bottom/left) and of average irradiance-weighted module temperature (bottom/right).

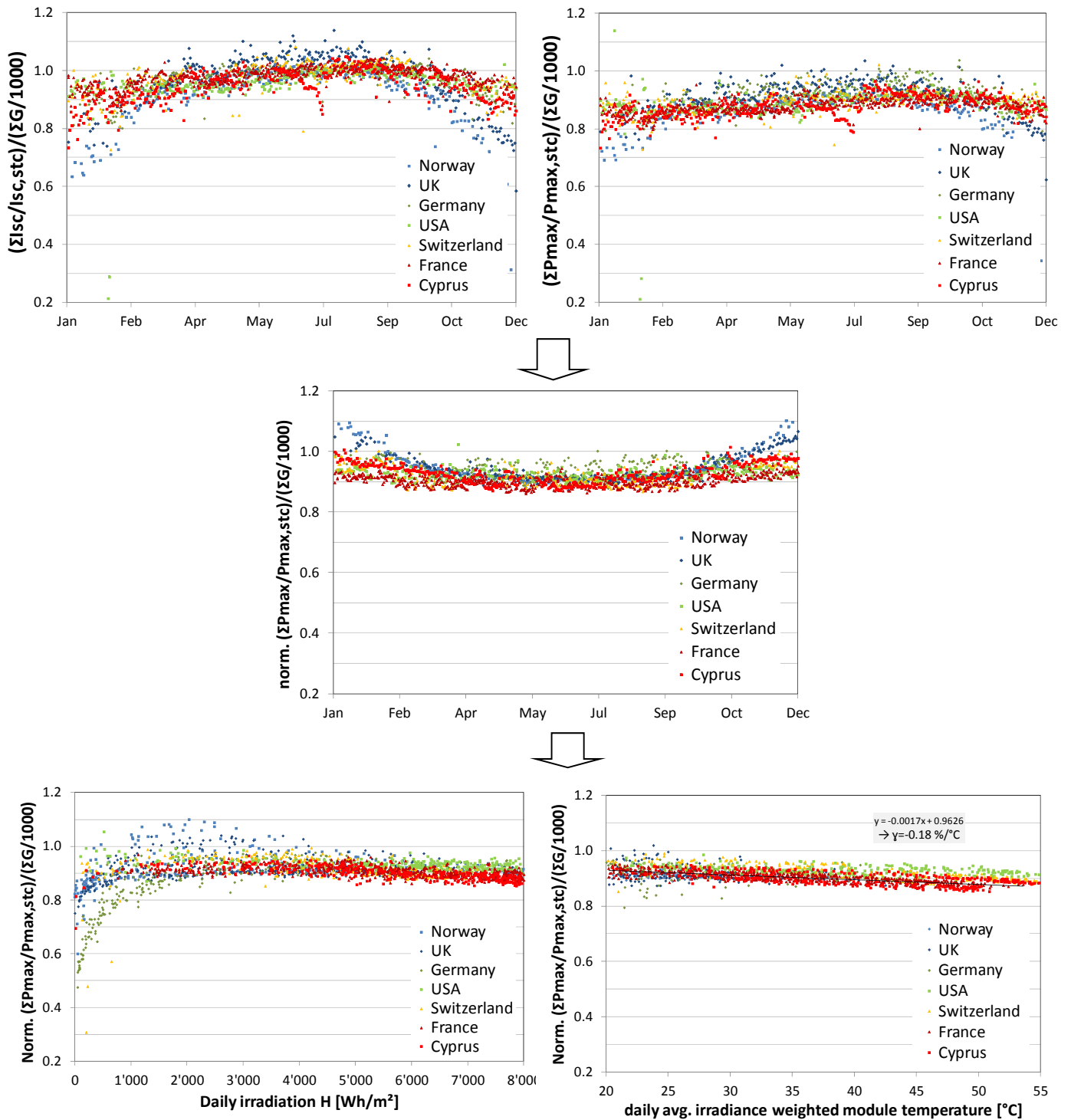


Figure 5.12: Example of analysis approach with daily performance ratio PR(Pm) (top/right) and PR(Isc) (top/left) of 7 different **a-Si-based silicon modules** measured at different locations. Step 1: merge to normalized performance ratio norm PR(Pm) and Step 2: plot in dependence of daily irradiation (bottom/left) and of average daylight module temperature (bottom/right).

6. MODELLING OF THIN FILM OUTDOOR PERFORMANCE

Background:

The energy output of a PV module in operation depends on its response to several external influence factors (irradiance, temperature, spectrum and mounting conditions) and on the stability of the module parameters over time (i.e. STC power, temperature coefficients, low irradiance performance, spectral response). Thin film module manufacturers often claim that their products display a higher performance under diffuse irradiance conditions, a better spectral response or lower temperature coefficient. The validity of these claims can only be verified by separating the contributions of each single effect on the overall energy production of a PV module.

Scope of the project:

- Link performance of indoor modules to that of outdoor modules.
- Evaluate thermal, irradiance, spectral and angular losses and their impact on the energy yield of single PV modules.
- Distinguish between irreversible degradations and seasonal oscillations of some technologies (e.g. amorphous silicon modules).
- Include Staebler-Wronsky degradation in the modelling for a-Si based devices.
- Investigate different spectral modelling approaches (i.e. APE, AM, etc).

Results:

- The implementation of spectral and angle of incidence losses within our models allowed us to distinguish between the single contributions and to better understand the measured differences in outdoor performance.
- The analysis of 4 years of outdoor data for 11 different thin film modules showed that spectral effects are crucial for all thin film technologies, with the highest influence for a-Si-based technologies and lower for a-Si/ μ c-Si. For a-Si/ μ c-Si, the spectral gains in summer are partly compensated for by higher thermal losses and lower thermal annealing (flatter PR trend). CIS and CdTe show a similar trend in PR to c-Si, but with remarkably different contributions from spectral and thermal losses.
- A simplified model, with a daily resolution (PRd), for the modelling of PV modules in operation was developed and validated against 3 years of data for the a-Si and c-Si technologies. The results are very encouraging for these technologies. The extension of this modelling approach to other technologies will be the subject of further work.
- A new approach for the modelling of the Staebler-Wronsky effect for amorphous silicon and different climates was implemented and validated for Lugano.

6.1 Basic equations

Several approaches exist today to describe the performance of PV devices under real operating conditions. These mathematical, electrical, empirical or semi-empirical models generally rely on a large number of input parameters which can be derived by outdoor or indoor characterization or which rely on the manufacturer's specifications for simplified models.

Instantaneous power model

Equation 6.1 describes the basic approach used at SUPSI to describe the power P_m of a module in dependence of the global in-plane irradiance (G) and module temperature (T_{mod}). The module parameters required for the calculation of the outdoor performance are usually extracted from measurements made in the laboratory under controlled testing conditions and are: the STC power (P_{stc}), the two parameters (a and b) extracted by fitting the relative efficiency curve $\eta_{rel}(G)$ calculated according to equation 5.3, and the P_{max} temperature coefficient (γ) expressed in %/°C. G_{stc} is the irradiance at STC, corresponding to 1000W/m².

$$P_m(G, T_{mod}) = P_{stc} \cdot G / 1000 \cdot [1 + a \cdot \ln(G / G_{stc}) + b \cdot \ln^2(G / G_{stc})] \cdot [1 + \gamma \cdot (T_{mod} - 25)] \quad (\text{equation 6.1})$$

In order to improve the modelling for thin film modules, a contribution for the spectral dependency was added to equation 6.1. The first approach, based on airmass (AM), can be applied in the absence of any spectral data. The second approach, requiring the average photon energy (APE) as an input, can be used only if spectral data are available.

$$P_m(G, T_{mod}, AM) = P_m(G, T_{mod}) \cdot [1 + c_1 \cdot (AM - 1.5)] \quad (\text{equation 6.2})$$

$$P_m(G, T_{mod}, APE) = P_m(G, T_{mod}) \cdot [1 + c_2 \cdot (APE - 1.634)] \quad (\text{equation 6.3})$$

The AM is a purely geometrical parameter which can be calculated for any given location. It is related to the length of the sunlight path through the Earth's atmosphere and can easily be calculated by or retrieved from meteorological software tools.

The APE index, described by equation 6.4, is defined as the ratio of the integrated irradiance to the integrated photon flux density. The index gives an idea of how red- or blue-shifted the spectrum is. An index of 1.634eV is achieved for the standard AM 1.5g when integrating the spectrum between 350 and 1600nm.

$$APE = \frac{\int G(\lambda) d\lambda}{q \int \Phi(\lambda) d\lambda} \quad (\text{equation 6.4})$$

How the relative spectral losses (expressed in %/APE or %/AM) are determined is described in Chapter 6.2.

An additional term for the modelling of reflection losses was added. The angular (AOI) correction is applied here to the direct irradiance only, whereas for the diffused irradiance no correction is applied.

$$G = G_{diff} + G_{dir} \cdot [1 + d_1 \cdot AOI^1 + \dots + d_6 \cdot AOI^6] \quad (\text{equation 6.5})$$

For clear days the angular correction is applied directly to the power equation:

$$P_m(G, T_{mod}, AM, AOI) = P_m(G, T_{mod}, AM) \cdot [1 + d_1 \cdot AOI^1 + \dots + d_6 \cdot AOI^6] \quad (\text{equation 6.6})$$

Performance Ratio (PR) model

Equation 6.2 can also be expressed as an instantaneous performance ratio $PR(t)$, the ratio between the instantaneous-measured efficiency $\eta = P_m/G$ and the laboratory-tested efficiency $\eta_{stc} = P_{stc}/G_{stc}$ at STC:

$$PR = \frac{P_m / P_{stc}}{G / G_{stc}} = [1 + a \cdot \ln(G / 1000) + b \cdot \ln^2(G / 1000)] \cdot [1 + \gamma \cdot (T_{mod} - 25)] \cdot [1 + c_1 \cdot (AM - 1.5)] \quad (\text{eq 6.7})$$

The normalization of the measured power P_m by P_{stc} and G allows the comparison of modules with different STC powers and modules exposed to different irradiances (different time frame, location or orientation).

By averaging over a full day we obtain the daily performance PR_d , which is defined as:

$$PR_d = \frac{E_d / P_{stc}}{H_d / G_{stc}} = \frac{\int P_m(t) / P_{stc} dt}{\int G(t) / G_{stc} dt} \quad (\text{equation 6.8})$$

where E_d (Wh) and H_d (Wh/m²) are, respectively, the daily energy production of the module and the daily insolation to which the module is exposed.

For clear days the angular correction can again be directly applied to the PR equation, and the clear sky daily performance ratio PR'_d can be written as:

$$PR'_d = \frac{\int G \left[1 + a \ln(G/1000) + b \ln^2(G/1000) \right] \cdot \left[1 + \gamma(T_{mod} - 25) \right] \cdot \left[1 + c_1(AM - 1.5) \right] \cdot \left[1 + d_1 AOI^1 + \dots + d_6 AOI^6 \right] dt}{\int G dt} \quad (\text{equation 6.9})$$

In the *simplified model* described below (see Chapter 6.4), the instantaneous values G , T_{mod} , AM and AOI are replaced by daily irradiance average values for the same parameters weighted on the irradiance profile (G_w , $T_{mod,w}$, AM_w and AOI_w). The equation reduces to:

$$PR'_d = \left[1 + a \ln(G_w / 1000) + b \ln^2(G_w / 1000) \right] \cdot \left[1 + \gamma(T_{mod,w} - 25) \right] \cdot \left[1 + d_1(AM_w - 1.5) \right] \cdot \left[1 + c_1 AOI_w^1 + \dots + c_6 AOI_w^6 \right] \quad (\text{equation 6.10})$$

The weighted values are calculated by multiplying the single parameter (as a function of daytime) by the irradiance profile $G(t)$ and normalizing over the full insolation of the day. Here we show an example for the module temperature T_{mod} .

$$T_{mod,w} = \frac{\int T_{mod}(t) \cdot G(t) \cdot dt}{\int G(t) \cdot dt} \quad (\text{equation 6.11})$$

The same approach is used for all other parameters. For the thermal and spectral components, the use of weighted values is equivalent to the use of instantaneous values, whereas this is a simplification for the angular and irradiance components. However, these latter components, as will be shown later, have a limited influence on clear days and optimally-oriented modules. The calculations with instantaneous values are expected to have a higher accuracy and to be independent of the day type or orientation of the module, whereas the simplified model has the advantage of being less computing intensive, though still quite accurate.

The equations 6.9 and 9.10 can also be expressed as:

$$PR_{d,clear} = \int G \cdot \varepsilon_G \cdot \varepsilon_T \cdot \varepsilon_{AM} \cdot \varepsilon_{AOI} / \int G \quad (\text{equation 6.12}) \text{ or}$$

$$PR_{d,clear} = \varepsilon_{w,G} \cdot \varepsilon_{w,T} \cdot \varepsilon_{w,AM} \cdot \varepsilon_{w,AOI} \quad (\text{equation 6.13})$$

where we define ε as a performance factor which determines the loss in performance with respect to STC conditions for each impact factor ($x=G$, T_{mod} , AM and AOI). The specific loss factors L_x , as calculated in Chapter 6.3, are defined as:

$$L_x = \varepsilon_x - 1 \quad (\text{equation 6.14})$$

6.2 Spectral modelling

Two different approaches were tested within the project: the Airmass (AM) and the Average Photon Energy (APE) approach. The AM approach can also be applied in the absence of any spectral data and could be applied in this way to model the full 4-year data set, whereas the APE requires spectral data as input.

Airmass (AM) model

The AM dependence was modelled, according to [PMTHIN 20], using the measured SRs of the modules and the global irradiance spectral data for the Lugano testing site generated with the application SMARTS (*Simple Model of Atmospheric Radiative Transfer of Sunshine*) developed by Gueymard (see Figure 6.1). Values of between AM 1 and 3 (the yearly range of oscillation of AM at solar noon for Lugano) were used in the calculation. The short-circuit current I_{sc} of the test devices as a function of AM is calculated as:

$$I_{sc} = \int E_{\lambda}^{AM}(\lambda) \cdot SR(\lambda) \cdot d\lambda \quad (\text{equation 6.15})$$

where $SR(\lambda)$ is the spectral response of the test devices, and $E_{\lambda}^{AM}(\lambda)$ is the spectral irradiance of the sunlight for different AM values weighted at 1000 W/m^2 . This variation in the I_{sc} is expected to be directly translated into variations of the power of the device. Figure 6.10 shows two examples of linear dependencies of a c-Si and a single-junction amorphous-silicon module as calculated with this approach.

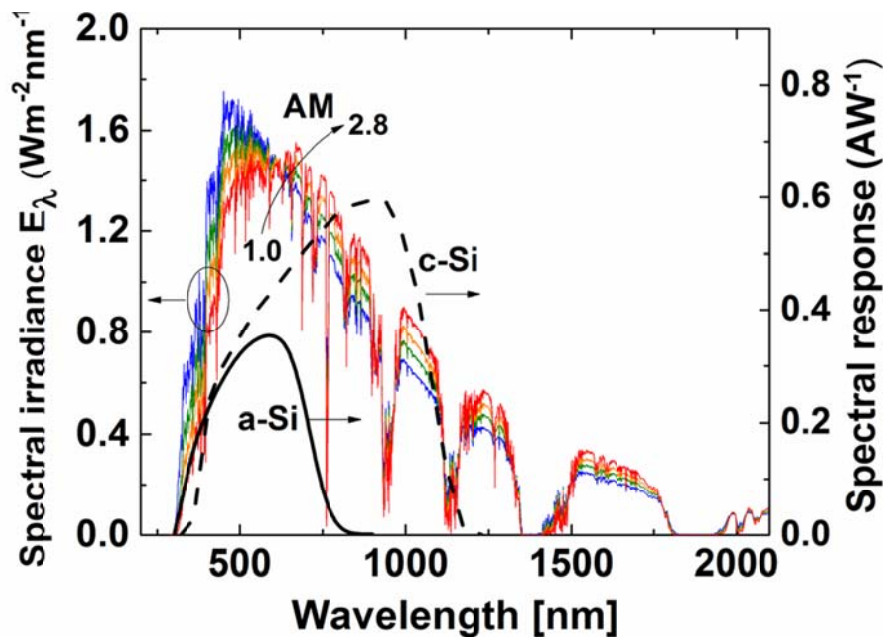


Figure 6.1: Sun spectra - weighted at a total irradiance of 1000 W/m^2 - generated as a function of AM values with SMARTS. For more clarity, only AM 1, 1.5, 2, 2.3 and 2.8 spectra are shown, illustrating a shift towards the red/infra-red for higher AM-values. SR data used to model the AM dependence of the a-Si and c-Si modules under investigation are also shown.

Average Photon Energy (APE) model

The APE dependence was determined by using the spectral irradiance data measured with the EKO MS-710/712 as input (see Chapter 5.1). The APE was calculated for each minute according to equation 6.4. The next step was to plot the temperature- and irradiance-corrected P_{max} values (1000 W/m^2 and 25°C) versus APE. The values were limited to $950 \text{ W/m}^2 < G < 1050 \text{ W/m}^2$ and values with good irradiance and thermal stability. A linear fit was performed on the data and the slope was determined. The slope corresponded to the parameter (c) required for the calculation of $P(G, T_{mod}, APE)$ according to equation 6.3. Figure 6.2 shows an example for one of the a-Si modules. $P_{max,corr}$ is here normalized to

the value at APE=1.634. Due to the very short time period (July to September) of these data and the limitation to 1000W/m², the APE range covered is very limited. A high linearity is obtained.

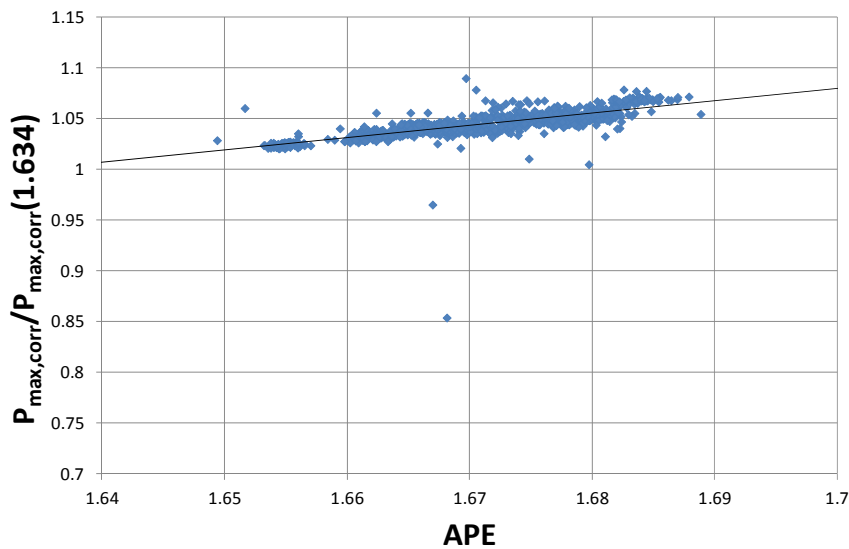


Figure 6.2: Normalized $P_{\max,corr}$ versus APE with linear fit for a single-junction a-Si module..

Figure 6.3 shows the calculated linear dependency for all the modules of the cycle 12 measurement campaign. The narrower the spectral response of the module technology, the stronger the spectral dependency becomes, and consequently the greater the slope of the lines. The typical changing slope at APE=1.634, when the current limitation changes from one sub-cell to another, is not visible here, as only APE values above 1.634 were available for the linear plot.

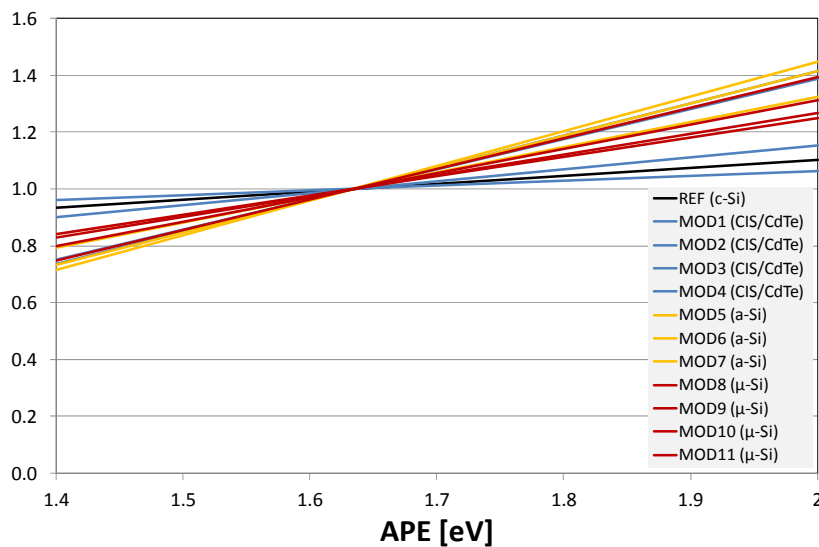


Figure 6.3: Calculated APE dependencies for all test cycle 12 modules.

The spectral modelling approach based on the average photon energy (APE) was validated on a set of data. Figure 6.4 shows the differences between measured and calculated energy yield, with APE (in red) and without APE (in blue), and how the results are influenced by correcting the original reference STC power to the value determined from the linear fit at APE=1.634 (in green). The inter-comparison of spectrally uncorrected data shows that in summer the spectral effect contributes up to 4% for a-Si (single- and multi-junction), a bit less for a-Si/ μ c-Si and below 1% for CIS (CuInS₂) and CdTe. For c-Si and broadband CIS (CuInGaSe₂ and Cu(InGa)(SeS)₂) technologies the effect is almost negligible.

The difference between measured and calculated values diminished significantly for some of the technologies when corrected with APE and increased significantly for all micromorph technologies. A closer look at the mean bias (mbd) and random mean square error (rmsd) highlighted that most of the deviations are due to offset errors. The offsets are probably due to: (1) the change of STC power of a-

Si based technologies due to annealing and the subsequent difficulty in defining an appropriate reference power P_{ref} , (2) the meta-stabilities in CIS and CdTe modules which influence the indoor measurements and, to a minor extent, (3) the mismatch error as calculated and listed in Table 5.5. By utilizing the STC power determined from the linear fit at $APE=1.634$ instead of the original reference power, the deviations were reduced to $\pm 1\%$ (green bars). The energy yield of the a-Si/ μ c-Si modules is also probably slightly underestimated due to the fact that the change in current limitation from bottom (μ c-Si) to top (a-Si) cell is not considered. The effective losses under red shift conditions ($APE < 1.634$) are therefore probably higher than those depicted in Figure 6.3.

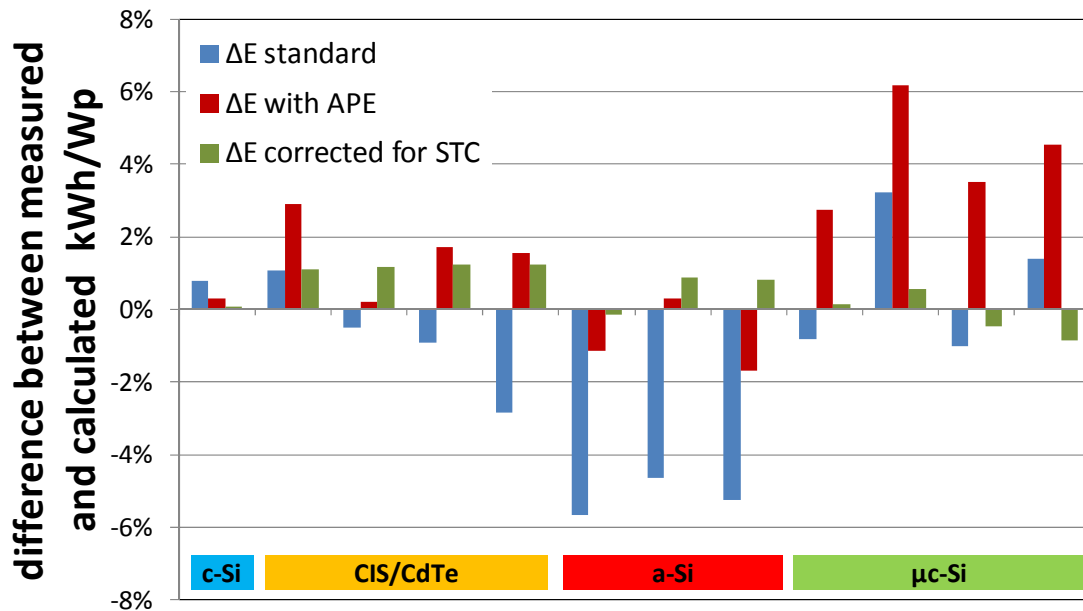


Figure 6.4: Differences between measured and predicted energy yield for the 3 months July-September 2012. Legend: (blue bars) basic approach considering only the parameters a, b, c and d; (red bars) advanced modelling with APE; (green bars) advanced modelling with index and STC power extracted from the linear interpolation of P_{max} versus APE.

6.3 Loss factor analysis

In addition to a better understanding of the outdoor performance, the goal of a loss factor analysis is to improve the translation from indoor to outdoor performance data. The separation of the single losses allows us to distinguish between spectral, degradation and/or meta-stability effects, as well as SWE within amorphous silicon. Starting from instantaneous data, daily optical (L_G , L_{AOI} and L_{AM}) and thermal losses (L_{Tmod}) were calculated for each module, according to the equations described in Chapter 6.1. The module parameters used for the calculations are summarized in Table 5.6. The same angle of incidence behaviour, for which data were taken from the literature, was assumed for all modules.

Figures 6.5 to 6.7 show three examples of loss factors calculated for: a CIGS (CIS1), an a-Si/ μ c-Si (μ -Si4) and an a-Si (a-Si1) module respectively. By counter-applying the losses to the measured PR values, one could theoretically extrapolate the STC power (P_{stc}) of the module and its evolution over time. If no degradation occurs over time, the corrected (and normalized) STC power should be equal to 1, without any measurement uncertainties. Part b of the figures shows the normalized daily average P_{stc} values of the module together with its indoor-measured STC power (red dots). In Figure 6.5b the data for the c-Si reference module were added to show how close it is to 1 for a stable module and low measurement uncertainties.

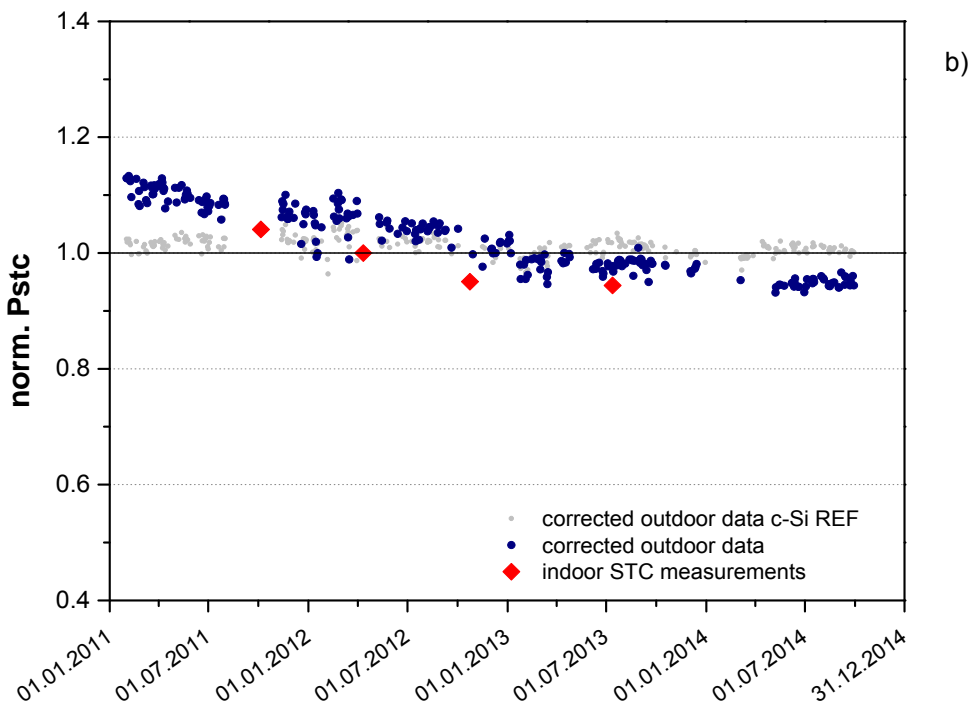
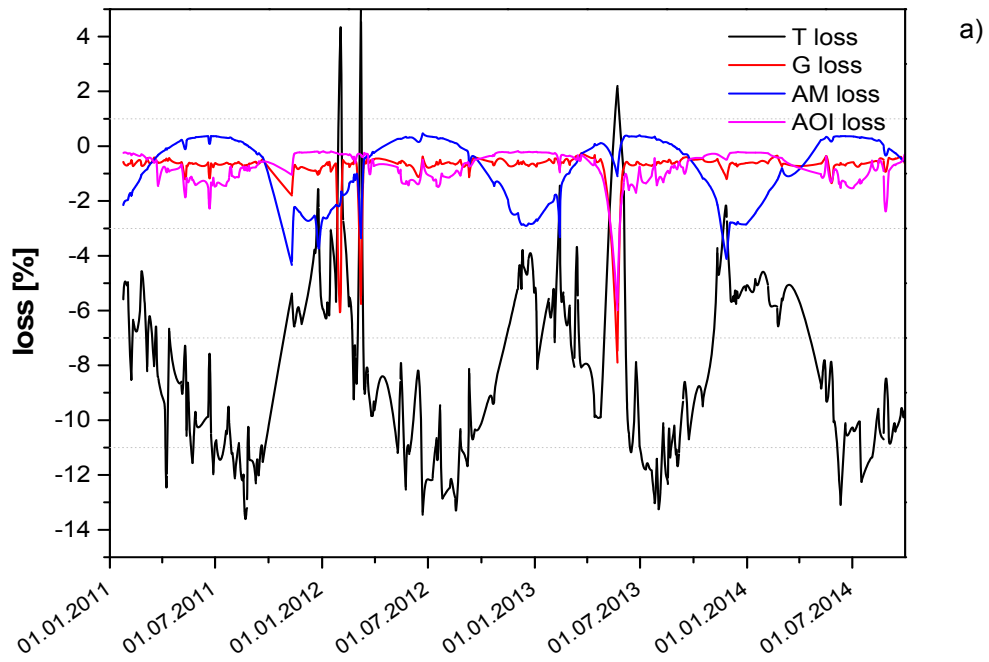


Figure 6.5: (a) Seasonal variation of the calculated performance losses: temperature, irradiance, angle of incidence and spectrum. (b) Indoor- and outdoor-determined STC power over time for a CIS module (CIS1) and in grey for the c-Si reference module.

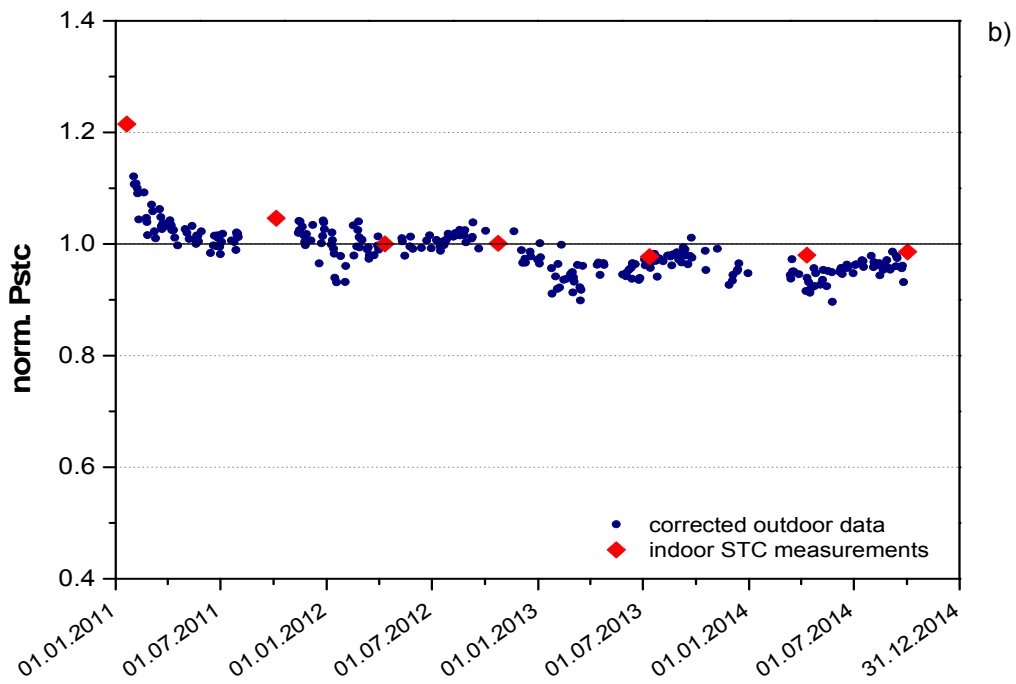
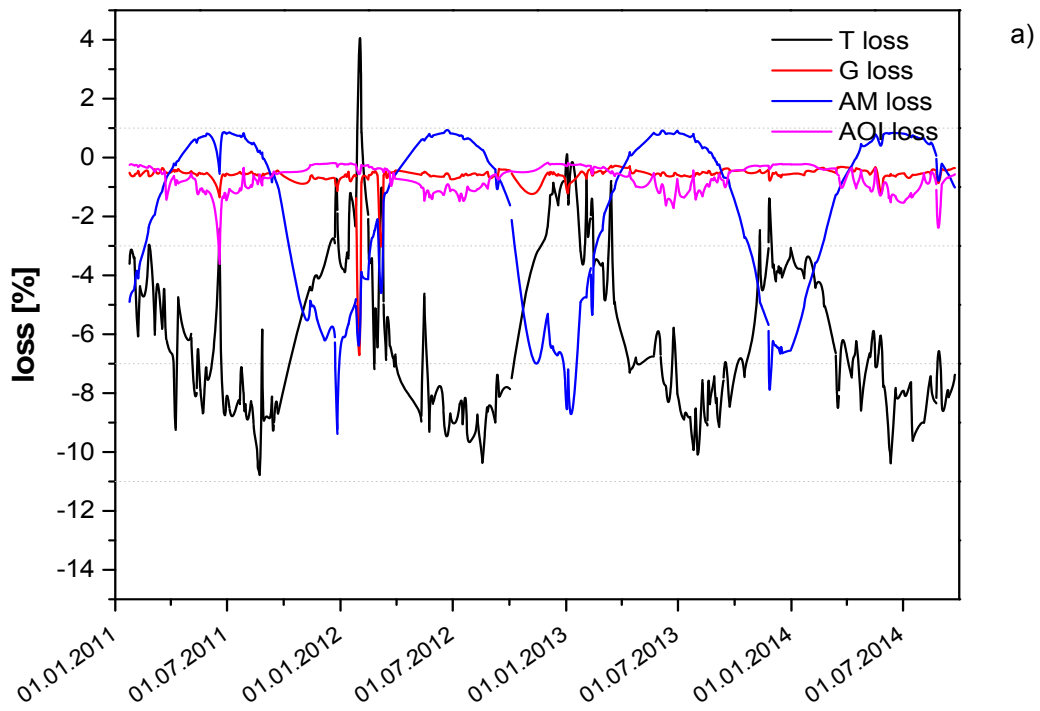


Figure 6.6: (a) Seasonal variation of the calculated performance losses: temperature, irradiance, angle of incidence and spectrum. (b) Indoor- and outdoor-determined STC power over time for an μ -Si module (μ -Si4).

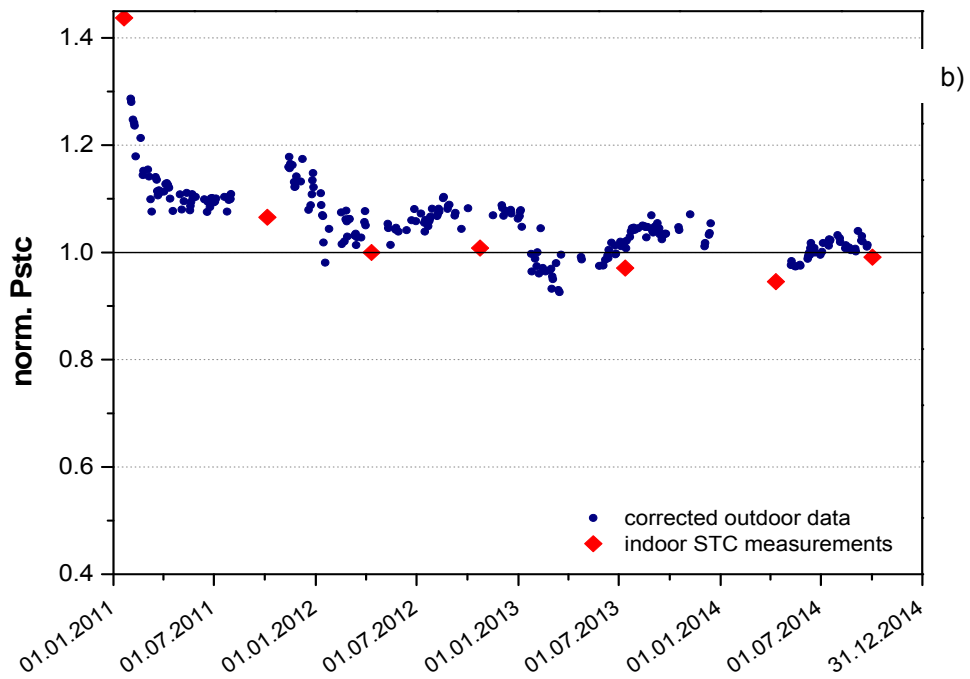
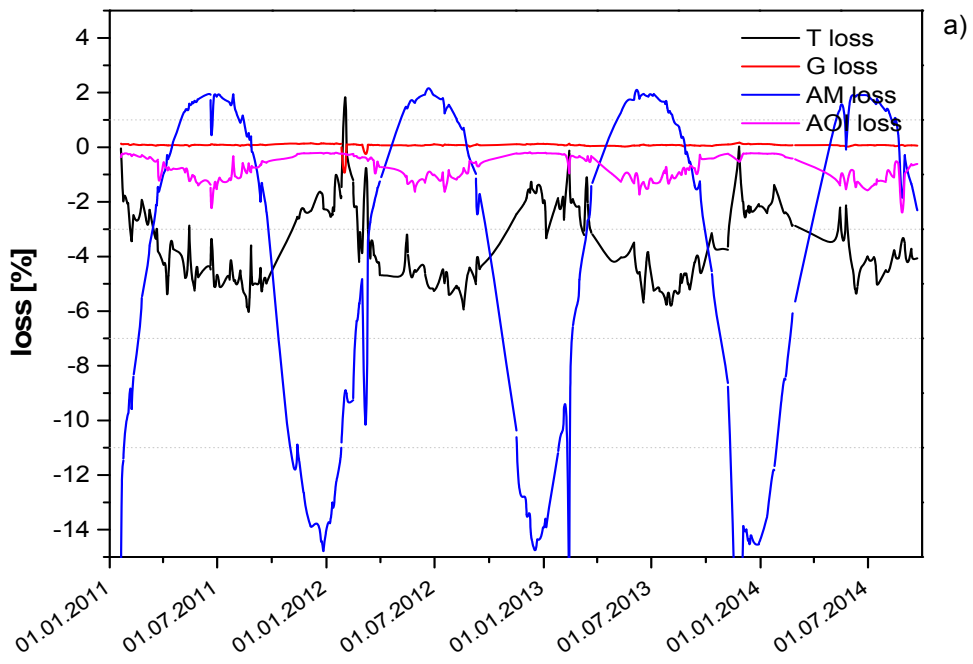


Figure 6.7: (a) Seasonal variation of the calculated performance losses: temperature, irradiance, angle of incidence and spectrum. (b) Indoor- and outdoor-determined STC power over time for an a-Si module (a-Si1).

The loss analysis of 4 years of outdoor data from 11 different thin film technologies showed that spectral effects are crucial for all technologies, with the highest influence for a-Si based technologies and the lowest for μ c-Si. For μ c-Si, the spectral gains in summer are partially compensated for by higher thermal losses and lower thermal annealing, resulting in flatter PR curves (see Figure 5.8). CIS and CdTe have a similar PR trend to c-Si (no Staebler-Wronsky effect), but with different contributions from spectral and thermal losses. In general, losses at low irradiances play a major role under cloudy conditions and cannot, therefore, be neglected in the annual performance analysis.

Degradation/meta-stability seems to be an issue in many of the thin film technologies investigated in this work. Figure 6.5 shows an almost constant degradation over the first two years for the module CIS1, with a slightly reduced degradation afterwards. Outdoor and indoor data show a similar trend. The a-Si 1 and μ -Si 4 modules show a clear negative trend (degradation), in combination with a seasonal variation due to the Staebler-Wronsky effect for the two amorphous silicon technologies. The separation of seasonal variations from long-term degradations is difficult to quantify here, but a slight negative trend is visible, which could be explained by only a partial recovery, which leads to an effective efficiency loss over time.

6.4 Simplified model with aggregate inputs

6.4.1 Model description

A novel simplified model, which is used to model the energy performance of PV modules in operation with a daily resolution [REF 6.1], was developed within the framework of the PM-THIN project. The simplified model, rather than examining the instantaneous power, focuses on the *larger picture* and attempts to provide a description of the daily energy performance of the device (PR_d). This allows us to introduce a number of simplifications: it reduces the number of input parameters; it does not make reference to any electrical circuits (1- 2-diode models) and, most notably, manages much smaller data sets, i.e. daily values versus instantaneous values with a resolution of minutes. The conceptual diagram of Figure 6.8 summarizes and clarifies the logic behind the model, which is used to describe the daily average performance ratio PR_d of a PV module for days of clear-sky conditions.

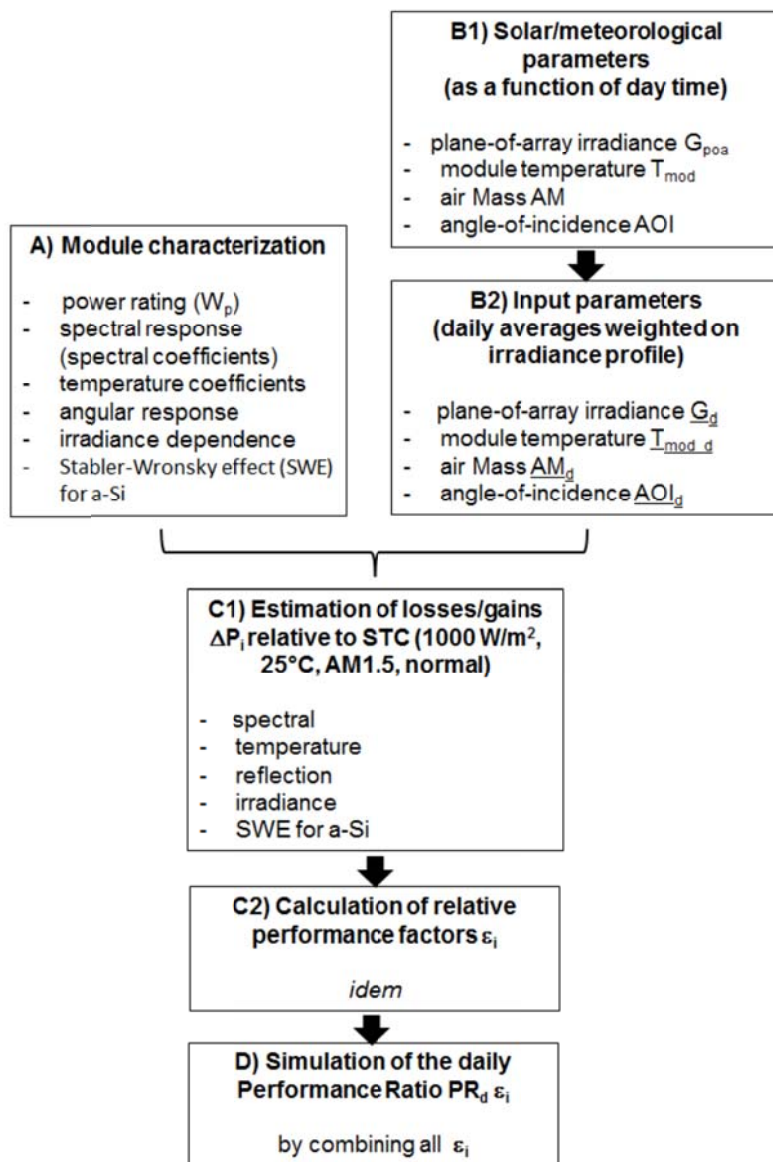


Figure 6.8: Conceptual schema summarising and clarifying the logic behind the model.

Due to the great amount of noise and scatter, *cloudy* and *overcast* days are filtered, allowing us to recognize a clear trend in the measured PR_d data. The model only focuses, therefore, on days of clear-sky conditions and on 4 *loss/gain mechanisms*: (1) *temperature*, (2) *spectral-effects*, (3) *reflection*, (4) *irradiance*, with the addition for *a-Si* of the *Staebler-Wronsky effect* (SWE), i.e. an intrinsic degradation/regeneration of the electrical properties of the semiconductor (typical of amorphous Si) promoted by exposure to light/thermal annealing.

Input parameters

As described by equation 6.11, the inputs for our simulations are *daily aggregate data* weighted on the irradiance profile for the temperature of the module (T_{mod}), the air mass (AM), the angle-of-incidence (AOI), and the irradiance G . AM and AOI (with respect to the module's normal) are geometrical parameters which can be calculated for any given location or retrieved from software applications. In this work T_{mod} , the ambient temperatures T_{amb} , and the plane-of-array irradiance G are directly monitored. As these parameters are instantaneous values, the idea of focusing on aggregate values - weighted on the irradiance profile - reflects the fact that in a single day the energy generation of a solar module is perfectly phased with the irradiance profile, so that values of T_{mod} , AM, AOI, and G are given a higher weight around solar noon when the energy production reaches a maximum. Figure 6.9 shows daily values of AOI and AM, respectively, and G_{poa} at a 45° -tilt at winter/summer solstices and at the equinoxes for Lugano ($46^\circ 0' \text{N}$, $8^\circ 57' \text{E}$, 273 m). On clear days, AM values reach a minimum when the sun is at the Zenith and a maximum when the sun is at the Horizon. An increase towards larger AM is associated with a red shift in the solar spectrum, whereas lower values of AM correspond to an increase in the blue component of the sun spectrum.

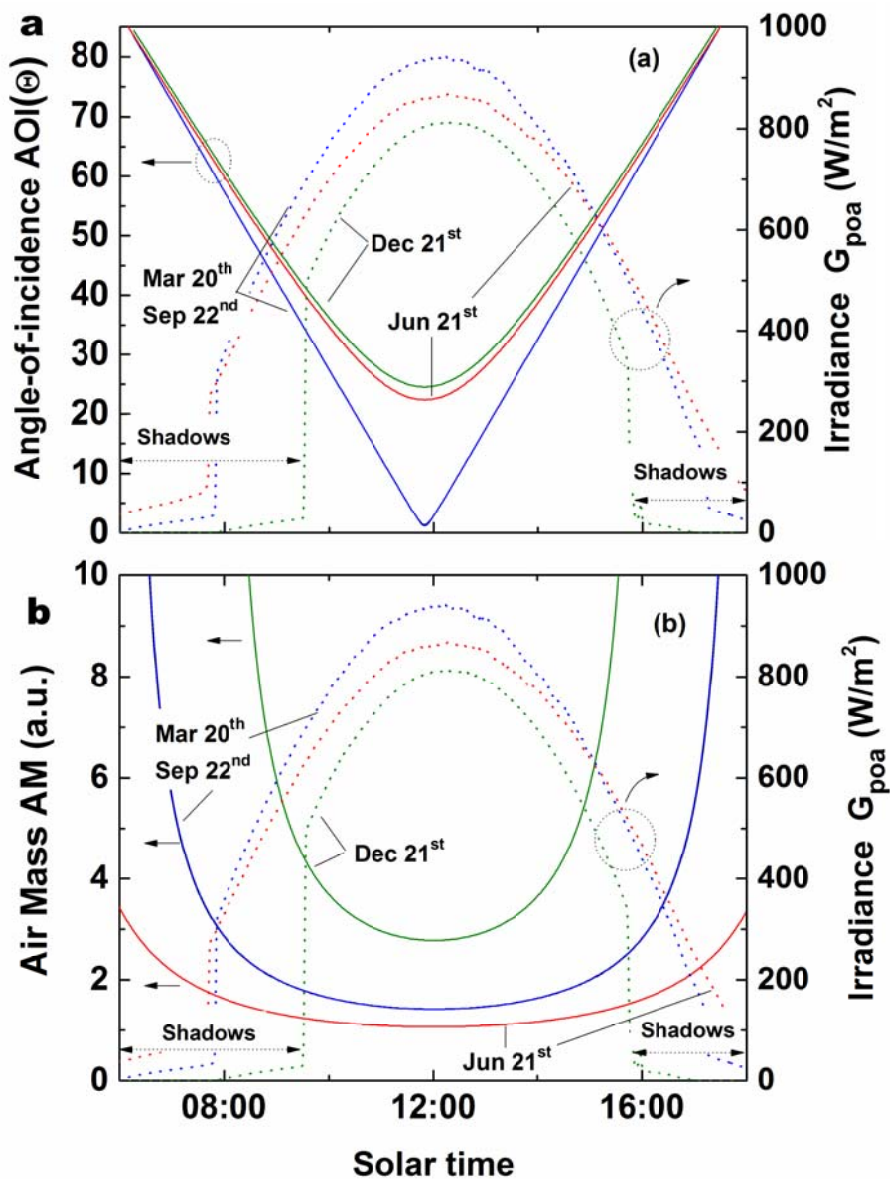


Figure 6.9: Solar input parameters: simulated daily (a) angle-of-incidence AOI and (b) air-mass AM values at winter/summer solstices and at the equinoxes in Lugano. The measured plan-of-array global irradiance G_{poa} at a 45° -tilt for the same days is also shown, and is used to calculate *daily weighted average* values for these parameters.

Module characterization

As for the device, the model requires a full characterization of the device under testing: (1) power at STC, (2) temperature coefficients, (3) spectral (SR) and (4) angular response, and (5) irradiance dependence. So far, the model does not predict any variation of the temperature coefficient with irradiance. Figure 6.10 shows the temperature coefficient and spectral dependence of the performance on the air mass AM for two modules taken as examples for the demonstration of the model.

Due to the much narrower spectral sensitivity of a-Si as compared to c-Si (in the range ~300–800 nm and ~300–1100 nm respectively), this technology is strongly affected by variations in the incident spectrum, rather than simply by a change in the total irradiance. It therefore significantly loses power when the light turns red-rich ($\alpha_{sp} = -6.44 \text{ \%/AM}$, from a linear fit to the data of Figure 6.10 a). An opposite trend, though lower in magnitude, ($\alpha_{sp} = +2.05 \text{ \%/AM}$), is observed for c-Si. It should be noted that in the AM range under consideration I_{sc} has a linear dependence on AM, a relation that does not necessarily hold for higher AM values [REF 6.3].

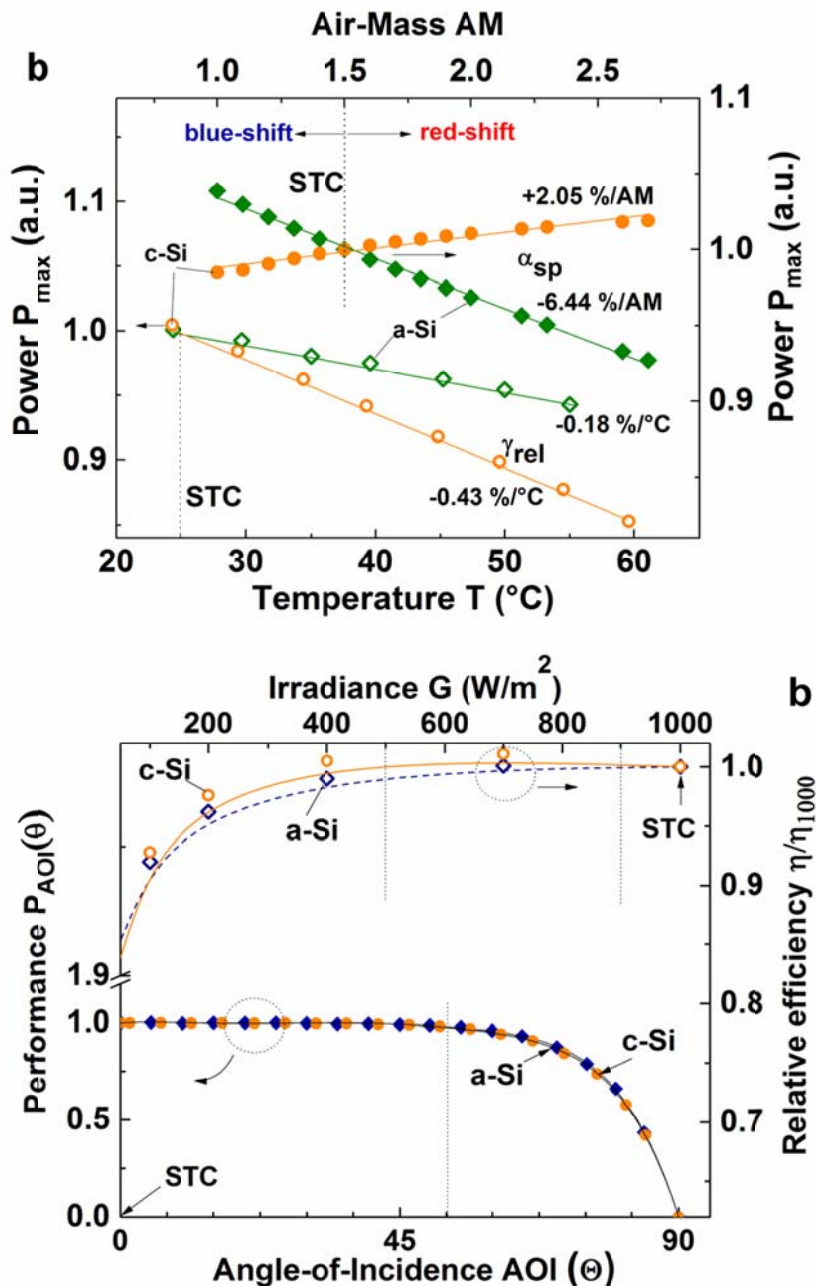


Figure 6.10: a) Indoor-measured temperature and simulated air mass AM dependence of the performance of a-Si and c-Si modules. b) Modules' performance versus angle-of-incidence (AOI) used to model reflection losses and indoor-tested irradiance dependence for the a-Si and c-Si devices.

The input to model *reflection losses* is the module's performance P_{AOI} (power or current) versus AOI. The literature values for conventional flat panel devices with conventional untextured front glasses are used here [REF 6.4]. As Figure 6.10 b) shows, $P_{AOI}(\Theta)$ is well fitted by a 6th-grade polynomial. For values of AOI in the range 0-50°, reflection losses can be quasi-neglected ($\leq 1\%$). Furthermore, Figure 6.10b) presents the indoor-tested *low-irradiance* behaviour of the two devices under testing. Both are nearly flat in the range 400-1000 W/m².

6.4.2 Losses/gains and relative performance factors

Relative daily average *performance losses* (or *gains*) ΔP_i with respect to STC (in %) for each device and single contribution were then modelled by inserting the input parameters into the following expressions:

(1) Spectral losses/gains

$$\Delta P_{sp}(AM) = [P(\underline{AM}_d) - P(1.5)] / P(1.5) = \alpha_{sp} \cdot (\underline{AM}_d - 1.5) \quad (\text{equation 6.16})$$

(2) Temperature losses/gains

$$\Delta P_{temp}(T) = [P(\underline{T}_{mod_d}) - P(25)] / P(25) = \gamma_{rel} \cdot (\underline{T}_{mod_d} - 25) \quad (\text{equation 6.17})$$

(3) Reflection (AOI) losses

$$\Delta P_{AOI}(\Theta) = [P(\Theta) - P(0)] / P(0) \quad (\text{equation 6.18})$$

with $\underline{AOI}_d = \Theta$ and $P_{AOI}(\Theta)$ defined in equation (3)

(4) Irradiance losses/gains

$$\Delta P_G(G) = [P(\underline{G}_d) - P(1000)] / P(1000) \quad (\text{equation 6.19})$$

with $P(G) = \eta(G) \cdot G$ and G defined in equation (4)

(5) SWE losses/gains

For amorphous silicon devices, we need to consider seasonal oscillations of the performance of the device which are directly related to SWE. Previous works have reported that this seasonality for a-Si-based devices in Lugano (and other neighbouring locations) can be modelled with $\pm 4\%$ amplitude fluctuations around a yearly average value [PMTHIN 20, PMTHIN 21, REF 6.1]. This trend, described relatively well by a sinusoidal or 4-th grade polynomial, reaches a maximum in late summer (i.e. mid-August/early-September) and a minimum in wintertime (i.e. February).

It is understood that a correct trend describing SWE strongly depends on the actual meteorological conditions and on a relatively long time scale. This behaviour could, therefore, vary from year to year and from one device to another. Particularly prolonged cold/rainy or, conversely, hot periods would affect the symmetry of the SWE curve used to model losses/gains related to these phenomena without, however, having a major impact on the amplitude or on the time phase (maxima/minima) of the oscillations. We are therefore confident that the trend shown in Figure 6.11 provides a reasonable approximation of the oscillatory phenomenon for our testing site. Previous works have attempted to model the SWE for different locations in Europe and Africa based on local meteorological data series (see e.g. PMTHIN 19)

These contributions (ΔP_i plus SWE) are then translated into five distinguished *relative performance factors* ε_{sp} , ε_T , ε_{AOI} , ε_G , ε_{SW} (with $\varepsilon_i = 1$ corresponding to the performance at STC), which coupled express a *relative combined performance factor*, where $\varepsilon_i = (100 + \Delta P_i) / 100$; e.g. a power loss of 10% relative to a given temperature deviation from 25°C would correspond to $\varepsilon_T = 0.9$. For c-Si (or technologies other than a-Si) ε_{SW} is set to 1 or simply neglected.

Modelled losses/gains

Figure 6.11 illustrates *daily weighted average* values for days of clear-sky conditions from October 1st, 2011 to April 1st, 2013 (12 ± 3 months) for \overline{AM}_d , \overline{AOI}_d , (a-Si and c-si), and \overline{G}_d with the addition of $\overline{T}_{amb,d}$. For both devices, the difference between $\overline{T}_{mod,d}$ and $\overline{T}_{amb,d}$ is nearly constant over the year and approximately equal to $22^\circ\text{C} \pm 3^\circ$ (for clear days).

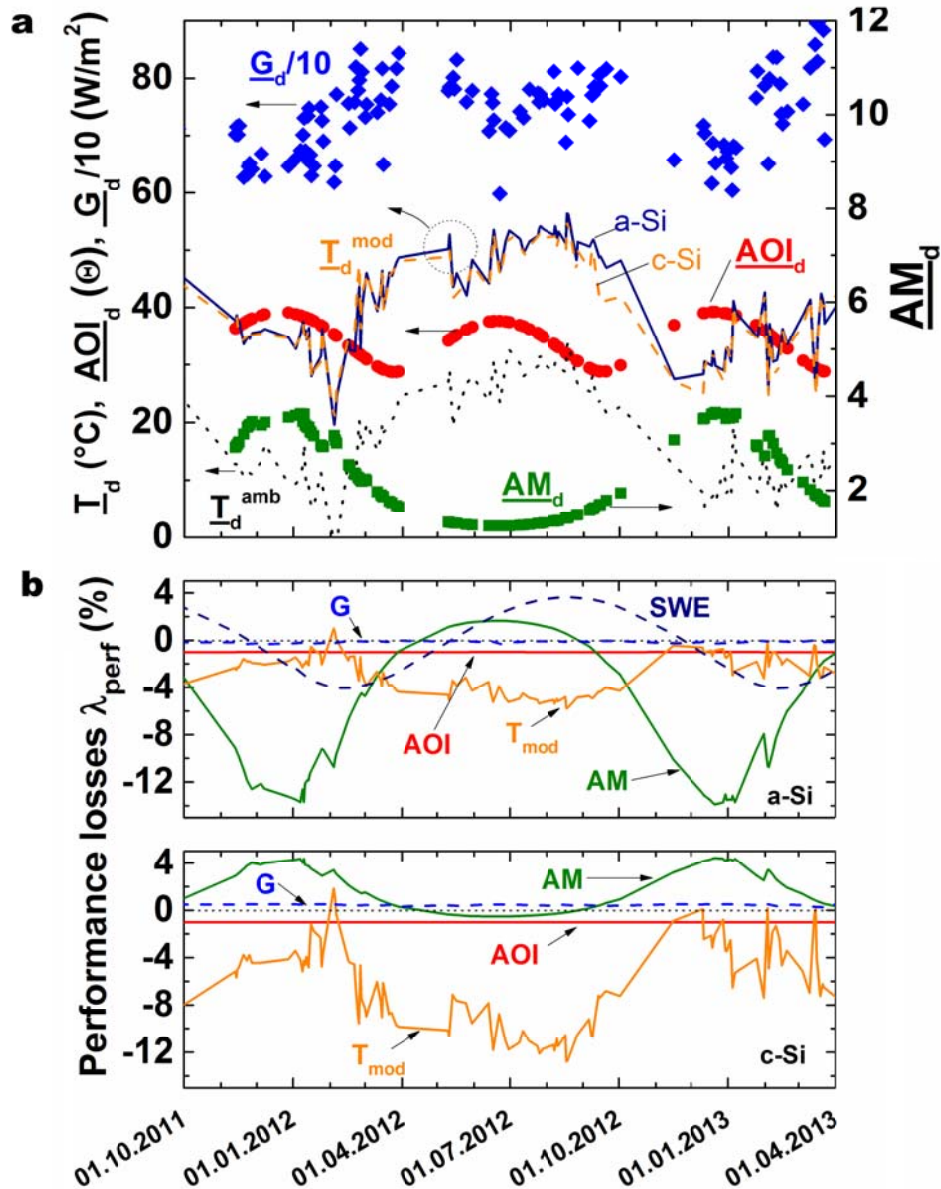


Figure 6.11: **a)** *Daily weighted average* values for the angle-of-incidence \overline{AOI}_d , the air-mass \overline{AM}_d , and the irradiance \overline{G}_d ($\overline{G}_d/10$) for days of clear-sky conditions from October 1st, 2011 to April 1st, 2013 (12 ± 3 months). Furthermore, the temperatures $\overline{T}_{mod,d}$ for the investigated modules (a-Si and c-Si) are shown together with daily weighted average *ambient temperatures* $\overline{T}_{amb,d}$. Missing data correspond to periods for which the acquisition system was not working properly or in which the modules were removed for indoor control testing. **b)** Distinguished contributions to *performance gains/losses* - relative to STC conditions - for a-Si and c-Si solar for the same period: (1) spectral effects (AM), (2) temperature (T_{mod}), (3) reflection (AOI), (4) irradiance (G), and (5) Staebler-Wronsky effect (SWE) for a-Si.

Using Equations 6.16 to 6.19 (and the SWE contribution for a-Si), the solar and temperature input parameters for the same period are translated into *relative performance losses/gains* for the devices under testing, which are shown in Figure 6.11b.

Spectral losses/gains for both technologies are perfectly harmonized with the solar phases (solstices), but are countercyclical. The red shift of the sun spectrum in *winter* induces pronounced losses (down to -12% compared to STC) in the performance of a-Si and a moderate gain for c-Si (~+4%). Contrarily, the blue shift of the sun spectrum induces a modest gain at *summer* solstice for a-Si (~+2%) and very modest losses for c-Si (-0.8%).

Temperature losses are naturally predominant in summer, and - due to the low temperature coefficients - limited to ~-4% for a-Si. Losses become much more severe (threefold) for c-Si, whereas *gains* in wintertime are practically negligible for both technologies, reflecting the fact that *daily weighted average module temperatures* $T_{mod,d}$ for both technologies on clear days reach values of ~20°C even on the coldest winter days (see Figure 6.11a).

As values of AOI_d for both devices (at a 45° tilt) vary between 30° and 40° over the course of the year (see Figure 3b), average *reflection losses* are nearly constant all year long (~-1.1%).

In the same way, we plot *irradiance losses/gains* which, due to the relatively high values of G_d (~570-900 W/m²) for days of clear-sky conditions in Lugano and to the good *irradiance dependence* of both devices (see Figure 3b), are nearly negligible over the whole year for a-Si (i.e. oscillating between -0.4% and -0.05%) and for c-Si (i.e. oscillating between +0.2% and +0.5%).

In addition, Figure 6.11 illustrates the modelled *SWE contribution* for the a-Si module.

Measured versus simulated PR_d

Field-measured *daily performance ratio* PR_d values (clear-sky conditions) for the full monitoring period are shown in Figure 6.12a together with the modelled *relative combined performance factor* ϵ_{comb} .

For a-Si, a typical seasonal behaviour can be observed, with a maximum around August and a minimum in February. Maxima and minima originate mainly from the super-position of spectral and SWE phenomena, which are clearly distinguished but act in similar time-phases (see Figure 6.11b) and Ref. [PMTIN 20]), and to a lesser extent from temperature effects.

Besides the very steep decrease (>20%) for PR_d in the first three months of operation (SWE), the model fits the measured data for year 2012 well, whereas it slightly underestimates and overestimates data for years 2011 and 2013 respectively. We believe that this discrepancy could be an indication of an intrinsic degradation of the module's performance and, in particular, of the electronic properties of the amorphous silicon *pin* junction. In principle, by using a non-constant value for P_{max} in Eq. (1), but different average P_{max} values for each year (i.e. a higher value for year 2011 and a lower one for 2013 consistent with an expected long-term degradation of the module's performance), the model would also come closer to the measured PR_d for years other than 2012.

In order to highlight what we believe to be a long-term degradation, we prefer to avoid applying to the data of Figure 6.12a-b the year-to-year compensation of P_{max} in calculating PR_d (this is later applied in Table I). A linear fit of PR_d performed - to avoid potential biases - excluding the entire first year of operation is shown in the same Figure, indicating a yearly performance loss rate of -1.3%/year, consistent with the observations of other works for a-Si [REF 6.2].

Nevertheless, we need to stress the fact that the late winter and the entire spring of year 2013 were on average rainier and colder than usual. The adverse meteorological conditions may have contributed to slowing down the SWE recovery for that year. This fact may explain the slightly more pronounced deviation from the model of the measured PR_d data in the spring and summer of 2013. If this observation is correct, the yearly performance loss rate for the a-Si module under investigation could presumably be lower. A long-term monitoring of a PV device over several years is in fact required to avoid seasonal biases and determine more reliable degradation rate factors.

Consistent with the observations of Figure 6.11b that temperature in summer time is the principle loss mechanism for c-Si, we observe seasonal oscillations for this device as well, with a reduced performance in summer and values just slightly above STC in winter when spectral gains also contribute to influencing the outdoor performance of the modules. As the linear fit in Figure 6.12b illustrates, the average PR_d of the c-Si device under testing in the first three years of operation is quite stable, indeed showing a very modest gain of +0.3%/y.

The counter-cyclical seasonal behaviour of both technologies is well described by the model and can clearly be appreciated in Figure 6.12b, where the two data sets directly overlap.

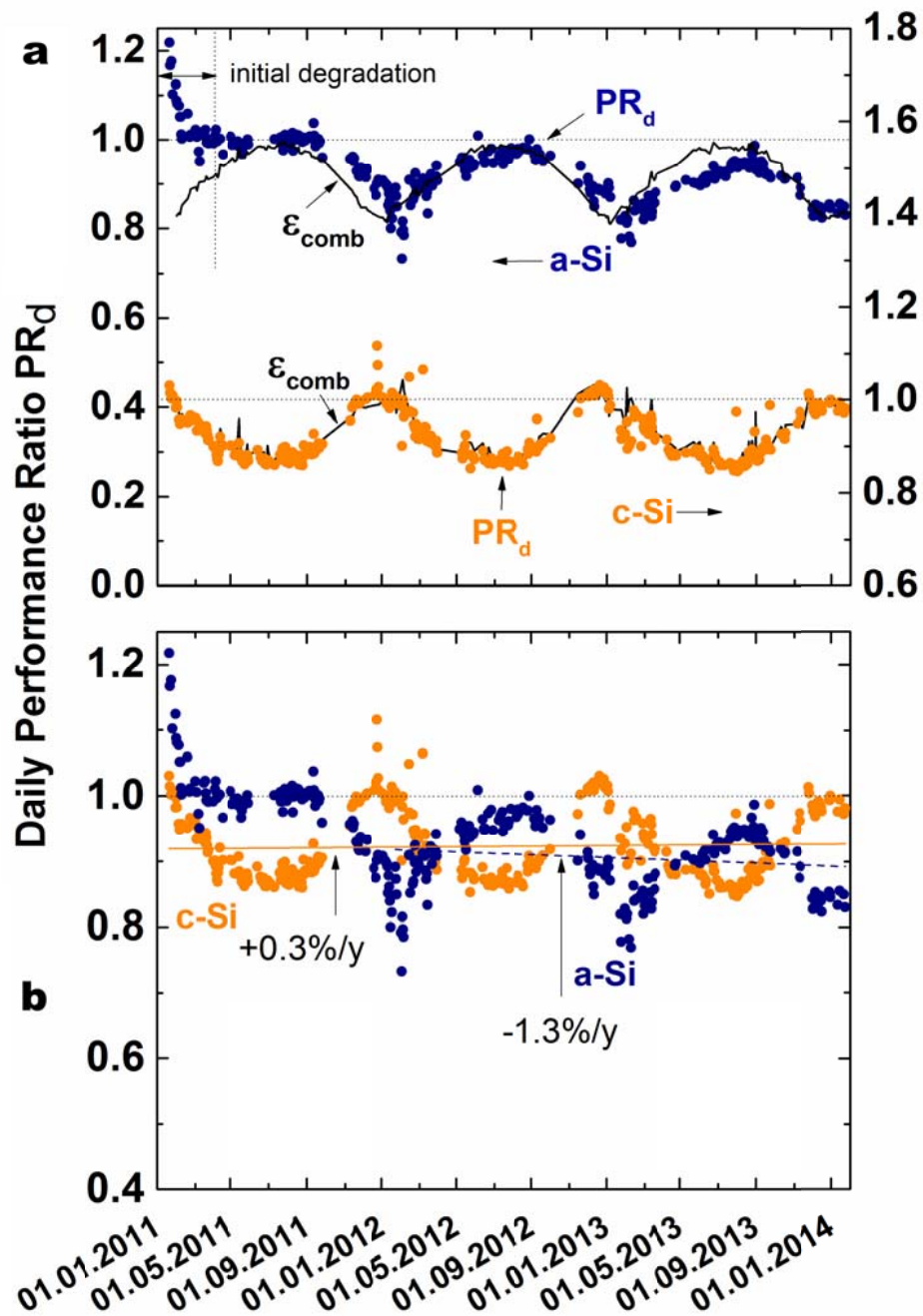


Figure 6.12: a) Daily measured PR_d (DC) for days of *clear-sky conditions* (i.e. from February 1st, 2011 to January 31st, 2014) for the a-Si and c-Si modules with the corresponding modelled *relative combined performance factor* ϵ_{comb} (solid black line). The offset between the two data sets is due to the use of different y-axes. b) PR_d data for both devices overlap here. In order to assess the long-term stability of the different technologies, linear fits to PR_d are applied to the entire interval (3 years) to c-Si (solid line) and, excluding the first full year of operation when the degradation is more pronounced, to 2 years for a-Si (dashed line).

6.5 Extension of the model to other geographical locations

In this Section we extend the *simplified model* with aggregate data described in the previous Section so as to model the performance of a-Si for different geographical locations in Europe [see PMTHIN 22]. In order to do this, we consider installing the same module at an optimal tilt - with identical characteristics (i.e. temperature coefficients, spectral response, etc.) - in three geographical locations representative of different climatic zones in Europe, and we attempt to model its climatic-dependent energy performance.

The selected sites are Sevilla (ES, 37°N), Lübeck (DE, 53°N), and Tallin (EE, 59°N) which we consider to be representative, respectively, of a typical Mediterranean, Northern-European and Scandinavian climate, therefore covering nearly all of Europe.

Whereas meteorological and solar data for the Lugano testing site were directly monitored, in extending the simulations to other locations in Europe we used full-time data series for the irradiance and ambient temperature provided by *GeoModel Solar*.

Using the same data series, a previously proposed model [PMTHIN 19] describing the Staebler-Wronsky effect (SWE, i.e. a degradation/regeneration of the electrical properties of a-Si, due to light exposure and temperature annealing), was used to model this phenomenon for the different sites.

Solar and meteorological input parameters

In extending the modelling to other geographical locations in Europe, meteorological data (solar irradiance and ambient temperature) from GeoModel were used. Solar irradiance data were derived from satellite data using Meteosat satellite and atmospheric models. Time resolution of the applied data was 15 minutes. Ambient temperature was derived from *The Climate Forecast System Reanalysis* (CFSR) - a global meteorological model - covering years 1979-2010 and *Seasonal Climate Forecast version 2* (CFSv2), covering years from 2011-2014. Both systems, focused on the conditions of the oceans and the atmosphere, are run by the National Oceanic and Atmospheric Administration (NOAA) agency of the US Department of Commerce.

The model comprises different meteorological parameters, such as the ambient air-temperature (at a height of two metres), humidity and pressure, water vapour and several others. The spatial resolution of the models in central Europe is about 35x30 km² and 22x19 km² for CFSR and CFSv2, respectively, and the time step is 60 minutes.

From the original raw resolution, using site-specific temperature gradients for the region and a 1-km resolution digital terrain model, ambient temperature was disaggregated down to a 1x1 km² resolution.

In order to model the performance of the module, one must translate ambient temperature values into module temperature T_{mod} . The temperature is derived from a regression formula, using the air temperature, the irradiance G_{poa} and the classical Nominal Operating Cell Temperature (NOCT=42.4°C) relation ($T_{mod} = T_{amb} + c_T * G_{poa}$), with the temperature coefficient c_T obtained by fitting outdoor data for Lugano and the year 2012. The same value was then used for all sites to obtain the T_{mod} versus T_{amb} relation for sunny days. No wind correction was applied at T_{mod} in this study.

Furthermore, for the different locations, modules were considered to be installed open-rack mounted, south-facing and at an optimal tilt. The yearly energy optimization took into account irradiation, temperature and also the local horizon. Optimal tilts were 33° for Sevilla, 39° for Lugano, and 38°/40° for Lübeck and Tallin, respectively. The higher value for Lugano, compared to Lübeck, is due to the horizon and the presence of the surrounding mountains.

Finally, in order to classify a day as clear for a given site (and hence use it in our calculations), we have defined a clear-sky ratio $H_s = G_{diff}/G_{poa}$ (with G_{diff} the diffused irradiance). Clear-sky days are those with $H_s < 0.35$. This relatively high threshold, used for all testing sites, was set because of the extreme difficulty in retrieving sunny days in wintertime for Lübeck, and most notably Tallin, due to the high ratio of days which may be classified as cloudy or overcast for these sites and period of the year.

Modelling the SWE in different geographical locations

So far, the model could be adapted to any technology, particularly crystalline-silicon (c-Si). For a-Si, however, we additionally needed to model the SWE, a dynamic phenomenon which acts on a relatively long timescale (days, weeks, months) depending on the climate of the installation site.

Simulation of the energy yield for a-Si modules is further complicated due to the huge spread of performance parameters between different manufacturers of amorphous silicon and the typical seasonal patterns of their outdoor performances.

The SWE model used in Ref. [PMTHIN 22] is briefly mentioned here. In this study, time series comprising 9 years (2005-2013) of irradiance G_{poa} and temperature T_{amb} were used for all four sites.

The SWE_n state of the module on day n depends on the state on the previous day (SWE_{n-1}), i.e. the junction temperature and the amount of solar insolation faced by the module on the previous day, i.e. a first order discrete differential equation, which is written as:

$$dTot = AN_{coef} \sum_{\text{daily where } (T_{mod}-T_{min})>0} (T_{mod} - T_{min}) * dt + LS_{coeff} \sum_{\text{daily}} GTI * dt \quad (\text{equation 29})$$

$$\text{if } dTot > 0 \\ d = SWE_{max} - SWE_n \quad (\text{equation 30})$$

$$\text{if } dTot < 0 \\ d = SWE_n - SWE_{min} \quad (\text{equation 31})$$

$$SWE_{n+1} = SWE_n + dTot * d \quad (\text{equation 32})$$

The values of the model parameters, given in Table 6.1, were obtained by fitting the equation to experimental data for the Lugano testing site. The results are shown in Figure 6.17.

Parameter	Description	Used value
SWE_{max}	Maximum state of the module	1.045
SWE_{min}	Minimum state of the module	0.945
SWE_{n+1}	Module's state in day n +1	-
SWE_n	Module's state in day n	-
G_{poa}	Global plane-of-array irradiance	-
T_{mod}	Temperature of the PV module (NOCT standard formula)	$T_{mod} = T_{amb} + c_T * G_{poa}$
c_T	Parameter that depends on the module construction and materials as well as on the mounting configuration of the module.	0.028 [W/°C] for open rack
T_{min}	Min. temperature triggering the annealing effect.	40
LS_{coef}	Light-soaking coefficient.	-0.0000011
AN_{coef}	Annealing coefficient.	0.00047

Table 6.1: Model parameters obtained by fitting the equation to experimental data for the test site of Lugano.

Modelling results

The single loss factors and the performance ratio were calculated for all locations. The final PR values are presented in Figure 6.13, confirming that, for clear-sky days, a-Si is a technology more suited to warmer climates and, due to the considerable spectral losses in wintertime at high latitudes, to latitudes (for the northern hemisphere) between 0° and, speculatively, 45-50° N.

For cloudy/overcast days, which the majority of the days in wintertime for Tallin and Lübeck are, the

argument that a-Si is more suitable, due to its better spectral-match and to typical blue-rich diffused spectra, is true. Nevertheless, it should be considered that the irradiance level on such days varies roughly in the range 50-300 W/m₂. The low-irradiance performance of the device under testing therefore becomes a much more critical parameter.

Furthermore, if the solar module is operating at low temperatures, due to the different temperature coefficients (~ -0.4 and ~ -0.2 %/°C, respectively, for c-Si and a-Si), the gain for c-Si will be twice as high: e.g. +6%, and +3%, respectively, compared to STC if the device is operating at 10°C.

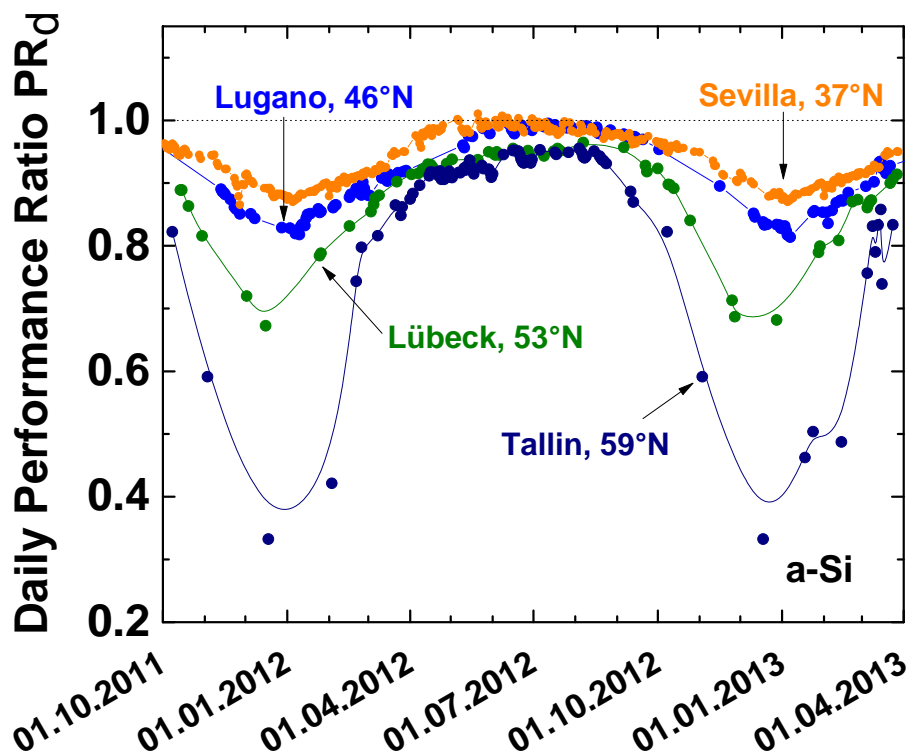


Figure 6.13: Combination of the different contributions (losses/gains with respect to STC) for the different geographical locations aiming at modelling the daily performance ratio PR_d .

The single losses and gains (with respect to STC) related to the different phenomena for sunny days and the selected locations are shown in Figures 6.14 to 6.16.

Reflection losses (at optimal tilt) are nearly negligible in Sevilla and Lugano all year long, whereas in wintertime losses reach a maximum at solar solstice, accounting for up to -2.3%, and -1.7% for Tallin and Lübeck respectively.

Spectral losses/gains are perfectly harmonized with the sun phase (maximum and minimum at solstices), and, as shown in Figure 6.15, become very pronounced on sunny days for Tallin and Lübeck in wintertime (-65%, and -30%, respectively, at winter solstice). Spectral losses in wintertime are also significant in Lugano (-12%) and, to a lesser extent, in Sevilla (-8%).

As expected, **temperature losses** for the a-Si module are predominant in Sevilla and Lugano in summertime, although limited to a maximum of -7% and -5%, respectively, due to the modest temperature coefficient (-0.18 %/°C). Conversely, in wintertime in Tallin and Lübeck, due to the average low temperatures, the device experiences a gain as compared to STC.

Due to the excellent low-light behaviour of the investigated device, **irradiance losses** (not shown here) are very modest and limited to winter days in Tallin (maximum -1.8%) and Lübeck (maximum -0.6%).

Finally, Figure 6.17 shows the simulated SWE for the 4 different locations, where the effect has been scaled to the Lugano testing site, for which there is a cross-check between simulations and experimental data.

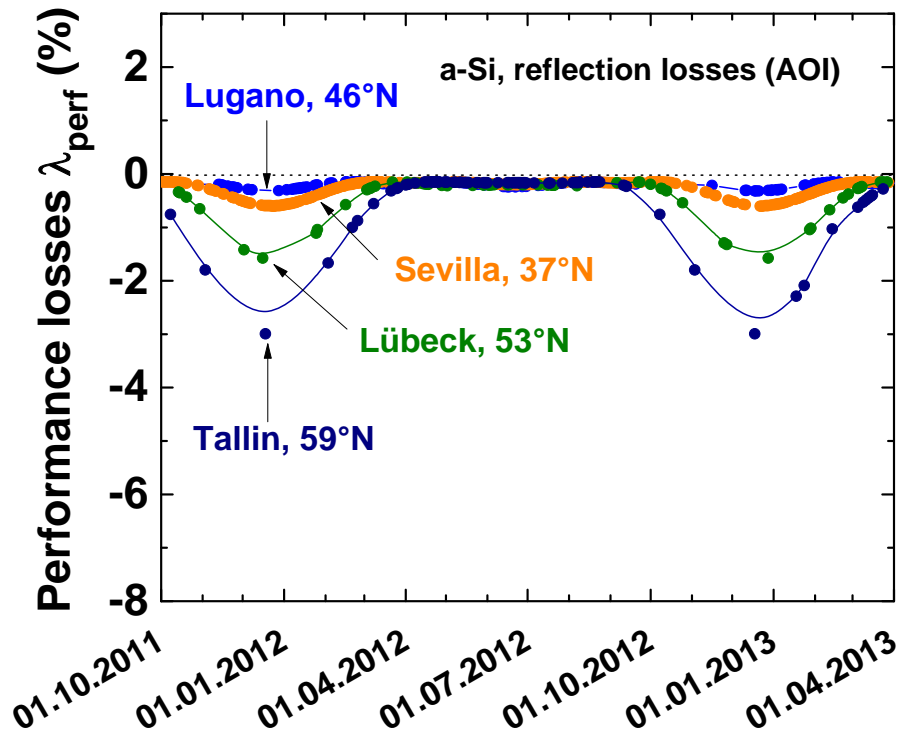


Figure 6.14: Reflection losses with respect to STC calculated for the different geographical locations.

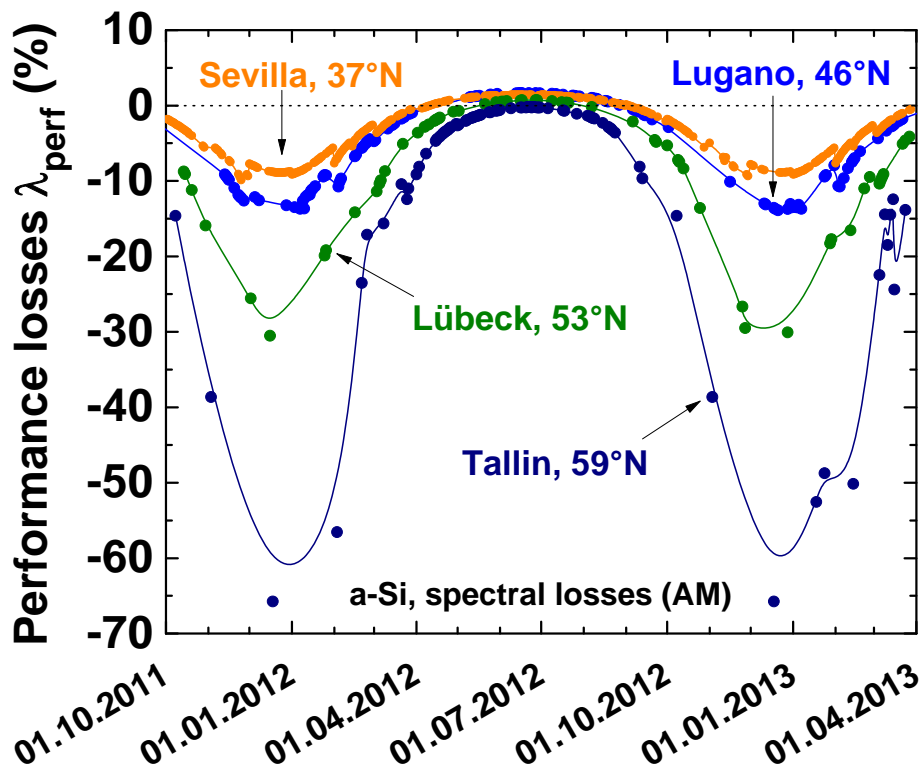


Figure 6.15: Spectral losses/gains with respect to STC calculated for the different geographical locations.

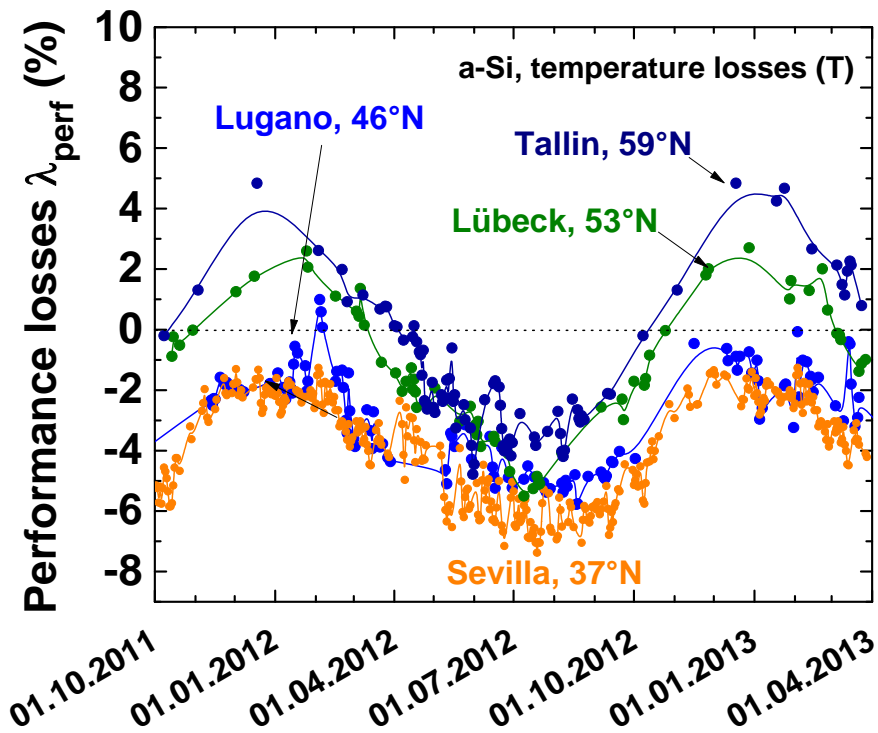


Figure 6.16: Temperature losses/gains with respect to STC calculated for the different geographical locations.

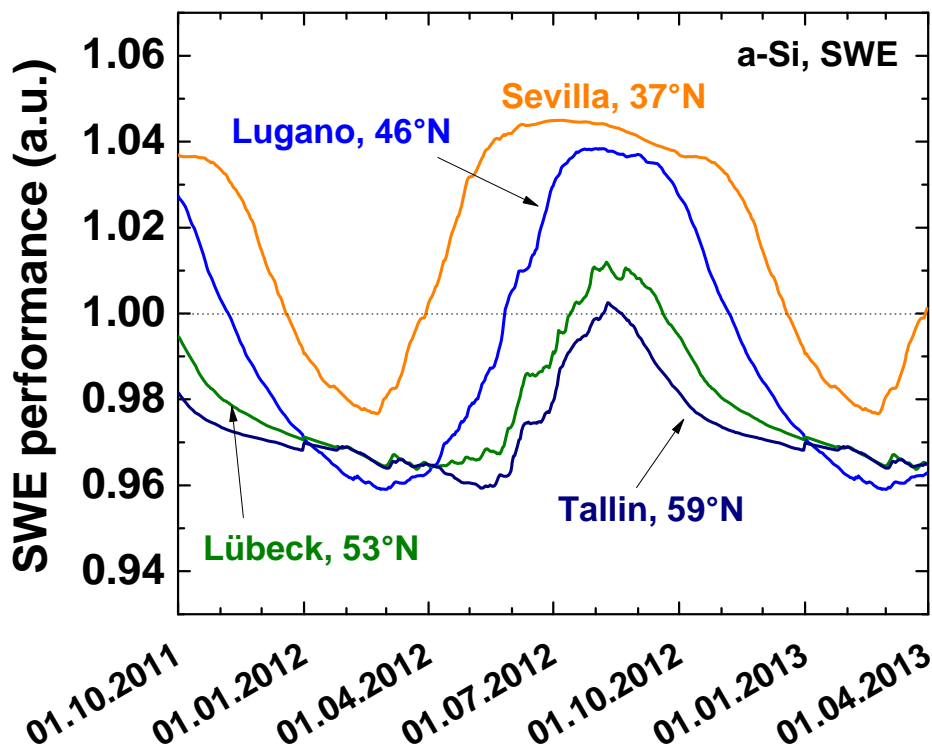


Figure 6.17: SWE effect modelled for the different geographical locations. The yearly average value for Lugano, validated against experimental data, is used as a scaling factor for the other curves.

7. CONCLUSIONS AND FUTURE PERSPECTIVES

The upgrade of some of the indoor and outdoor testing facilities at SUPSI, in combination with the implementation of new testing procedures and the extension of the performance models which were used, allowed SUPSI to significantly improve its measurement accuracies and to gain further insight into the behaviour of thin film modules. Important collaborations were started, (e.g. round robins with industry partners and research laboratories in order to validate the new measurement procedures), and an exchange program was initiated for the outdoor data.

The main achievements of the project have been:

- A new measurement setup for the spectral responsivity measurement of multi-junction modules, in line with the pre-normative activities of IEC TC 82, where the authors were directly involved in the definition of a new international standard for multi-junctions.
- A new measurement procedure for indoor performance testing of multi-junction large area modules, with outstanding measurement uncertainty in line with the uncertainty for single-junction modules. With this result, SUPSI is now among very few testing centres worldwide which are capable of testing multi-junction modules at STC, via spectrometric characterization.
- A new indoor pre-conditioning procedure for the stabilization of CIGS and CdTe modules based on light soaking and dark current soaking was introduced at SUPSI, allowing a higher degree of control of the stabilization process. Outdoor and indoor preconditioning approaches proved to be comparable within a limited uncertainty of $\pm 2\%$.
- 4 years of outdoor measurements were concluded successfully, demonstrating differences in annual energy production of up to $\pm 10\%$ within different thin film technologies. CIS and a-Si/ μ c-Si modules slightly underperformed or performed very closely to c-Si, whereas CdTe and a-Si tended to overperform, due to their much better temperature coefficients. A slight negative trend (i.e. degradation) was visible for all a-Si-based technologies, which could only be explained by a partial recovery of defects generated by SWE, and a subsequent accumulation of these defects with an effective loss of efficiency over time.
- The consideration of spectral and reflection effects allowed us to improve our modelling capabilities of the energy performance of single PV modules in operation, to distinguish between the single contributions and to better understand the measured differences in outdoor performance.
- A new approach for the modelling of the Staebler-Wronsky effect for amorphous silicon and different climates was implemented and validated for Lugano.
- A simplified model, with a daily resolution (PR_d), for the modelling of PV modules in operation was developed and validated for single junction a-Si and c-Si technologies. The results are very encouraging for these technologies.
- A new approach to the representation and analysis of PV module field data was defined in the framework of the International Agency's Photovoltaic Power System Programme (IEA PVPS) Task 13. The approach allows a comparison of data measured in different climates and conditions, as well as of data acquired during different testing periods, and to correct for spectral effects, thus allowing an extraction of the thermal performance under real operating conditions.

Besides these encouraging results, the project has also identified some criticalities, which will be the subject of future work. The major ones are listed here:

- As expected, the accuracy of spectral irradiance measurements is of great importance for providing reliable characterization of PV modules, particularly for thin films. It was shown that the uncertainty that may arise from spectral irradiance measurements in the infrared region has a significant impact on the measurement accuracy of triple- and multi-junction devices for concentrating or space applications, but this may also affect any technology with relevant spectral mismatch, even on a Class A+ solar simulator.
- Observed differences between dark current soaking (CS) and light soaking (LS) could be an indicator for a degradation mechanism occurring in the very first seconds or minutes of dark storage or for current soaking pushing the module into a different state from a light soaking approach. Furthermore, how effective the new stabilization procedure for CIGS and CdTe modules is in reducing the spread of performance measurements between laboratories still needs to be demonstrated via round robin campaigns, also given the fact that changes in these technologies are occurring very rapidly. SUPSI is currently involved in various collaborations whose aim is to demonstrate the validity of the new draft procedure.
- The repetition of temperature coefficient measurements on a set of modules exposed outdoors for over 4 years, as well as laboratory inter-comparisons (round robins), has shown significant discrepancies and variations over time, the origins of which are under investigation. These discrepancies translate directly into a higher uncertainty in energy ratings and predictions. For CIGS and CdTe, these discrepancies can possibly be attributed to meta-stabilities, which are much more difficult to control over the time required to perform a full temperature coefficient measurement (i.e. 2-3 hours). Besides, other factors, so far not considered, such as spectral mismatch errors or the influence of the reference cells, could be sources of uncertainty.
- The modelling accuracy of diffuse days is still in need of improvement in order to reach an acceptable level even for cloudy days. This is also of importance for the validation of the draft Energy Rating Standard IEC 61853-part3.
- Deviations between measured and predicted performance of multi-junction modules could be partially attributed to the missing simulation of current-matching mechanisms. The modelling of the sub-cells will be implemented in the future in combination with indoor characterization methods for the determination of spectral module parameters, which are fast, repeatable and possibly independent of a spectral response measurement.
- In order to better understand the outdoor-observed long-term degradations within thin film modules and to be able to include the degradation in simulation tools, the degradation parameters with their time dependencies and values should be analyzed in more detail in the future by extending the current outdoor analysis with new parameters.
- More outdoor data from labs all over the world will be collected in the future within IEA Task13, while the methods for data evaluation and the result plots for the comparison of different PV module technologies will be further developed. A clear need was identified in this work for consistency among the laboratories performing outdoor testing.

The expertise and competency on the electrical characterization of thin film PV technologies developed at SUPSI during the PM-Thin Project now also allows us to deal with (and test) the new PV technologies, which will be present on the market - or the subjects of extensive research - in the very near future.

The same methods expressly developed for the testing of tandem micromorph devices may be used to characterize all multi-junction devices, such as III-V compounds for concentrated PV (CPV) or very innovative structures, such as organic/inorganic tandems (e.g. perovskite/c-Si or perovskite/CIGS cells). Pre-conditioning procedures developed for II-VI (CdTe) and I-III-VI (CuInSe₂) polycrystalline compounds are still being actively applied. Presently, CdTe is in fact the only technology competing with c-Si on a price level, and CIS-based devices are, among all TF technologies, the ones exhibiting

the highest efficiencies, with many groups and individuals still working extensively on these technologies. Finally, SUPSI has notably increased its modelling capabilities and its understanding of how multiple factors (i.e. temperature, reflections, irradiance, and spectral effects) affect the operation of PV modules under real operating conditions. With the proper adaptations, these capabilities could be extended to model any PV technology.

References

- [REP 01] G. Friesen et al.: Final report ISAAC-TISO test centre, quality and energy yield of photovoltaic modules, period VIII, 2007-2010.
- [REP 02] T. J Silverman, G. Friesen and M. Pravettoni et al., Characterization of Performance of Thin-film Photovoltaic Technologies, Report IEA-PVPS T13-02:2014, May 2014

Chapter 3

- [REF 3.1] J. Burdick and T. Glatfelter, "Spectral response and I-V measurements of tandem amorphous-silicon alloy solar cells", *Solar Cells* **18**, 301-314 (1986)
- [REF 3.2] ASTM E 2236-10 "Standard test method for measurement of electrical performance and spectral response of nonconcentrator multijunction photovoltaic cells and modules", *Annual Book of ASTM Standards*, vol. 12.02 (2015)
- [REF 3.3] M. Pravettoni et al., "Spectral response measurements of double-junction thin-film photovoltaic devices: the impact of shunt resistance and bias voltage", *Meas. Sci. Technol.* **22**, 045902 (10pp) (2011)
- [REF 3.4] IEC 60904-8.1 *Photovoltaic devices: Part 8.1: Measurement of spectral response of multi-junction photovoltaic (PV) devices* (draft)
- [REF 3.5] IEC 60904-7:2008 *Photovoltaic devices - Part 7: Computation of the spectral mismatch correction for measurements of photovoltaic devices*
- [REF 3.6] IEC 60904-1.1 *Photovoltaic devices - Part 1.1: Measurement of current-voltage characteristics of multi-junction photovoltaic (PV) devices* (draft)
- [REF 3.7] M. Meusel et al., "Spectral mismatch correction and spectrometric characterization of monolithic III-V multi-junction solar cells", *Prog. Photovolt: Res. Appl.* **10**, 234-255 (2002)
- [REF 3.8] ISO/IEC Guide 98-1, *Uncertainty of Measurements - Part 1: Introduction to the expression of uncertainty in measurement* (2009)
- [REF 3.9] H. Müllejans et al., "Analysis and mitigation of measurement uncertainties in the traceability chain for the calibration of photovoltaic devices", *Meas. Sci. Technol.* **20**, 075101:1-12 (2009)
- [REF 3.10] M3003 "The Expression of Uncertainty and Confidence in Measurement", UKAS, Ed. 3 (2012), p. 32

Chapter 4

- [REF 4.1] A. Avellán et al., "Challenges in measuring the true efficiency of CIGS modules" in *28th EU PVSEC*, Paris, 2013, p. 2118-2124.
- [REF 4.2] IEC 61646, "Thin-film terrestrial photovoltaic (PV) modules - Design qualification and type approval", second edition, 2008-05.
- [REF 4.3] M. Gostein and L. Dunn, "Light soaking effects on photovoltaic modules: overview and literature review" in *37th IEEE Photovoltaic Specialist Conference*, 2011, p. 3126-3131.
- [REF 4.4] A. Virtuani et. al., "Comparison of indoor and outdoor performance measurements of recent commercially available solar modules" in *Progress in Photovoltaics*, 2011.
- [REF 4.5] A. Virtuani et. al., "Comparison of Indoor and Outdoor Performance Measurements on CIS Thin Film Solar Modules" in *22th EU PVSEC*, Milan, 2007, p. 2421- 2425.
- [REF 4.6] J.A.del Cueto, C.A. Deline and S. Rummel, "Analysis of Alternate Methods to Obtain Stabilized Power Performance of CdTe and CIGS PV Modules" *Reliability Workshop*, Denver, 2011.

Chapter 5

- [REF 5.1] G. Friesen et al., kWh/Wp measurements and predictions of 13 different PV modules, 37th IEEE PVSC, Seattle (USA), June 2011.
- [REF 5.2] D. Chianese et al., MPPT3000 Multifunction Testing Device for PV Modules, 23rd EPVSEC, Valencia (ES), September 2008.
- [REF 5.3] Guideline for PV power measurement in industry, ISBN 978-92-79-15780-6.
- [REF 5.4] P. Grunow et al.; Weak light performance and annual yields of PV modules and systems as a result of the basic parameter set of industrial solar cells, 19th EUPVSEC.
- [REF 5.5] M. Schweiger et al., Fabrication tolerance of PV-module I-V correction parameters for different PV-module technologies and impact on energy yield prediction, 29th EUPVSEC
- [REF 5.6] M. Schweiger et al.; Non-linearity of temperature coefficients. Equivalent cell temperature and temperature behaviour of different PV module technologies; 28th EUPVSEC

Chapter 6

- [REF 6.1] L. Fanni, A. Virtuani, and D. Chianese, *A Detailed Analysis Of Gains And Losses Of A Fully Integrated Flat Roof Amorphous Silicon Photovoltaic Solar Plant*, Solar Energy 85 (2011) 2360–2373.
- [REF 6.2] D. C. Jordan and S. R. Kurtz, *Photovoltaic Degradation Rates—an Analytical Review*, *Prog. Photovolt: Res. Appl.* (2011), DOI: 10.1002/pip.1182.
- [REF 6.3] DL King, WE Boyson, JA Kratochvill, *Photovoltaic Array Performance Model*, Sandia Report 2004-3535, Sandia National Laboratories, Albuquerque, 2004;
- [REF 6.4] N. Martin, J.M. Ruiz, *Calculation Of The PV Modules Angular Losses Under Field Conditions By Means, Of An Analytical Model*, Sol. En. Mater. Sol. Cells 70 (2001) p. 25- 38.

Annex 1: List of publications

- [PMTHIN 1] M. Pravettoni et al., "A Filtered Pulsed Solar Simulator for Spectral Response Measurements of Multi-junction Modules of Commercial Size" Proceedings of the 27th European Photovoltaic Solar Energy Conference, Frankfurt, 2012.
- [PMTHIN 2] M. Pravettoni, "To Bias or Not to Bias? An 'How-To' Guide for Spectral Response Measurements of Thin Film Multi-Junction Photovoltaic Modules" MRS Proceedings, 1426, pp 81-86. doi:10.1557/opl.2012.838.
- [PMTHIN 3] M. Pravettoni et al., "Spectral Mismatch Effect to the Open-circuit Voltage in the Indoor Characterization of Multi-junction Thin-film Photovoltaic Modules", 39th IEEE PVSC, Tampa (2013), 706-711.
- [PMTHIN 4] M. Pravettoni, "Characterization of the electrical performance of photovoltaic cells and modules: a review", in Compendium of Energy Science and Technology, Vol. 9, in press.
- [PMTHIN 5] V. Paraskeva et al., "The effect of shunt resistance on external quantum efficiency measurements at high light bias conditions", 40th IEEE PVSC, Denver, 2014, 3664-3669.
- [PMTHIN 6] V. Paraskeva et al., "Voltage and light bias dependent quantum efficiency measurements of GaInP/GaInAs/Ge triple junction devices, Solar Energy Material & Solar Cells **116**, 55-60 (2013)
- [PMTHIN 7] M. Pravettoni et al., "Light Emitting Diodes in the Experimental Practice for the Characterization of Novel Photovoltaics", 2015 MRS Spring Meeting, in press.
- [PMTHIN 8] R. Galleano and M. Pravettoni et al., "Comparison of spectral characterization measurements on pulsed solar simulators and impact on the calibration of a multi-junction thin-film module", 29th EU PVSEC, Amsterdam, 2014
- [PMTHIN 9] M. Pravettoni et al., "Results of the fourth international spectral measurement inter-comparison of a steady-state AM0 solar simulator", 6th WCPEC, Kyoto 2014, 1041-1042
- [PMTHIN 10] R. Galleano et al., "Second international spectroradiometer intercomparison: results and impact on PV device calibration", Prog. Photovolt: Res. Appl., published online (2014)
- [PMTHIN 11] R. Galleano and A. Virtuani et al., "Intercomparison campaign of spectroradiometers for a correct estimation of solar spectral irradiance: results and potential impact on photovoltaic devices calibration, Prog. Photovolt: Res. Appl. 2014; 22:1128–1137
- [PMTHIN 12] G. Belluardo et al., "Solar spectral characterization of three different locations at alpine latitudes using average photon energy", Eurosun 2014 ISES Conference Proceedings
- [PMTHIN 13] S. Dittmann et al., "Current-Soaking and Dark Storage Effects of Polycrystalline Thin Film Solar Modules", 40th IEEE PVSC, Denver, 2014
- [PMTHIN 14] S. Dittmann et al.: Energy yield measurements at SUPSI - importance of data quality control and its influence on kWh/Wp inter-comparisons, 26th EPVSEC, Hamburg (D), September 2011.
- [PMTHIN 15] G. Friesen et al. "Detailed analysis of thin film module performance based on indoor and outdoor tests" Proceedings of the 27th European Photovoltaic Solar Energy Conference, Frankfurt, 2012.
- [PMTHIN 16] G. Friesen et al., "A 4 year energy yield inter-comparison of thin-film modules: linking indoor to outdoor performance data", 6th WCPEC, Kyoto 2014.

- [PMTHIN 17] B. Mihaylov and G. Friesen and S. Dittmann, Results of the SOPHIA module inter-comparison part-1: STC, low irradiance conditions and temperature coefficients measurements of c-Si technologies, 29th EUPVSEC, Amsterdam 2014.
- [PMTHIN 18] B. Mihaylov and G. Friesen and S. Dittmann, Uncertainty in energy yield estimation based on c-Si module round robin results, 6th WCPEC, Kyoto 2014.
- [PMTHIN 19] A. Skoczek, A. Virtuani, T. Cebecauer, and D. Chianese, "Energy Yield Prediction Of Amorphous Silicon Modules Using Full Time Data Series Of Irradiance And Temperature For Different Geographical Locations", 26th EUPVSEC, Hamburg, 2011.
- [PMTHIN 20] A. Virtuani et al., "Seasonal power fluctuations of amorphous silicon thin film PV modules: distinguishing between different contributions", Prog. Photovolt: Res. Appl. (2012), DOI: 10.1002/pip.2257.
- [PMTHIN 21] A. Virtuani et al., "A simple approach to model the performance of amorphous silicon PV modules in operation", 28th EUPVSEC, Paris, 2013.
- [PMTHIN 22] A. Virtuani et al., "Modelling The Performance Of Amorphous Silicon Photovoltaic Modules In Different Geographical Locations In Europe", 29th EUPVSEC, Amsterdam 2014.

Annex 2: Module table

LABLE	TECHNOLOGY	MANUFACTURER	MODULE TYPE
c-Si REF	mc-Si	Conergy	PowerPlus 220P
a-Si 1	a-Si	Nexpower	NH-100AX-1
a-Si 2	a-Si/ a-Si	Schott	ASI 100
a-Si 3	a-Si/ a-Si	EPV	EPV-5X
μ-Si 1	a-Si/μc-Si	Bosch	Vega-T 115
μ-Si 2	a-Si/μc-Si	Inventux	X120
μ-Si 3	a-Si/μc-Si	Mitsubishi	MT130
μ-Si 4	a-Si/μc-Si	Pramac	Luce MCHP
CIS 1	CIS	Sulfurcell	SCG55-HV-F
CIS 2	CIGS	Solibro	SL1-85F
CIS 3	CIGS	Avancis	PowerMax 110
CIS 4	CIGS	Solar Frontier	SF165-S
CIS 5	CIGS	Avancis	PowerMax Smart
CIS 6	CIGS	Solibro	LS2-120
CdTe 1	CdTe	Firstsolar	FS-275
CdTe 2	CdTe	Firstsolar	FS-382

List of modules tested in the framework of this project and the correlation of the labels used in this report to the manufacturer, module type and technology
